2010-03

Climate analysis of lightning launch commit criteria for Kennedy Space Center and Cape Canaveral Air Force Station

Muller, Eric C.

Monterey, California. Naval Postgraduate School

NAVAL POSTGRADUATE SCHOOL

MONTEREY, CALIFORNIA

THESIS

CLIMATE ANALYSIS OF LIGHTNING LAUNCH COMMIT CRITERIA FOR KENNEDY SPACE CENTER AND CAPE CANAVERAL AIR FORCE STATION

by

Eric C. Muller

March 2010

Thesis Advisor:	Tom Murphree
Thesis Co-Advisor	Mary S. Jordan

Approved for public release; distribution is unlimited

THIS PAGE INTENTIONALLY LEFT BLANK

REPORT DOCUMENTATION PAGE		Form Approved OMB No. 0704-0188

1. AGENCY USE ONLY *(Leave blank)*	2. REPORT DATE	3. REPORT TYPE AND DATES COVERED
	March 2010	Master's Thesis

4. TITLE AND SUBTITLE
Climate Analysis of Lightning Launch Commit Criteria for Kennedy Space Center and Cape Canaveral Air Force Station

5. FUNDING NUMBERS

6. AUTHOR(S) Muller, Eric C.

7. PERFORMING ORGANIZATION NAME(S) AND ADDRESS(ES)
Naval Postgraduate School
Monterey, CA 93943-5000

8. PERFORMING ORGANIZATION REPORT NUMBER

9. SPONSORING /MONITORING AGENCY NAME(S) AND ADDRESS(ES)
N/A

10. SPONSORING/MONITORING AGENCY REPORT NUMBER

11. SUPPLEMENTARY NOTES The views expressed in this thesis are those of the author and do not reflect the official policy or position of the Department of Defense or the U.S. Government.

12a. DISTRIBUTION / AVAILABILITY STATEMENT
Approved for public release; distribution is unlimited

12b. DISTRIBUTION CODE

13. ABSTRACT

We have conducted climate analyses of natural lightning activity at Kennedy Space Center and Cape Canaveral Air Force Station (KSC/CCAFS). These analyses were conducted to improve forecasts of lightning related hazards for, and the planning of, space vehicle launches at KSC/CCAFS. If a space vehicle is hit by lightning during launch, the vehicle and payload may sustain irreparable damage. In this research, we investigated one aspect of the lightning related rules governing launches—the natural lightning launch commit criteria. Our goal was to improve the scientific basis for skillful forecasting of the probability of lightning hazards. Such forecasts have the potential to reduce lightning related risks to personnel and equipment, and to save millions of dollars in preparation and launch costs. Using cloud-to-ground lightning strike data from the National Lightning Detection Network during January 1989 through December 2008, we identified events in which the KSC/CCAFS natural lightning criteria for launches were violated—that is, when excessive lightning activity prevented or would have prevented launches from occurring. Based on these events, we developed daily and multi-day probabilities of lightning violations. We also developed and applied an objective statistical method for determining the seasonality of lightning and for identifying six lightning violation seasons through the course of the calendar year. These seasons were used as the basis for characterizing the temporal and spatial patterns associated with climate scale variations in lightning at KSC/CCAFS. We used atmospheric reanalysis data to analyze the physical processes that lead to interannual variability in: (a) lightning violations in each season; and (b) the start and end dates of the main lightning season. These analyses led to the identification of regional and global scale processes that tend to increase and decrease the probability of lightning violations, including: (1) shifts in the strength, latitude, and zonal extent of the Bermuda High; (2) alterations of regional scale divergence and convection, and (3) teleconnections to global scale climate variations. The results of this study help form the foundation for improvements in the analysis and forecasting of natural lightning violations, and in the planning of launches at KSC/CCAFS.

14. SUBJECT TERMS
Cape Canaveral Air Force Station, Climate Analysis, Climate Variations, Climatology, Kennedy Space Center, Lightning Launch Commit Criteria, Lightning Probability, Long Range Forecasting, National Lightning Detection Network, Reanalysis, Space Vehicle Launch, Teleconnections, Triggered Lightning

15. NUMBER OF PAGES
147

16. PRICE CODE

17. SECURITY CLASSIFICATION OF REPORT	18. SECURITY CLASSIFICATION OF THIS PAGE	19. SECURITY CLASSIFICATION OF ABSTRACT	20. LIMITATION OF ABSTRACT
Unclassified	Unclassified	Unclassified	UU

NSN 7540-01-280-5500

Standard Form 298 (Rev. 8-98)
Prescribed by ANSI Std. Z39.18

THIS PAGE INTENTIONALLY LEFT BLANK

Approved for public release; distribution is unlimited

CLIMATE ANALYSIS OF LIGHTNING LAUNCH COMMIT CRITERIA FOR KENNEDY SPACE CENTER AND CAPE CANAVERAL AIR FORCE STATION

Eric C. Muller
Captain, United States Air Force
B.S., Valparaiso University, 2001

Submitted in partial fulfillment of the
requirements for the degree of

MASTER OF SCIENCE IN METEOROLOGY

from the

NAVAL POSTGRADUATE SCHOOL
March 2010

Author: Eric C. Muller

Approved by: Tom Murphree
Advisor

Mary S. Jordan
Associate Advisor

Philip A. Durkee
Chairman, Department of Meteorology

THIS PAGE INTENTIONALLY LEFT BLANK

ABSTRACT

We have conducted climate analyses of natural lightning activity at Kennedy Space Center and Cape Canaveral Air Force Station (KSC/CCAFS). These analyses were conducted to improve forecasts of lightning related hazards for, and the planning of, space vehicle launches at KSC/CCAFS. If a space vehicle is hit by lightning during launch, the vehicle and payload may sustain irreparable damage. Lightning-based rules for conducting launch and vehicle preparation activities have been developed by launch managers at KSC/CCAFS. In this research, we investigated one aspect of these—the natural lightning launch commit criteria. Our goal was to improve the scientific basis for skillful forecasting of the probability of lightning hazards. Such forecasts have the potential to reduce lightning related risks to personnel and equipment, and to save millions of dollars in preparation and launch costs.

Using cloud-to-ground lightning strike data from the National Lightning Detection Network during January 1989 through December 2008, we identified events in which the KSC/CCAFS natural lightning criteria for launches were violated—that is, when excessive lightning activity prevented or would have prevented launches from occurring. Based on these events, we developed daily and multi-day probabilities of lightning violations. We also developed and applied an objective statistical method for determining the seasonality of lightning and for identifying six lightning violation seasons through the course of the calendar year. These seasons were used as the basis for characterizing the temporal and spatial patterns associated with climate scale variations in lightning at KSC/CCAFS. We used atmospheric reanalysis data to analyze the physical processes that lead to interannual variability in: (a) lightning violations in each season; and (b) the start and end dates of the main lightning season. These analyses led to the identification of regional and global scale processes that tend to alter the probability of lightning violations, including: (1) shifts in the strength, latitude, and zonal extent of the Bermuda High; (2) alterations of regional scale

divergence and convection, and (3) teleconnections to global scale climate variations. Several of these processes tend to be important in all or most of the six lightning violation seasons. The results of this study help form the foundation for improvements in the analysis and forecasting of natural lightning violations, and in the planning of launches at KSC/CCAFS.

TABLE OF CONTENTS

LIST OF FIGURES

THIS PAGE INTENTIONALLY LEFT BLANK

LIST OF TABLES

THIS PAGE INTENTIONALLY LEFT BLANK

LIST OF ACRONYMS AND ABBREVIATIONS

14 WS	14th Weather Squadron
45 WS	45th Weather Squadron
4DLSS	Four-Dimensional Lightning Surveillance System
AC-67	Atlas-Centaur-67 rocket
AFSPC	Air Force Space Command
AMU	Applied Meteorology Unit
CCAFS	Cape Canaveral Air Force Station
CG	cloud-to-ground lightning
CGLSS	Cloud-to Ground Lightning Surveillance System
CONUS	contiguous U.S.
CPC	Climate Prediction Center
DoD	Department of Defense
EFM	Electric Field Mill
EN	El Niño
ENLN	El Niño/La Niña
ESE-erly	east-southeasterly
ESRL	Earth System Research Laboratory
FAA	Federal Aviation Administration
GPH	geopotential height
IOZM	Indian Ocean Zonal Mode
km	kilometer(s)
KSC	Kennedy Space Center
LAP	Lightning Advisory Panel
LN	La Niña
LDAR	Lightning Detection and Ranging
LLCC	Lightning Launch Commit Criteria
LTM	long term mean

MATLAB	Matrix Laboratory
m	meter
mb	millibar(s)
m/s	meters per second
NASA	National Aeronautics and Space Administration
NE	northeast
NE-erly	northeasterly
nm	nautical mile(s)
NPS	Naval Postgraduate School
NCAR	National Center for Atmospheric Research
NCEP	National Centers for Environmental Prediction
NLDN	National Lightning Detection Network
NOAA	National Oceanic and Atmospheric Administration
NW-erly	northwesterly
OLR	outgoing longwave radiation
ONI	Oceanic Niño Index
Pa/s	Pascal per second
R1	NCEP/NCAR Reanalysis Projects
RH	relative humidity
SE	southeast
SE-erly	southeasterly
SE-ward	southeastward
SH	specific humidity
SST	sea surface temperature(s)
SW-erly	southwesterly
STD	standard deviation
TOA	time-of-arrival
U.S.	United States
USAF	United States Air Force

W/m^2	Watts per meter squared
WNW-erly	west-northwesterly
WSW-erly	west-southwesterly

ACKNOWLEDGMENTS

This thesis would not have been possible without the contributions of several individuals. I would like to first thank my advisors, Dr. Tom Murphree and Ms. Mary Jordan for their wisdom, patience, and guidance throughout this research process. Thanks to Mr. William Roeder from the USAF's 45th Weather Squadron for providing his expertise on all aspects of launch weather support. This research was supported by USAF funds provided to the Naval Postgraduate School by the 45th Operations Group.

Also, I would like to thank my fellow classmates for providing periods of laughter and sanity throughout this long and often stressful process. Last, but certainly not least, I would like to thank my wonderful wife and daughter, Erinn and Taegan. Their love and support, for which I am forever grateful, provided motivation as I spent long hours away from home working on this thesis.

THIS PAGE INTENTIONALLY LEFT BLANK

I. INTRODUCTION

A. BACKGROUND

Safety is paramount in the U.S. space program. The United States Air Force (USAF) 45th Weather Squadron (45 WS) plays an essential role in ensuring the safety of space flight. The 45 WS provides comprehensive weather services to the space program for pre-launch, launch, and post-launch operations at Kennedy Space Center (KSC) and Cape Canaveral Air Force Station (CCAFS). One of the most important operational tasks of the 45 WS is evaluating and forecasting lightning and lightning favorable conditions that will exceed the established thresholds prior to and during launches from KSC/CCAFS. These thresholds are described by the Lightning Launch Commit Criteria (LLCC; Roeder and McNamara 2006). The LLCC describe lightning-related conditions under which space launch is hazardous. Approximately 30 percent of the weather related delays and scrubs at KSC/CCAFS during 1988-2002 were due to violations of the LLCC, making LLCC violations the largest source of weather impacts on space launches (FAA 2003). Each inaccurate forecast of the LLCC can cost up to $1M, or in the worst cases, result in a catastrophic loss of mission and personnel (Roeder et al. 1999). In addition, delays and cancellations create backlogs in future launch schedules and take an immeasurable physical and mental toll on personnel executing launches.

Familiarity with Earth's climate system is fundamental to developing and applying LLCC-based mission planning products. Advanced high-resolution datasets and new forecasting techniques, developed primarily by the civilian community, have allowed for significant progress in understanding natural climate variations. A number of research studies have established the importance of climate analysis (e.g., the identification of climate variations) in developing a foundation for skillful long range forecasts (lead times of two weeks or longer) for military operations (e.g., Hildebrand 2001; LaJoie 2006; Vorhees 2006; Stepanek 2006; Hanson 2007; Moss 2007). Several of these studies have

resulted in skillful long-range forecasting techniques for Department of Defense (DoD) areas of operation (e.g., Iraq, Afghanistan, western North Pacific, North Atlantic; Hanson 2007; Moss 2007; Mundhenk 2009; Raynak 2009).

This thesis will focus on providing space weather personnel with detailed natural lightning related climatologies and climate analyses that: (a) apply state-of-the-science data sets and methods; (b) are based on the most current operational LLCC; and (c) improve the use of the LLCC in reducing launch delays and cancellations.

B. LIGHTNING LAUNCH COMMIT CRITERIA

Natural and rocket triggered lightning pose a significant threat to space launch operations at KSC/CCAFS. The LLCC is a set of 11 rules that was developed to minimize natural and rocket-triggered lightning hazards to launch operations. These rules are very complex and atypical within operational meteorology in that they require clear evidence of compliance before a launch can occur (Roeder and McNamara 2006). If just one LLCC violation occurs, the mission gets delayed or scrubbed dependent on how much launch opportunity remains. The analysis and forecasting of LLCC for violations does not occur on a daily basis; rather it is executed only during actual launch windows starting at lead times of three days before the planned launch time.

Descriptions of all eleven of the LLCC are contained in Air Force Space Command Manual 91-710 (Air Force Space Command 2004). An updated version of the LLCC will soon be available (William Roeder, personal communication). However, the main elements of the natural lightning criterion, the LLCC on which we focused this research, can be summarized as shown below.

1. The launch operator must not initiate flight for 30 minutes after any type of lightning occurs within 10 nautical miles (nm) of the flight path.

2. If lightning has occurred within 10 nm of the flight path, launch may occur only if all of the following conditions are satisfied:

   a. The cloud that produced lightning is greater than 10 nm from the flight path.

   b. There is at least one working electric field mill (EFM) less than five nm from the lightning discharge.

   c. Absolute values of all EFM measurements within five nm of the flight path and at each EFM specified in paragraph 2.b have been less than 1000 volts/meter for 15 minutes or longer.

1. History

The danger of rocket triggered lightning was first realized in 1969 when the Apollo-12 launch induced two rocket-triggered lightning flashes (explained below), one cloud-to-ground (CG) and one intracloud, during launch through a weak cold front which was not producing natural lightning (Uman and Krider 1989). Prior to Apollo-12, the only LLCC was for lightning within 10 nm (Poniatowski 1987). Fortunately, the Apollo-12 mission was completed successfully with minimal damage. However, the triggered lightning problems spawned the first set of LLCC that resemble modern rules.

The next significant event in the evolution of the LLCC occurred in 1987 when an unmanned Atlas-Centaur (AC-67) rocket launched into conditions similar to those present at the launch of Apollo-12 and triggered a CG discharge (Uman and Krider 1989). However, the impacts were catastrophic, as the vehicle guidance system was disrupted inducing an erroneous sideways turn. The associated stresses caused the rocket to begin breaking up, forcing range control to destroy it to protect populated areas.

Shortly after the AC-67 accident, the 45 WS and NASA formed the Lightning Advisory Panel (LAP) to advise the USAF and NASA on LLCC issues. The panel, made up of representatives from government agencies and

academia, continuously reviews and modifies the LLCC based on operational incidents, scientific improvements, and new weather sensors (Roeder and McNamara 2006). Since the formation of the LAP, there have been no triggered lightning strikes to launch vehicles at KSC/CCAFS (Roeder and McNamara 2006).

2. Rocket Triggered Lightning

The LLCC were designed primarily to deal with rocket triggered lightning hazards. Rocket triggered lightning is an electrical discharge caused by the rocket and its electrically conductive exhaust plume passing through a sufficiently strong pre-existing electric field (Figure 1; Roeder and McNamara 2006). Amplification of the electric field can occur during rocket launch and significantly increase the pre-existing electric field near the rocket (Roeder 1999). Electric field breakdown can occur (air becomes conductive) and a lightning strike can be triggered (Roeder and McNamara 2006).

The difference between triggered and natural lightning is critical, since the atmosphere, under certain conditions, can produce electric fields sufficient for a triggered lightning threat, but not natural lightning (Roeder 1999). This is because electric fields required for triggered lightning can be 100 times less than that required for natural lightning (Roeder and McNamara 2006). As such, 10 of the 11 LLCC are specifically for triggered lightning. Even the one natural lightning rule is mostly for triggered lightning, due to the presence of an increased electric field rather than the lightning bolt actually striking the launch vehicle.

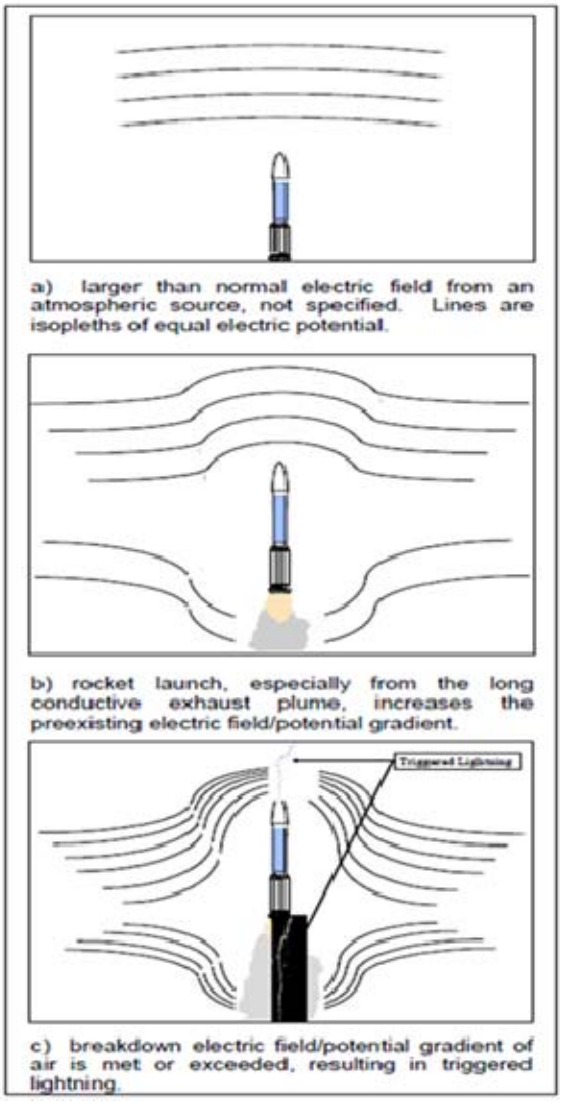

Figure 1. Schematic description of the rocket-triggered lightning process (image from Roeder and McNamara 2006).

C. FLORIDA CLIMATOLOGY

Lightning on the Florida Peninsula and at KSC/CCAFS is strongly determined by long-term mean (LTM) climate patterns and processes, and potentially, by variations in those patterns and processes. A major climate factor affecting the weather experienced across much of the southeast (SE) U.S. throughout the year is the Bermuda High, a semi-permanent, lower tropospheric,

subtropical high pressure system that resides in the North Atlantic Ocean between 20°N and 40°N (Glickman 2000). The seasonal impacts of the Bermuda High are summarized below.

1. Winter (Dec-Feb)

In winter, the Bermuda High is relatively weak and centered in the central North Atlantic near 25°N and 45°W (Figure 2a). During this season, the Bermuda High is located far enough to the south and east that extratropical cyclones and associated frontal systems are frequently able to move through the SE U.S., producing conditions that are generally unfavorable for lightning in the SE U.S. However, for short periods during the winter, the Bermuda High may intensify and expand northward and westward over the Gulf of Mexico and nearby regions (14 WS 2010). During these periods, warm moist air tends to be advected from the tropical southwestern flank of the Bermuda High northward and eastward into the SE U.S. This advection can lead to thunderstorms and lightning in the SE U.S. (Hodanish et al. 1997).

2. Spring (Mar-May)

Early in the spring, extratropical cyclone passage is still quite common as a weak Bermuda High remains east of the region. However, dynamically driven severe weather can occur in Florida due to an increase in solar insolation and low-level moisture, along with cool temperatures aloft (Hodanish et al. 1997). Forcing mechanisms shift from synoptic to mesoscale as the season progresses. The intensification and westward expansion of the Bermuda High allows fewer frontal systems to push through the region (14 WS 2010). Weaker steering currents allow the sea breeze to intensify, increasing the frequency of afternoon showers and thunderstorms across the Florida Peninsula including at KSC/CCAFS (Hodanish et al. 1997).

3. Summer (Jun-Aug)

The Bermuda High dominates summer weather as it expands westward over Florida (Figure 2b). It blocks extratropical synoptic systems from affecting the region, leaving mainly local effects to cause precipitation outside of the occasional easterly wave or tropical cyclone (14 WS 2010). The sea breeze on the east coast of the Florida Peninsula is prominent during summer afternoons near KSC/CCAFS, interacting with the warm moist low-level flow causing thunderstorms to develop almost every afternoon somewhere in the area (Simpson 1994). The precise strength, position, and orientation of the Bermuda High ridge axis, which varies throughout the season, are critical to the direction of the low-level winds (Hodanish et al. 1997). The low-level wind pattern determines where sea breeze thunderstorms are concentrated (e.g., southwesterly (SW-erly) winds occur when the ridge axis is south of KSC/CCAFS keeping thunderstorms concentrated along the east coast of Florida; 45 WS 2007). LTM summer conditions generally produce low level southeasterly (SE-erly) to SW-erly flow over the Florida Peninsula, which is favorable for lightning somewhere over Florida.

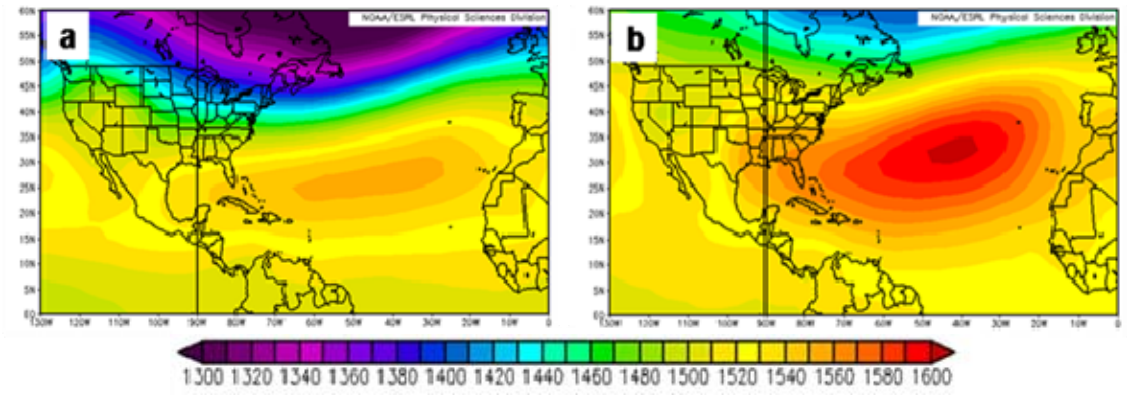

Figure 2. 850 mb geopotential height (GPH) (m) LTM (1968–1996) for the U.S. and North Atlantic regions for (a) Dec-Feb and (b) Jun-Aug.

4. Fall (Sep-Nov)

A moist tropical air mass remains in place over Florida as fall begins. Convection associated with the sea breeze is still quite common along the Florida east coast but is less common than in the summer. However, as fall progresses, the land and water contrast becomes less pronounced weakening the sea breeze (Hodanish et al. 1997). Additionally, as the Bermuda High migrates eastward, more extratropical low-pressure systems are able to affect the region producing unfavorable conditions for lightning (14 WS 2010). Behind these systems, large anticyclones enter the SE U.S. The northeasterly (NE-erly) flow over Florida produced by the anticyclones has continental origins, which brings cooler, more statically stable air into the region (Hodanish et al. 1997).

D. RESEARCH MOTIVATION AND SCOPE

1. Prior Work

Several prior studies developed statistical methods to describe the probability of lightning for KSC/CCAFS during the warm season (May-Sep; Neumann 1971; Everitt 1999; Lericos et al. 2002; Lambert et al. 2005). These studies focused on two important aspects of thunderstorm development in the region, static stability and low-level winds. Neumann (1971) developed a linear regression equation for each month (May-Sep) to describe the relationships between lightning and low level wind, moisture, and stability parameters. Everitt (1999) developed a logistic regression equation describing the probability of lightning based on wind and stability parameters for each month (May-Sep).

The location of the Bermuda High influences the mesoscale processes that drive convection during the warm season across the Florida Peninsula. Lericos et al. (2002) investigated the relationship between low level flow (1000-700 mb layer averaged wind direction) associated with the Bermuda High and Florida convection using National Lightning Detection Network (NLDN) data. His work identified six specific flow regimes that most commonly produced convection over the Florida Peninsula (i.e., calm flow, northwesterly (NW-erly)

flow, subtropical ridge to the north of the peninsula, subtropical ridge to the south of the peninsula, subtropical ridge between Tampa Bay and Jacksonville, and subtropical ridge between Tampa Bay and Miami). For each of these flow regimes, Lericos et al. identified a characteristic pattern of convection over Florida. Figure 3 shows regimes that are favorable (subtropical ridge to the south) and unfavorable (subtropical ridge to the north) for lightning in the KSC/CCAFS area along with the associated daily flash densities. The low-level flow dictated by the position of the Bermuda High ridge axis, focuses sea breeze convection along the east (west) coast of the peninsula in the favorable (unfavorable) flow regime. Lambert et al. (2005) incorporated these six flow regimes into an objective lightning forecast tool for KSC/CCAFS. In addition to modifying the low-level flow regimes developed by Lericos et al. (e.g., added a NE-erly flow regime), Lambert et al. included stability parameters to create a logistic regression equation specific to KSC/CCAFS. Their results suggested that the best flow regime for convection at KSC/CCAFS is a ridge between Tampa and Miami, followed closely by the ridge south of Florida, both of which produce a SW-erly flow over the KSC/CCAFS area.

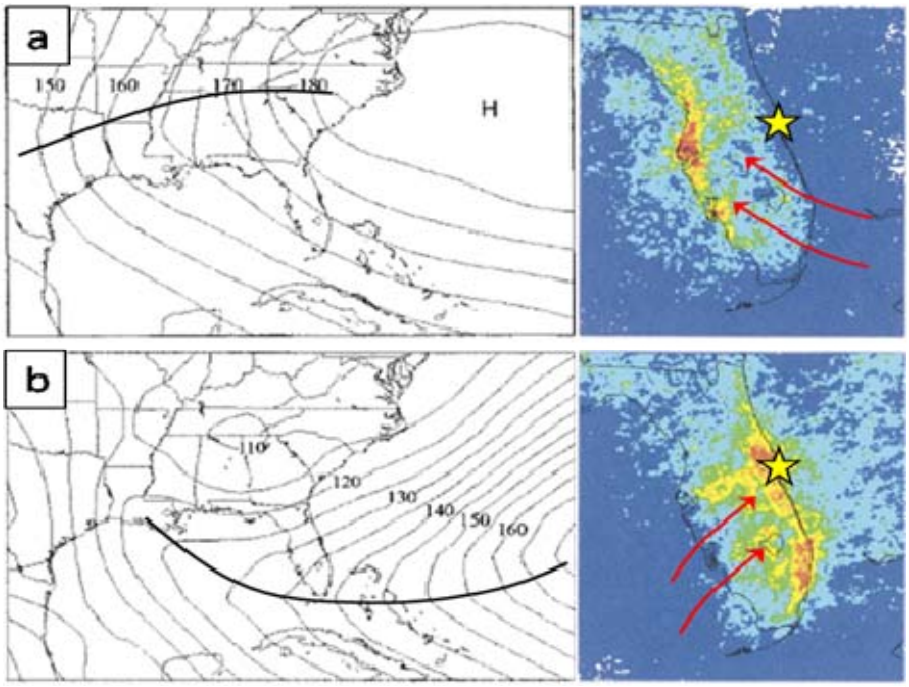

Figure 3. Average 1000 mb GPH (m) contours and daily natural lightning flash densities for summer (May-Sep) flow regimes that are unfavorable and favorable for convection and lightning at KSC/CCAFS: (a) unfavorable regime with subtropical ridge to the north of KSC/CCAFS; and (B) favorable regime with subtropical ridge to the south of KSC/CCAFS. The bold black lines show the axis of the subtropical ridge or Bermuda High at 1000 mb. Red arrows represent the 1000 mb flow. The yellow star indicates the approximate position of KSC/CCAFS.

These prior studies have helped identify important factors leading to violations of the LLCC, however, research that directly investigates the probability of violating the LLCC is still lacking. Goetz (2000) made an attempt at developing limited LLCC climatologies. His research focused on developing LLCC climatology for the natural lightning and cumulus criteria. Goetz examined NLDN data from 1989–1998 for CG flashes within 12 nm of KSC/CCAFS. After filtering the data, he produced hourly violation probabilities for each day of the year and for each month. Goetz built his cumulus climatology based on surface observation cloud codes and precipitation groups for 1992–1998. He divided the cumulus violation data into four seasons (Nov-Feb cool season, Mar-May spring

season, Jun-Aug warm season, and Sep-Oct autumn season) and then calculated hourly violation probabilities for each season.

However, the Goetz study had several important limitations. First, the data periods were relatively short for developing reliable climatologies (ten years for the NLDN data, seven years for the cumulus data). The full range of climate system variability at a location can be very difficult to determine from such short periods. Second, the cumulus violation probabilities were defined for seasons based on calendar months rather than observed variations of lightning and associated cumulus activity. Seasons based on observed variations are more likely to produce reliable descriptions of violation probabilities. This is especially true if one part of a month is active while another part is inactive. Finally, the daily probabilities produced by Goetz (2000) include large day-to-day variations (e.g., 70 percent probability on one day followed by 20 percent probability on the next day). These large variations are likely the result: (a) the limited data periods; and (b) the complexity of the mesoscale processes that determine lightning violations in the KSC/CCAFS region. Such large and questionable day-to-day variations can be very problematic when used in mission planning.

An important stage in quantifying CG lightning at a given distance from a point is determining how to account for the horizontal distance CG lightning travels from its source point aloft to its strike point on the ground. McNamara (2002) tackled this problem by using both NLDN data and data from the lightning detection and ranging (LDAR) system for approximately a four-year period (Mar 1997–Dec 2000). McNamara used a flash grouping algorithm, originally developed by NASA, to determine which sources were associated with a single lightning flash. All sources satisfying the time and spatial constraints were considered by McNamara to be part of the same flash and thus were consolidated into a single flash origin point. Those flashes were then matched to NLDN ground strikes points to determine how far the CG lightning traveled from its original source aloft. This technique matched 60.4 percent of LDAR flashes to NLDN ground strikes yielding an average horizontal distance traveled of 4.7 nm.

Additionally 71.6 percent of CG strikes occurred within 5 nm of the source point. Numerous other studies by Renner (1998), Cox (1999), Lopez and Holle (1999), Poehler (1978), Krider (1988), and Parsons (2000), produced results comparable to McNamara's using different datasets and methods. Table 1 is a summary of prior work investigating the horizontal distance CG lightning travels from its origin source aloft.

Table 1. Summary of previous studies of the horizontal distance CG lightning travels from its origin aloft.

Method	Researcher	Location	Scope	Results
WSR-88D Storm Centroid Method	Renner	Gulf Coast Southern Plains	April-July	75% < 10 nm
	Cox	Southeast Coast	April-July	32%-39% > 5 nm
Distance Between Successive Flash Method	Krider	Florida	3 Storms	Avg 1.9–2.5 nm
	Lopez Holle	Florida, Oklahoma Colorado	1995 1 Storm 1996	75% < 4.9 nm
	Cox	Southeast Coast	April-July	30% > 5 nm
	Parsons	Continental US	1995-1999	65 < 5 nm
LDAR Based Method	Poehler	Florida	1 Storm 13 CG Flashes	100% < 4.8 nm
	McNamara	KSC	March 1997-December 2000	71.6% < 5 nm

Several of the prior studies have emphasized long-term mean descriptions of convection and lightning (e.g., Goetz 2000; McNamara 2002). Others have focused on the regional scale processes that lead to LTM seasonal and intraseasonal patterns in convection and lightning (e.g., Lericos et al. 2002; Lambert et al. 2005). Analyses of climate variations (deviations from LTM patterns and processes) and the mechanisms for those variations are also needed in conducting a complete climate analysis and developing the basis for skillful long-range forecasts of lightning violations. A number of prior studies have shown the value of climate variation analyses and long range forecasting for a wide range of variables and locations (e.g., Hildebrand 2001; Vorhees 2006; Lajoie 2006; Stepanek 2006; Moss 2007; van den Dool 2007; Murphree 2008b;

Raynak 2009). Similar studies of convection and lightning have the potential to significantly improve the ability to analyze and forecast LLCC violations at KSC/CCAFS.

2. Research Questions

Violations of the LLCC are a leading source of weather delays and cancellations at KSC/CCAFS. Thus, objective, quantitative estimates of the probability of violating the LLCC for a given time of year and time of day would be very useful in developing analyses and forecasts to support the planning of space launches (Roeder and McNamara 2006). However, there is no dataset of observed LLCC violations on a daily, multi-decadal basis. Thus, reliable LLCC violation probabilities cannot be directly calculated. In this study, we explored the viability of inferring LLCC violation probabilities using daily resolution, multi-decadal lightning and atmospheric reanalysis datasets. Our major goal was to provide space launch weather personnel with detailed LLCC related climate analyses and climatologies that help limit future launch delays and cancellations.

Our research was primarily focused on the following questions:

1) Can the probability of violating the natural lightning LLCC be accurately inferred from observational data (e.g., NLDN, LDAR)?

2) How do the violation probabilities for KSC/CCAFS change with time of year and time of day, and from year to year?

3) What regional and global scale processes lead to intraseasonal to interannual variations in LLCC violations at KSC/CCAFS?

3. Thesis Organization

To address these research questions, we followed a systematic approach, first focusing on developing the LLCC climatologies and then investigating climate scale variations in lightning violations.

Chapter II defines the study region and period, and then provides details concerning the data sets used in this research, as well as the methods used in developing our LLCC climatologies and in assessing climate variations. Chapter III presents our results, with a focus on the major features of the climatologies, and the climate variations associated with anomalous violation periods. Chapter IV provides a summary of our results and conclusions and offers suggestions for future research.

II. DATA AND METHODS

A. STUDY REGION AND PERIOD

Our research centered on the KSC/CCAFS region of the Florida Peninsula. More specifically, we focused our efforts within a 20 nm radius around the average location of the five most active launch sites as shown in Figure 4.

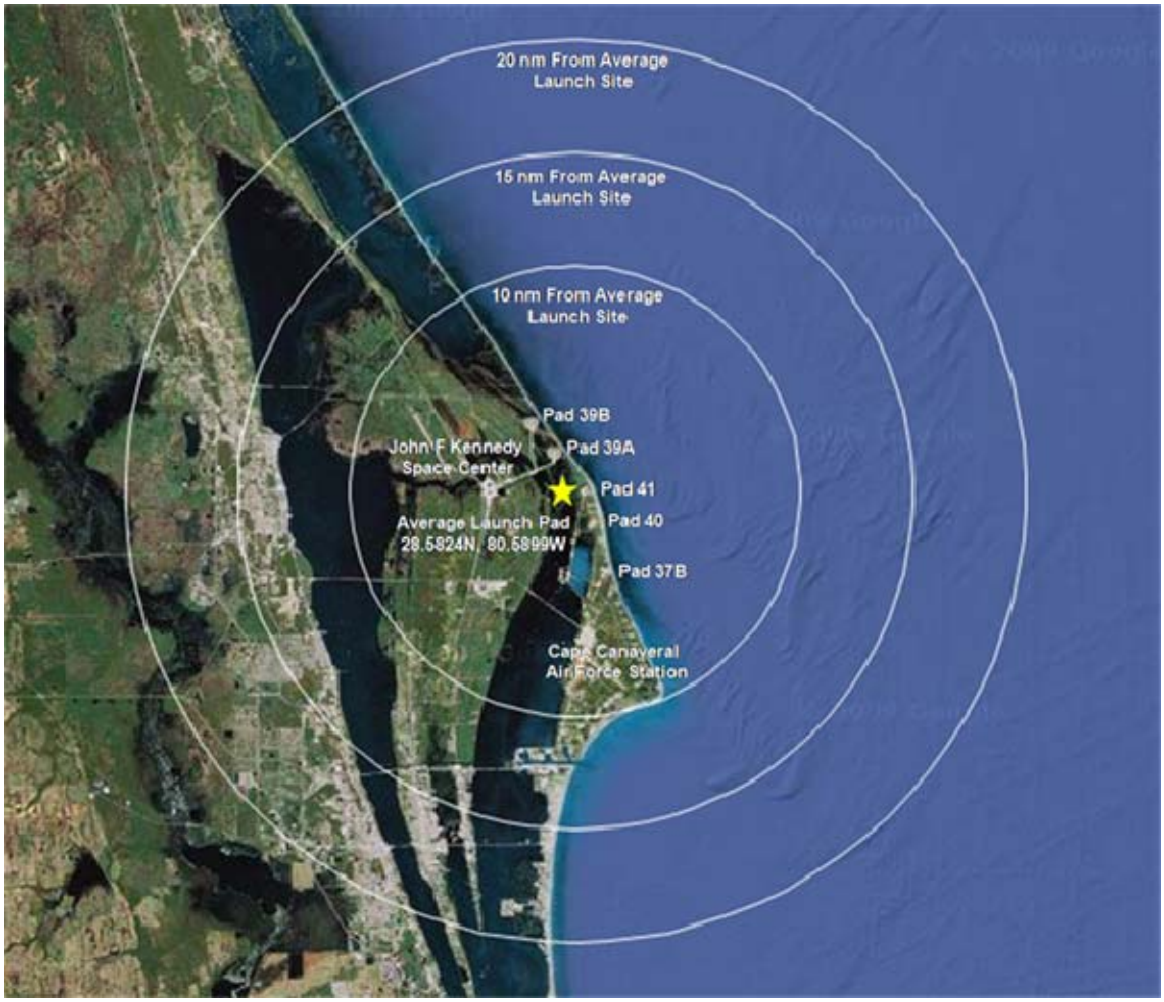

Figure 4. The region of interest for this study. Average launch site (yellow star) is the average location of the five most active launch sites in the region (Pad 39B, Pad 39A, Pad 41, Pad 40, and Pad 37B). The range rings shown are radii in nautical miles from the average launch pad location. Image adapted from FreeMapTools.com [accessed online at http://www.freemaptools.com/radius-around-point.htm, January 2010].

We chose this small region because the natural lightning criterion (described in Chapter I.B.), is focused on lightning that occurs only within 10 nm of the average launch pad location. We chose a region with a 20, rather than 10, nm radius because the larger radius region includes the mesoscale topographic features (e.g., inland waterways, land-sea contrasts) that impact the development of sea-land breezes, convection, and lightning in the KSC/CCAFS region. The larger region also allowed us to work with larger datasets, which is useful in building robust climatologies.

Our study period was January-December of the 20-year period of 1989-2008, the maximum period for which NLDN data for the KSC/CCAFS region was available when we began the study. This 20-year period is shorter than the 30-year or longer period we would have preferred. Nevertheless, 20 years is long enough to develop initial climatologies that can be updated as data for additional years becomes available. A 20-year period is also long enough to allow us to identify and characterize intraseasonal and interannual climate variations. The 1989–2008 period also maximizes the incorporation of in situ and remotely sensed data in the atmospheric reanalysis dataset. Unlike previous studies which only investigated lightning during the warm season (e.g., Neumann 1971, Everitt 1999, Lericos et al. 2002, Lambert et al. 2005), we focused on the entire year and created climatologies and analyzed climate variations for each of six lightning violation seasons that span all months.

B. DATA SETS AND SOURCES

1. National Lightning Detection Network (NLDN)

The Vaisala National Lightning Detection Network (NLDN) consists of 113 Improved Accuracy From Combined Technology (IMPACT) sensors spaced 200-350 kilometers (km) apart. The NLDN provides near-real-time CG lightning information, including time, location, polarity, and peak current information for each individual return stroke (Ward et al. 2008). The IMPACT sensors, installed during the last system-wide upgrade in 2002, provide time-of-arrival (TOA) and

directional information on CG lightning. Figure 5 shows the NLDN sensors for the eastern contiguous U.S. (CONUS) with a closer view of the nine sensors covering our study region in Florida, Georgia, and the Bahamas (not shown). Cummins et al. (1998) estimated the flash detection efficiency as approximately 95 percent, the national average location accuracy as approximately 500 meters, and the location accuracy near KSC/CCAFS as approximately 600–700 meters.

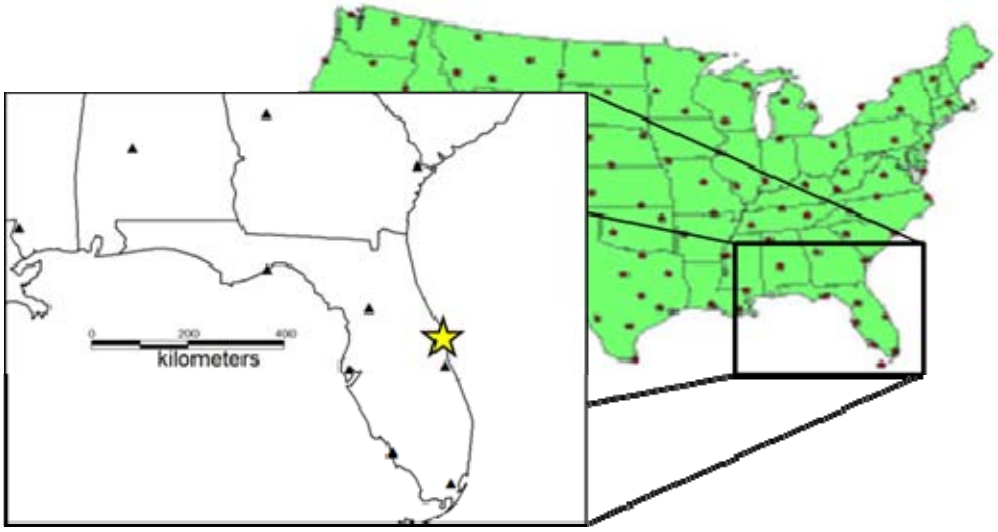

Figure 5. NLDN sensor locations for the eastern CONUS and an inset showing the locations of the nine sensors in Florida, Georgia, and the Bahamas (not shown) that cover our study region. The yellow star represents the approximate location of KSC/CCAFS. Images adapted from Ward (2006) and Grogan (2004).

The operation of the NLDN system involves the following steps and platforms (see Figure 6 and Ward et al. 2008). First, remote sensors detect electromagnetic pulses characteristic of an individual CG stroke (1 in Figure 6). The sensors then transmit the information to a central processing station via satellite (2-3 in Figure 6). Three downlink stations then forward data to the network control center located in Tucson, Arizona (4 in Figure 6). There, the data is processed and archived, with the results forwarded to users via terrestrial and satellite links (5-6 in Figure 6). This near real-time process takes place in a total of 30-40 seconds (Cummins et al. 2006). Flash-grouping algorithms commonly run to combine strokes into flashes, make the dataset less complex

(McNamara 2002). McNamara (2002), Cummins et al. (2006), and Ward et al. (2008) provide more information on the characteristics of the NLDN system. For this study, we received post-processed NLDN CG flash data from the USAF 14 WS (formerly the USAF Combat Climatology Center) in Asheville, North Carolina.

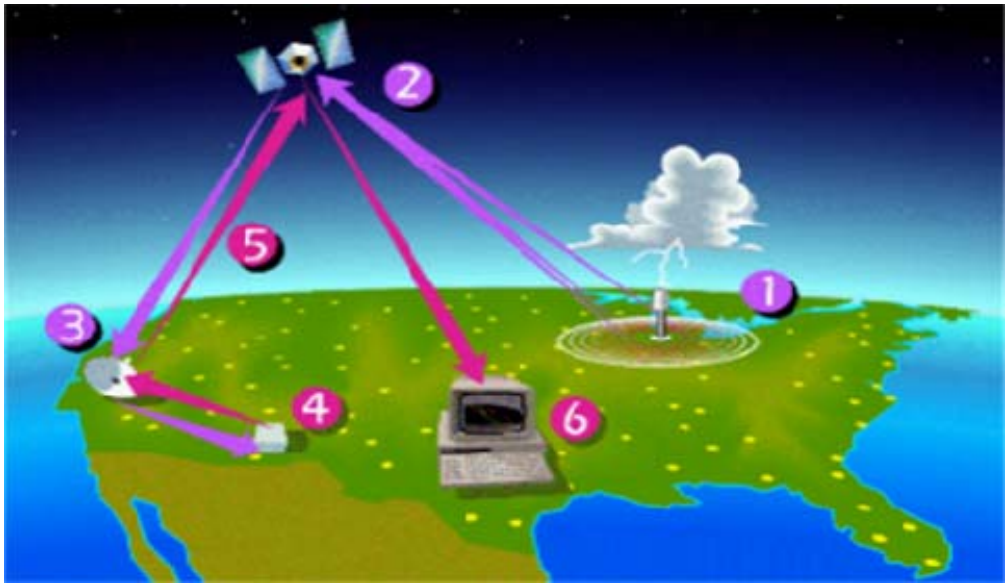

Figure 6. Schematic of the data flow in the NLDN system. The six steps shown in this figure are explained in Chapter II, Section B.1. Image from Cummins et al. (2006).

2. Four Dimensional Lightning Surveillance System (4DLSS)

Developed by Vaisala, in conjunction with NASA, the Four Dimensional Lightning Surveillance System (4DLSS) monitors lightning activity to at least 140 km from KSC/CCAFS using 15 sensors spaced approximately 15-25 km apart (Murphy 2008). The 4DLSS is comprised of two individual lightning detection systems, LDAR-II (formerly LDAR, upgraded to LDAR-II in 2007) and the Cloud-to-Ground Lightning Surveillance System (CGLSS). LDAR-II, which uses nine sensors to detect lightning-induced electromagnetic radiation, can detect in-cloud and CG lightning, but cannot locate ground strike points. This capability allows the LDAR-II system to produce a 3-D picture of lightning discharge activity. CGLSS, on the other hand, detects and locates CG ground strike points using six

of the same sensors as the NLDN system. Together, the LDAR-II and CGLSS systems provide a comprehensive representation of lightning activity at KSC/CCAFS (Murphy 2008). Murphy (2008) reported that 4DLSS has essentially 100 percent detection efficiency out to 50 km and one km location accuracy out to 75 km. LDAR/LDAR-II lightning data is available from 1993 to present and is accessible via the NASA weather archive (NASA 2009).

3. Atmospheric Reanalysis

The National Centers for Environmental Prediction / National Center for Atmospheric Research (NCEP/NCAR) Reanalysis I dataset is the product of assimilating numerous observational data sources into a global atmospheric model output to produce global retrospective analyses (i.e., reanalyses) that span from 1948 to the present. The reanalysis process uses spectral statistical interpolation analysis and a T62/28-level global spectral model for data assimilation (Kalnay et al. 1996). Observational data used in the reanalysis include observations from aircraft, land, and ocean surface platforms, rawinsondes, and satellites. All data undergoes a complex quality control check before creation of the reanalyses to minimize errors in the final output.

The NCEP/NCAR reanalysis dataset used in this study provides data at a 2.5° horizontal resolution, at standard tropospheric and stratospheric levels, and at a daily resolution (Kalnay et al. 1996). We chose to use this dataset primarily because of its ease of accessibility and its value in analyzing intraseasonal to interannual climate variations (e.g., climate variations that may be associated with anomalies in lightning violations at KSC/CCAFS). In our research, we evaluated data from 1989–2008 to be consistent with the NLDN data used to create the LLCC climatology. Further discussion of the reanalysis data used in our research is presented in the methodology portion of this chapter.

C. METHODS

1. Selection of Lightning and Electric Field Datasets

The NLDN dataset is readily processed, provides a relatively long period of record, and was recommended for our study by 45 WS. However, the NLDN dataset only represents CG lightning, which was problematic for our research since the natural lightning criterion is based on any type of lightning occurring near KSC/CCAFS. The LDAR/LDAR-II dataset provides a more comprehensive description of lightning near KSC/CCAFS, but it spans a shorter period of record and requires much more complex processing than the NLDN dataset (in part due to the large size of the dataset). We tested the feasibility of using the LDAR/LDAR-II dataset by processing data from two summers, and determined that the processing requirements and the short period of record made the LDAR/LDAR-II dataset less suitable than the NLDN dataset for our climate study.

We also checked the representativeness of the NLDN dataset by comparing the locations of the nearest CG strikes to the average launch site from both the NLDN and CGLSS datasets. In the 571 hours of lightning activity that we investigated, the closest NLDN and CGLSS strikes were collocated 53.9 percent of the time. The CGLSS dataset produced the closest strike 20.1 percent of the time while the NLDN dataset produced the closest strike 23.6 percent of the time. Each dataset produced the nearest strike about equally, and the average distances between the nearest strike and the average launch site were 2.5 and 2.9 nm, respectively. Thus, consistency between the two datasets supported our decision to use the NLDN dataset for our study.

The natural lightning criterion (see Chapter I, Section B) is quite complicated and includes several potential exceptions. The main issue we dealt with in determining whether to address these exceptions in our study was the feasibility of using the EFM dataset needed to deal with these exceptions. This dataset spans the period 1996-present for a region within 10 nm of the average launch site (NASA 2009). The EFM dataset is very large, and a significant effort

would be required to process each 30-minute data file for the multiple years needed for our climate study. The resulting electric field data files would then need to be merged with the NLDN data. This merger would be complicated by the limited spatial coverage of the EFM dataset (see also Chapter II, Sections A and C.2). We determined that working with the EFM dataset would not be appropriate for our study, mainly because: (a) the time we would spend processing the electric field data would preclude us from conducting other important parts of the study; and (b) the relatively short period of record for the EFM data available to us when we started our study (1996-2008) would limit its usefulness in our climate analyses. Thus, we limited our study to only part 1 of the natural lightning criterion (see Chapter I, Section B).

2. Determination of Relevant Distance from Average Launch Site

The next step in the research process was to determine the radial distance from the average launch site for which we would analyze lightning data. One factor we considered in making this decision was the location error associated with the NLDN, estimated to be about 600-700 meters (Cummins et al. 1998). Additionally, we wanted to focus on lightning violations within 10 nm of each of the main launch pads while still working with only the average launch site (Figure 4). The greatest distance between these pads is about 5 nm. Furthermore, we needed to select a maximum distance that would allow us to account for lightning aloft, since NLDN detects only CG strikes. McNamara (2002) and other studies have shown that CG lightning tends to travel an average horizontal distance from its origin point aloft of about 5 nm, and about 70 percent of CG lightning travels less than 5 nm (see Chapter I, Section D.1). These reasons, plus the need to conduct our analyses on a robust climate dataset that represents the mesoscale processes involved in creating lightning at KSC/CCAFS (see Chapter II, Section A), led us to choose 15 nm as the radial distance from the average launch site for which we would develop our lightning violation climatologies.

3. Development of Climate Analyses and Climatologies

We wrote programs, using the software MATLAB, to decode the 1989-2008 NLDN dataset. For the study, we converted the number and location of lightning strikes to LLCC violations. A violation is the occurrence of at least one lightning strike during the specified period of time—one calendar day or one hour of the day. We created four separate databases: (1) whether a violation occurred on each calendar day during the 20-year data record, (2) the number of violations occurring on one calendar day summed over the 20 years of data (i.e., the number of times in 20 years that lightning occurred on May 15), (3) whether a violation occurred during each hour on each calendar day during the 20-year data record, (4) the number of violations occurring during each hour of each day summed over the 20 years of data (i.e., the number of times in 20 years that lightning occurred at 0000 UTC on May 15). These four databases were also used to produce the subsets of data used in this study, such as the number of violations within a specified radius of the average launch pad location.

For this study, we define a *violation day* as the occurrence of at least one lightning strike during the calendar day. A *violation hour* is the occurrence of at least one lightning strike during one hour of the day.

a. Identification of Lightning Violation Seasons

We developed and applied an objective statistical method to use in identifying lightning violations seasons. The seasons were defined using the violation data within a 20 nm radius from the average launch site at KSC/CCAFS. We used a 20 nm radius to remove some of the temporal variability associated with mesoscale spatial variability within the KSC/CCAFS region (see Chapter II, Section A). We identified each violation day for each year with a “1” and each non-violation day with a “0,” allowing us to calculate multi-day means of the violation days as values between 0 and 1. Figure 7a displays 365 days of a

representative year in the dataset with each calendar day represented as a violation or non-violation day (i.e., 1 or 0). The five-day running mean of the data in Figure 7a is displayed in Figure 7b.

To identify the lightning seasons, we searched the violation day dataset for each year starting on 01 April to find the first date with a five-day mean of 0.8 or greater and with seven of the next ten dates also having violations (e.g., Figure 7). We identified this first date as the start of the ramp-up season for that year—that is, the spring period in which lightning increases prior to the onset of the summer period in which lightning is most frequent. This gave us 20 start dates for the ramp-up season in each of the 20 years in our study period. From this set of 20 dates, we removed the earliest and latest ramp-up start dates. We then identified the climatological start (end) date for the ramp-up season as the earliest (latest) of the remaining 18 start dates.

We used a similar method to determine the start and end dates of the ramp-down season—that is, the mid-summer period in which lightning decreases after the end of the summer period in which lightning is most frequent. However, for the start of the ramp-down season, we began searching on 01 August and searched for the first date with a five-day mean of 0.8 or less, and with seven of the next ten dates having no violations. We defined the period between the end of the ramp-up season and the beginning of the ramp-down season as the main lightning season.

We used a very similar technique to identify the beginning of the spring lightning violation season. In this case, we defined the first date of each year with a five-day mean lightning violation value of 0.4, and with four of the next ten days producing a violation, as the start of the spring lightning violation season for that year. We then deleted the earliest of the 20 start dates for the spring season, and defined the earliest of the remaining 19 start dates as the start of the spring season. We defined the end of the spring season as the date just prior to the start of the ramp-up season that we had previously defined.

Finally, we defined the winter lightning violation season as starting just after the end of the ramp-down season and ending just before the start of the spring season. The net result was the objective identification of five lightning violation seasons: winter, spring, ramp-up, main, and ramp-down.

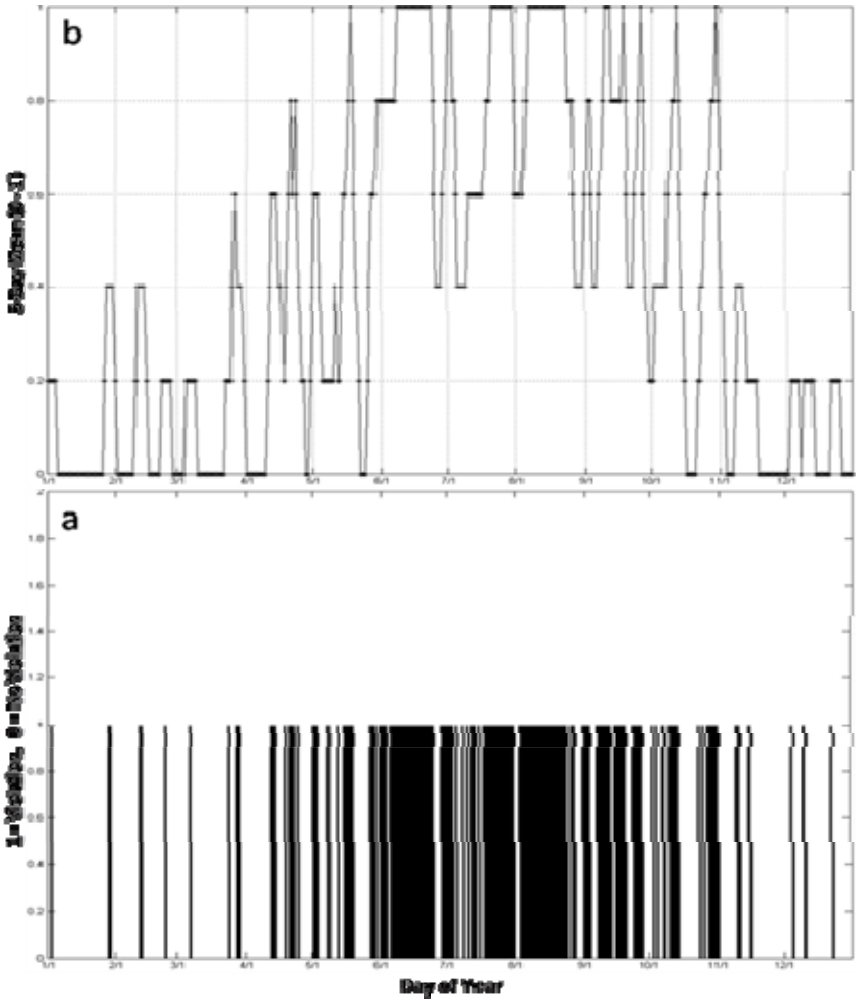

Figure 7. (a) Violation days and (b) 5-day mean of violation days for a representative year. A violation day in panel a corresponds to a value of 1.0, meaning there was at least one lightning strike during the day. Values in panel b were calculated from data in panel a. Results from both panels were used to define lightning violation seasons.

b. Sensitivity Analyses

We conducted sensitivity analyses to investigate the extent to which small changes in the 10 nm threshold distance specified in the natural lightning criterion would alter lightning violation probabilities. These analyses were done by varying the distance within which violations were calculated and then determining the change in the number and probability of violations. Such analyses are useful in identifying: (a) additional opportunities for launches that might be achieved by small reductions in the threshold distance; and (b) the reduction in launch opportunities that might be incurred by small increases in the threshold distance.

c. Analyses of Climate Variation in Lightning Violations

We analyzed lightning violations for each year and compared them to the long-term mean violations for each season. This allowed us to identify anomalous violation periods—for example, years with years with anomalous high and low numbers of seasonal violation hours. For each season, we conducted composite analyses of the three years with the highest number of violation hours and the three years with the lowest number of violation hours. In particular, we used the NCEP reanalysis dataset to analyze the regional and global atmospheric patterns and processes that are: (a) associated with anomalously high and low violation periods; and (b) favorable and unfavorable for violations during each lightning violation season at KSC/CCAFS. We conducted similar analyses of the three years in which the main lightning season started anomalously early and the three years in which this season started anomalously late. For these analyses, we composited the ten-day period both before and after the three earliest and three latest starts. For all of these analyses of climate variations in lightning violations, we calculated the composite anomalies as:

composite anomaly = conditional composite – long term mean

For these calculations: (a) the conditional composite was the composite based on a specified condition having been met (e.g., lightning violations in the top

three for the 20-year study period); and (b) the long term mean was the mean for the full study period, 1989-2008.

d. Generation of Operational Climate Products

We developed several climate products for operational use by 45 WS and others. These included figures and tables describing the probabilities of lightning violations based on 15-day means. The 15-day means were used to produce temporally smoother climatologies that reduce large day-to-day variations that are found in the unsmoothed probabilities. These large variations probably are due to the high degree of mesoscale variability in the KSC/CCAFS region (see Chapter I, Section A), and the short term, episodic nature of lightning activity, that are difficult to adequately represent in the relatively short NLDN period of record (20 years). The large day to day variations are also problematic when using the probabilities operationally, since they would indicate very different launch decisions should be made for successive days (e.g., for two successive days in August for which the probabilities vary by large amounts).

The products we produced included charts showing the probability of violation for a given time of day during each season. To accomplish this, we summed up the violations for a specific time of day during each season. Dividing by the number of days in each season and the 20 years in our study period produced the probability of lightning violations for a specific hour of the day during that season (i.e., 00 UTC during the main lightning season). We also created a product displaying the annual 15-day mean distribution of the average number of hours violated per day. Chapter III and the Appendix A show these products and other useful climatological statistics.

III. RESULTS

A. NATURAL LLCC CLIMATOLOGY

1. Daily Totals and Daily Long-Term Means

Figure 8 shows the total number of lightning strikes within 15 nm of KSC/CCAFS and the number of lightning violations at KSC/CCAFS for each day of the year when summed over the 20-year study period, 1989–2008. No temporal averaging or smoothing was used to produce these results. If at least one lightning strike occurs within 15 nm of KSC/CCAFS on one calendar day, a lightning violation is said to have occurred (see Chapter II, Sections A and C.2, for more on the 15 nm condition). Figure 8 shows that the greatest numbers of lightning strikes and violations occur in the summer months. However, a large (small) number of lightning strikes do not necessarily correspond to a proportionally large (small) number of violation days. For example, on April 7 over 2,700 lightning strikes occurred during the 20-year period, approximately four times the average for that time of year. However, the same date produced only one lightning violation over a 20-year period (i.e., all 2700 strikes occurred on April 7 of one year), below average for that time of year.

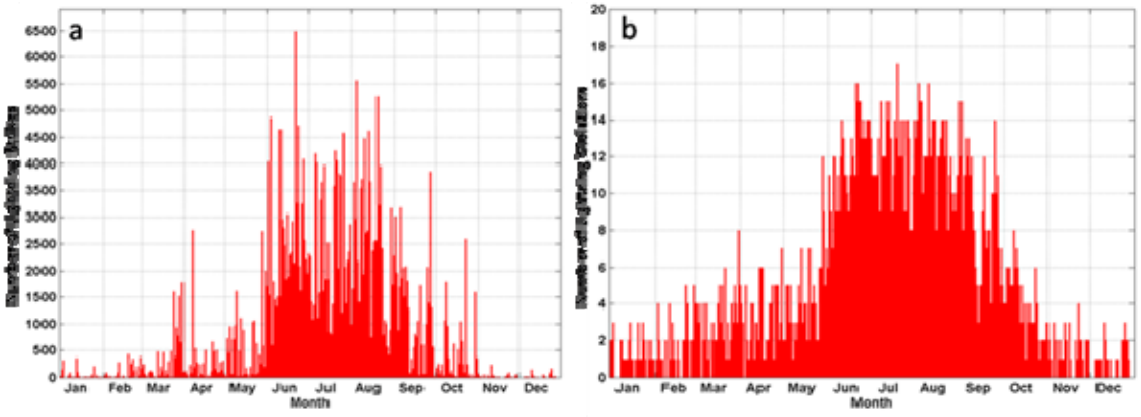

Figure 8. Total number of (a) daily lightning strikes and (b) daily natural lightning violations for KSC/CCAFS during the study period of 1989-2008.

Figure 9 shows the daily probabilities of lightning violation before and after applying a 15-day smoothing. Note that much of the day-to-day variability noticeable in the raw, unsmoothed results is absent in the 15-day mean results, providing temporally more consistent and more operationally useful climate information for mission planners (see Chapter II, Section C.3.d). Figure 9 shows that the probability of violations increases steadily beginning in early February with a rapid increase underway by late May. The highest violation probabilities (> 0.6) occur during late June through mid-August, before a decline commences in late summer. Probabilities are lowest during the winter months (i.e., Nov-Jan). Appendix A contains a table with the raw violation and 15-day mean probability data used to create Figure 9.

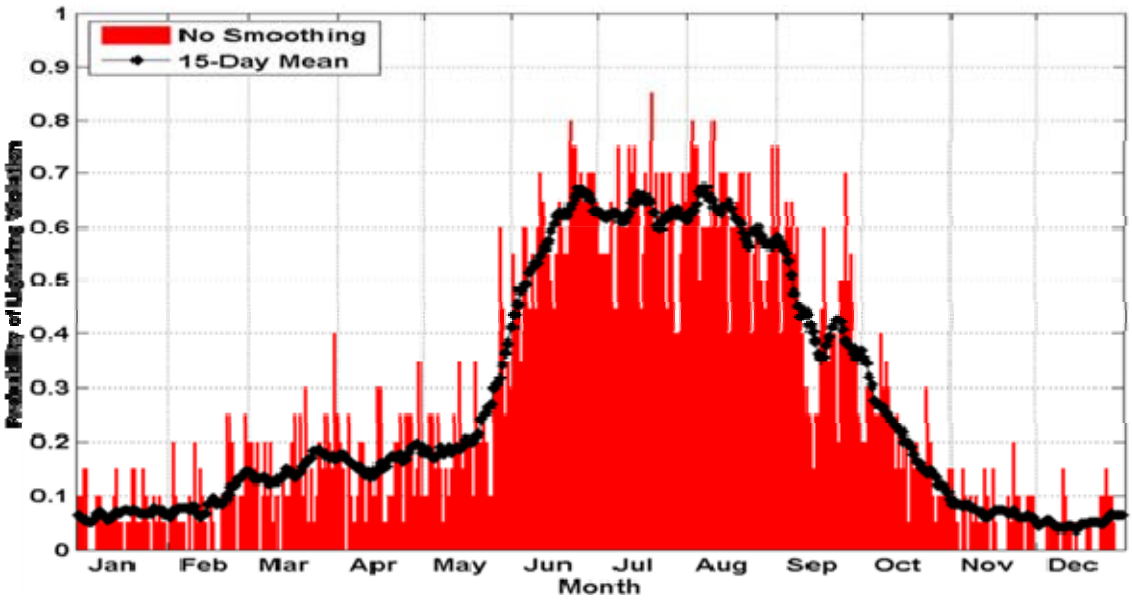

Figure 9. Daily natural lightning criterion violation probability for the study period of 1989-2008 before and after applying a 15-day smoother (red bars and black diamonds, respectively).

Figure 10 shows the average number of lightning violation hours per day for the study period. During the summer months, forecasters and mission planners at KSC can expect an average of two to three hours per day with a lightning violation. Similar to the lightning probabilities, the number of violation

hours quickly increase beginning in late May and decrease beginning in August. Throughout the colder months, lightning violations are rare, as indicated by values of less than 0.5 hours per day.

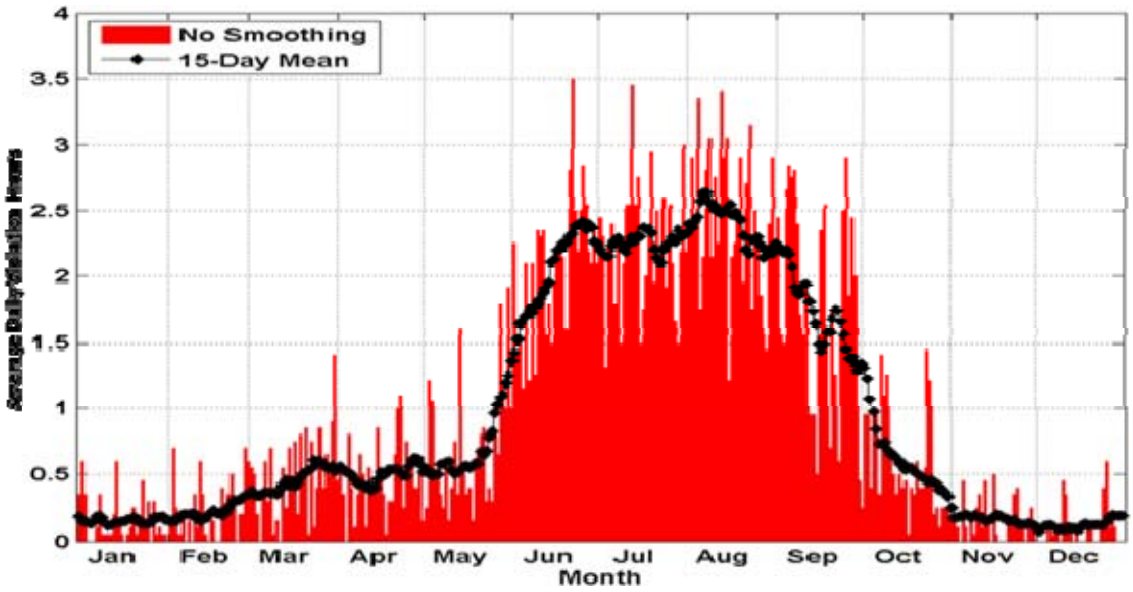

Figure 10. Average number of hours per day with a lightning violation within 15 nm of KSC/CCAFS during the study period of 1989-2008.

2. Lightning Violation Seasons

Table 2 and Figure 11 show the five lightning violation seasons we identified using the statistical methods described in Chapter 2.C.3.a. Table 2 also shows the five lightning violation seasons identified by the 45 WS for the spring, summer, and fall (AMU 2009) Our ramp-up, main lightning and ramp-down I seasons, which make up the bulk of the lightning violations, are similar to the ramp-up, lightning proper, and ramp-down I seasons developed by 45 WS. Our winter season is in addition to the 45 WS seasons, since the 45 WS did not attempt to identify seasons during the winter. The short pre-lightning season identified by the 45 WS seems to be unwarranted based on our data. The 45 WS ramp-down II season appears to be a continuation of the ramp-down season we identified, as indicated by the uniform downward trend during the ramp-down I and ramp-down II seasons shown in Figure 11. For our study, we settled on

using a set of six seasons based on merging the seasons identified by the 45 WS and us. This set of six seasons does not include the pre-lightning season but does include the ramp-down II season identified by the 45 WS, as well as the winter season identified by our study. We used the start and end dates identified by the 45 WS for the four merged seasons that are part of the 45 WS set of seasons, since these dates are very similar to those we identified. The decision to exclude the pre-lightning season but include the ramp-down II season was based in large part on the statistical results we obtained when analyzing these seasons and comparing them to the results obtained for the adjacent prior and subsequent seasons (e.g., results shown in Tables 3-4 and Figures 11-12). We developed and used the merged set of seasons to: (a) incorporate the improvements in the methods for identifying seasons that we developed for this study and applied to the entire year; and (b) provide consistency at the 45 WS in the identification of the seasons by retaining the seasons and seasonal start and end dates already in use at the 45 WS, to the extent justified by our results.

Table 2. Start and end dates (month/day) for the lightning violation seasons identified by the 45 WS (covers only May-Oct only) and by our study (NPS, covers the entire year). The merged seasons represent a consolidation of the 45 WS and NPS seasons, and are the six seasons we used in our study.

Season	45 WS	NPS	Merged
Spring	N/A	2/4 - 5/15	2/4 - 5/13
Pre-Lightning	5/1 - 5/13	N/A	N/A
Ramp-Up	5/14 - 6/22	5/16 - 6/25	5/14 - 6/22
Main Lightning	6/23 - 8/12	6/26 - 8/4	6/23 - 8/12
Ramp-Down I	8/13 - 10/12	8/5 - 10/14	8/13 - 10/12
Ramp-Down II	10/13 - 10/31	N/A	10/13 - 10/31
Winter	N/A	10/15 - 2/3	11/1 - 2/3

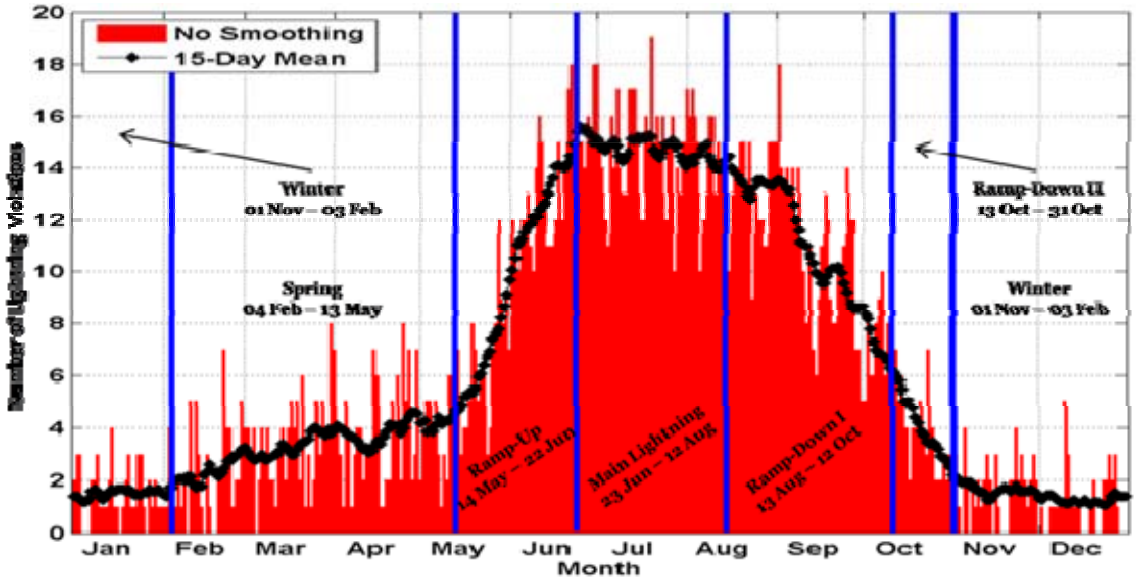

Figure 11. The six lightning violations seasons used in our study overlaid on the total number of natural lightning criterion violations for each calendar day within 15 nm of KSC/CCAFS summed over the study period of 1989-2008 (raw values in red bars and 15-day mean values in black diamonds). The blue lines mark the boundaries between the six seasons.

Violation statistics for each of our seasons are shown in Table 3. Mission planners can expect approximately 33 violation days in the main lightning season, with a daily average violation probability of 0.64. The ramp-up and ramp-down I season have the next highest daily violation probabilities, but also feature the largest standard deviations (STD). These large STD values represent considerable variability in the lightning violation totals during these transition periods, likely related to the variable start and end dates of these seasons from year to year. This variability has important implications for climate analysis and for the use of climate analysis results in planning launches. For example, the variability indicates that: (a) extra caution must be applied when using climate analysis results for these seasons; and (b).analyses of the transition seasons that help explain the variability and resolve the associated uncertainty during these seasons could be especially useful in improving

operational support during these seasons. These results were part of the motivation for the climate variation analyses described in the following sections of this chapter.

Table 3. Summary of key statistics related to the total natural lightning criterion violations for KSC/CCAFS based on data from our 1989–2008 study period for each of the six seasons used in our study. Left column: mean number of violation days by season. Middle column: standard deviation (in days) of the number of violation days by season. Right column: the daily probability of a lightning violation by season.

	Mean Violation Days	STD	Daily Violation Probability
Spring	14.1	4.22	0.14
Ramp-Up	16.9	5.65	0.42
Main Lightning	32.5	3.62	0.64
Ramp-Down I	28.3	4.31	0.46
Ramp-Down II	2.9	2.72	0.15
Winter	5.9	2.69	0.06

Table 4 presents the average seasonal violation hours for KSC/CCAFS. The main lightning season and ramp-down I season have similar average numbers of violation hours. However, the average number of hours violated per day is higher in the main lightning season, because the main lightning season is shorter than the ramp-down I season.

Table 4. Summary of key statistics related to the total natural lightning criterion violation hours for KSC/CCAFS based on data from our 1989–2008 study period for each of the six seasons used in our study. Left column: mean number of violation hours for the entire season. Right column: mean number of violation hours per day by season.

	Mean Violation Hours	Mean Violation Hours / Day
Spring	42.4	0.43
Ramp-Up	56.5	1.41
Main Lightning	118.3	2.32
Ramp-Down I	112.2	1.84
Ramp-Down II	8.4	0.44
Winter	14.1	0.15

Figure 12 shows the diurnal cycle of lightning violations for each season. As expected, the winter curve shows very little probability of a lightning violation throughout the day. In the ramp-up season, lightning violation probabilities are greater, with a peak during the afternoon and evening hours (1900-2200 UTC). This peak also occurs in the ramp-up, main lightning, and ramp-down I seasons. The probability of lightning violations during the afternoon-evening peak of the ramp-up season is nearly triple that of the spring season. The main lightning season peak is nearly double that of the ramp-up season and the ramp-down I season. The ramp-down II diurnal curve resembles the spring season curve but with a peak that is centered more in the evening. The ramp-down I season has the highest probability of nighttime lightning violations, followed by the main lightning season. Lericos et al. (2002) suggested that nocturnal convection is more likely in the late summer and fall due to both a local strengthening of the land breeze associated with relatively warm ocean temperatures and inland thunderstorm activity that is advected toward KSC/CCAFS due to increased westerly flow aloft.

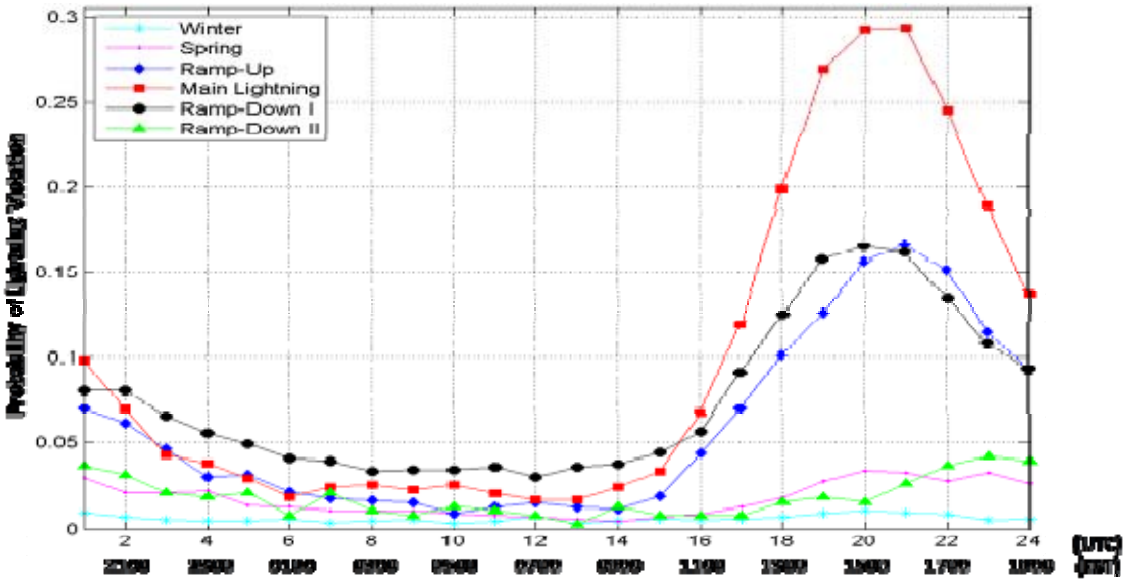

Figure 12. Diurnal cycle of lightning violation probability by season for KSC/CCAFS based on data from our 1989-2008 study period. The x-axis represents hour of the day, labeled both in UTC and Eastern Standard Time (EST; local time).

The results presented in the preceding sections should be useful to launch weather officers attempting to minimize delays and cancellations of space launches. To further improve the use of the natural lightning launch commit criterion, we conducted analyses of the sensitivity of lightning violations to small changes in the criterion distance (see Chapter I, Section B, and Chapter II, Section C.3.b). Our objectives were to assess: (a) the potential for changing the distance threshold in the criterion in a way that would yield a significant increase in launch opportunities, while not compromising the safety of launch personnel; and (b) the impact on violation probabilities and launch opportunities of increasing the threshold distance. Table 5 summarizes the results of these analyses for the three seasons with the greatest amount of lightning violations. The percent changes are calculated with respect to the probabilities for the 10 nm threshold distance (e.g., from 10 nm to 6 nm or from 10 nm to 15 nm). Negative (positive) percent changes indicate a decrease (increase) in the violation probability.

Table 5 shows that decreases (increases) in threshold distances lead to decreases (increases) in violation probabilities, as expected given the character of the natural lightning criterion. The largest percent changes, 31-33 percent, occur when the threshold distance is reduced from 10 nm to 5 nm. A reduction of the threshold distance to five nm is quite unlikely given the corresponding increase in lightning related hazards. However, even a one- or two-mile reduction in the threshold distance could yield exploitable reductions in the probability of lightning violations and increases in launch opportunities. In addition, increases in the threshold distance could cause significant increases in lightning violation probabilities and reductions in launch opportunities.

Table 5. Results from our sensitivity analysis for the three peak lightning seasons at KSC/CCAFS based on data from our 1989-2008 study period. The top half of the table shows the probability of violation for the indicated natural lightning criterion threshold distance (the distance from the average launch site for our study). The bottom half of the table shows the corresponding percent changes in the probability of violation for the indicated distance ranges. The percent changes are calculated with respect to the probabilities for the 10 nm threshold distance (e.g., from 10 nm to 9 nm or from 10 nm to 15 nm). Negative (positive) percent changes indicate a decrease (increase) in the violation probability.

	Probability of Lightning Violation for Indicated Threshold Distance								
	5 nm	6 nm	7 nm	8 nm	9 nm	10 nm	15 nm	20 nm	25 nm
Ramp-Up	0.18	0.20	0.22	0.24	0.26	0.27	0.34	0.39	0.43
Main Lightning	0.29	0.32	0.35	0.37	0.39	0.42	0.51	0.59	0.64
Ramp-Down I	0.20	0.22	0.25	0.27	0.29	0.30	0.37	0.44	0.48
	Percent Change in Violation Probability for Indicated Change in Threshold Distance								
	5-10 nm	6-10 nm	7-10 nm	8-10 nm	9-10 nm	10-15 nm	10-20 nm	10-25 nm	
Ramp-Up	-33.3	-25.9	-18.5	-11.1	-3.7	25.9	44.4	59.3	
Main Lightning	-31.0	-23.8	-16.7	-11.9	-7.1	21.4	40.5	52.4	
Ramp-Down I	-33.3	-26.7	-16.7	-10.0	-3.3	23.3	46.7	60.0	

B. CLIMATE VARIATION ANALYSES

During our work to define the lightning seasons, we observed considerable interannual variability in lightning violation days and lightning

violation hours in each of the seasons (see Appendix B, Figures 57-58). This indicated that long term mean (LTM) descriptions (i.e., traditional climatologies) of lightning violations may provide inadequate and potentially misleading representations of those violations. The seasonal mean lightning violation hours for many individual seasons will be well above or below the LTM, if there is large interannual variability for that season. An example of this is provided by the time series of the mean number of violation hours for each of the ramp-up seasons during the 1989–2008 study period (Appendix B, Figure 58c). The LTM number of lightning violation hours in the ramp-up season is approximately 55, but for most of the individual years, the number of violations hours is 45 percent above or below the LTM value. Similarly, the LTM number of lightning violation hours in the main lightning season is approximately 120, but in several years the violations hours were 20-30 percent above or below that LTM value (Appendix B, Figure 58d). For the ramp-down season, many of the individual years had lightning violation hour totals that were 30 percent above or below the LTM for that season (Appendix B, Figure 58e). Thus, climatologies based on LTM values must be used with caution, since the LTM will often provide a poor and possibly misleading representation of actual conditions. Advanced climatologies and other climate analyses that explicitly account for and exploit information about these interannual variations can be very useful in providing operational support (e.g., Vorhees 2006; LaJoie 2006; Moss 2007; van den Dool 2007; Murphree 2008b).

We investigated the interannual variations in lightning violation hours in order to understand the processes that create these variations, and their potential value in: (a) developing, understanding, and operationally applying LLCC climatologies; and (b) developing more useful forecasts of LLCC violation probabilities. Our investigation involved analyses of climate anomalies, or departures from LTM values—for example, anomalies in the 850 mb GPH field during main lightning seasons with anomalously high numbers of lightning violation hours. To analyze the mechanisms involved in creating anomalous

lightning violation hours, we created for each season conditional composites based on: (a) the three years with the highest lightning violation hour totals; and (b) the three years with the lowest lightning violation hour totals. Table 6 shows the three most above normal and three most below normal years, in terms of lightning violation hours, for each of the seasons. The remainder of this section discusses the environmental conditions associated with anomalous lighting violation hours in each of the seasons. Appendix B contains figures showing the interannual variability for each season for the entire study period (Figures 57–58), as well as additional anomaly figures for each season—in particular, specific humidity anomalies (Figures 59–66) that we used in combination with GPH anomalies and wind anomalies to infer moisture advection anomalies. In all of the following sections, the terms *above normal* and *below normal* refer to above normal and below normal lightning violations hours.

Table 6. The three years with the largest number, and the smallest number, of lightning violation hours at KSC/CCAFS for each of the six lightning seasons during the 1989-2008 study period. The three years with the largest (smallest) number are labeled the above (below) normal years. See Appendix B, Figure 58, for 1989-2008 time series of the number of lightning violation hours for each season. The atmospheric conditions of above (below) normal years were composited together and analyzed to determine the conditions and processes that create seasons with anomalously large (small) numbers of lightning violations hours.

	Above Normal Years	Below Normal Years
Spring	1991, 2003, 2005	1990, 2004, 2007
Ramp-Up	1992, 1994, 1999	1993, 1998, 2000
Main Lightning	1997, 2003, 2004	1989, 1992, 1999
Ramp-Down I	1992, 1993, 1995	1989, 2002, 2008
Ramp-Down II	1989, 2001, 2002	1992, 1996, 2000
Winter	1995, 1996, 1998	1990, 2000, 2001

1. Main Lightning Season

The main lightning season features the greatest number of lightning violations, but also high variability in violation totals from year to year (Appendix B, Figures 57d and 58d). During this time of year, the Bermuda High is the dominant low level synoptic feature influencing the region (Figure 13). Centered over the western North Atlantic (as shown in Figure 2), a ridge axis extends westward across the central Florida Peninsula and the northern Gulf Coast producing large scale mean west southwesterly (WSW-erly) flow for KSC/CCAFS.

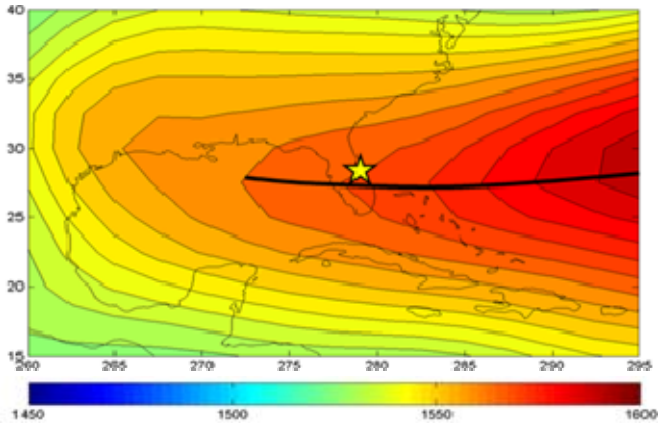

Figure 13. 850 mb LTM GPH (m) for the main lightning season during 1989-2008. The bold black line shows the axis of the ridge at 850 mb. The yellow star indicates the approximate location of KSC/CCAFS.

In the above normal cases, the actual composite mean indicates lower than normal heights over the peninsula with the ridge axis positioned farther south across southern Florida (Figure 14a). This change induces more of a SW-erly component to the low-level flow, allowing a greater transport of tropical moisture across the Florida Peninsula (Figure 15a). These factors, along with reduced subsidence created by the weaker high pressure make conditions more favorable than normal for lightning violations. In the below normal main lightning seasons, the position of the ridge axis is near normal, however, stronger than normal ridging is present (Figure 14b). This has two negative impacts on lightning violations. First, the stronger ridge increases the subsidence over the

region while a greater than normal westward extension of the ridge axis produces less favorable moisture transport across the Florida Peninsula, especially north of the ridge axis (Figure 15b).

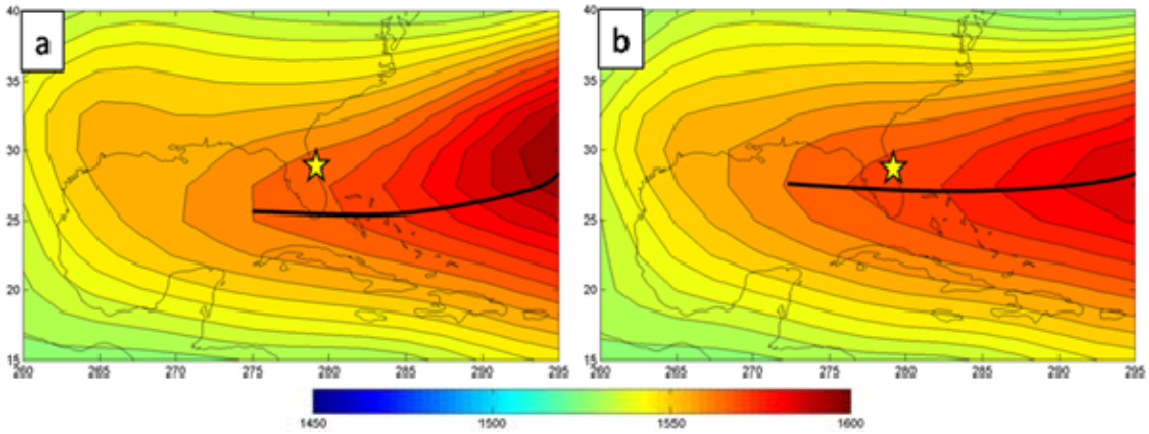

Figure 14. Composite mean 850 mb GPH (m) during the main lightning season for three years (see Table 6) in which there were: (a) above normal lightning violations and (b) below normal lightning violations. The bold black lines show the axis of the ridge at 850 mb. The yellow star indicates the approximate location of KSC/CCAFS.

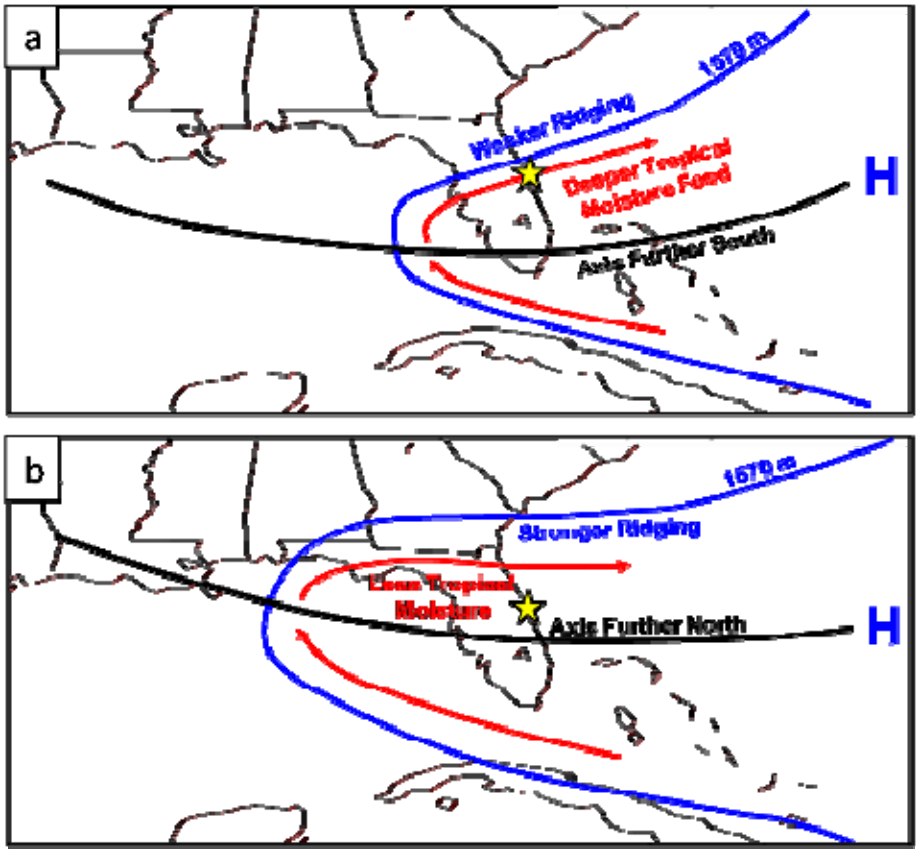

Figure 15. Schematic diagram of composite mean conditions during the main lightning season for the three years of (a) above normal lightning violations and (b) below normal lightning violations. The black line represents the position of the Bermuda High ridge axis. Red arrows represent 850 mb flow and the blue line is a representative 850 mb height contour. The yellow star indicates the approximate location of KSC/CCAFS.

The relatively subtle differences in the composite means (Figure 14) become more evident when analyzing the 850 mb GPH anomalies. Figure 16 shows a large negative height anomaly affecting much of the SE U.S. in the above normal main lightning seasons. The associated circulation on the southern side of this anomaly produces anomalous WSW-erly flow across the entire Florida Peninsula. This wind flow is favorable for lightning violations at KSC/CCAFS as the anomalous WSW-erly flow strengthens the LTM flow. This ushers more moisture into the region and increases the opposition to the east coast sea breeze front, helping to maintain it along the eastern coast of the

Florida Peninsula. Conversely, Figure 16 shows a positive height anomaly centered just west of KSC/CCAFS in the below normal main lightning seasons. The flow associated with this feature yields an anomalous NW-erly flow, aiding the introduction of drier, more stable air into the region. Additionally, subsidence linked to the positive height anomaly directly overhead further reduces the likelihood of lightning violations.

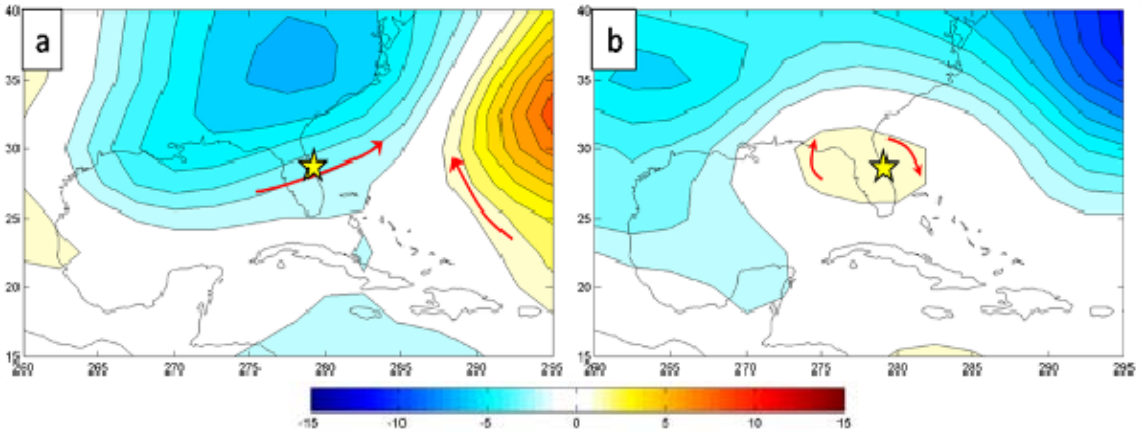

Figure 16. Composite 850 mb GPH anomalies (m) during the main lightning season for periods in which there were: (a) above normal lightning violations and (b) below normal lightning violations. Red arrows represent anomalous 850 mb flow. The yellow star indicates the approximate location of KSC/CCAFS.

Analyses of several other variables also provide insights on the mechanisms involved in creating the atmospheric patterns associated with the anomalous main lightning seasons. Zonal winds help highlight flow along the ridge axis. Figure 17 shows that in the above normal cases, there is a large positive zonal wind anomaly on the southern side of the negative height anomaly. Again, this helps maintain the east coast sea breeze over the eastern half of Florida while amplifying eastward propagation of the west coast sea breeze, increasing the likelihood of interaction of these two boundaries at or near KSC/CCAFS (Lambert et al. 2005). The zonal wind anomalies also provide a useful way of identifying the approximate position of the anomalous ridge axes. This position is approximately the boundary between the anomalous easterlies and westerlies (marked by the black lines in Figure 17). In the above normal

seasons, the anomalous ridge axis extends from the central Bahamas westward to the northern Yucatan Peninsula (Figure 17a). In the below normal seasons, the anomalous ridge axis is positioned similar to the LTM, stretching from the Bahamas across the central Florida Peninsula (Figure 17b). These anomalies help accentuate the anomalous locations of the Bermuda High shown in Figures 14–15, and help in identifying the processes that lead to above and below normal lightning violation in the main lightning season.

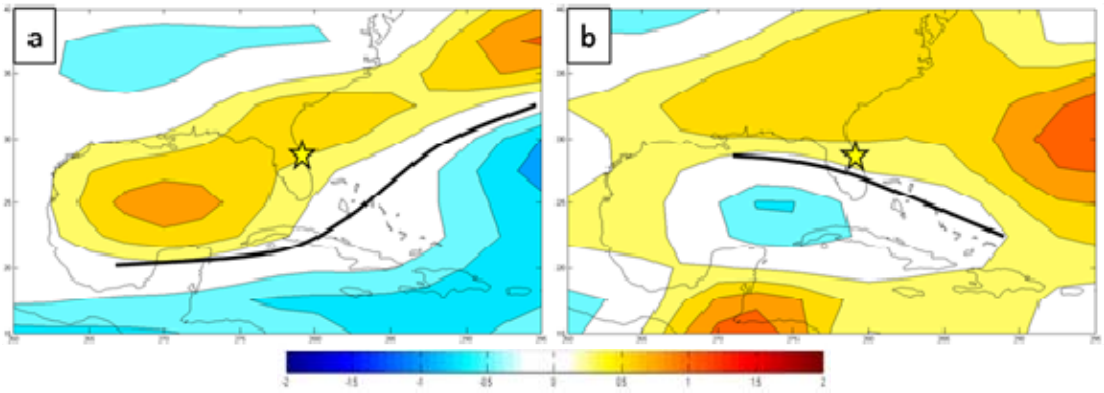

Figure 17. Composite 850 mb zonal wind anomalies (m/s) during the main lightning season for periods in which there were: (a) above normal lightning violations and (b) below normal lightning violations. The bold black lines indicate show the anomalous ridge axis at 850 mb. The yellow star indicates the approximate location of KSC/CCAFS.

Figure 18 shows 500 mb omega anomalies for both the above and below normal seasons. In the above normal composite (Figure 18a), a large area of negative anomalies from the northern Gulf of Mexico across Florida into the North Atlantic region indicates anomalously upward vertical motion. This area of anomalously upward motion tends to also be an area of negative outgoing longwave radiation (OLR) anomalies (Figure 18c). OLR is used as a proxy for deep convection, with negative (positive) OLR anomalies indicating anomalously strong (weak) convection. Near normal OLR conditions are present at KSC/CCAFS, but there is a pronounced region of negative OLR anomalies east of KSC/CCAFS that is roughly coincident with a region of pronounced upward anomalies. The patterns in the below normal composites (Figure 18b, d) are

roughly opposite to those in the above normal composites, with positive 500 mb omega and OLR anomalies for much of the Florida Peninsula and the adjacent North Atlantic.

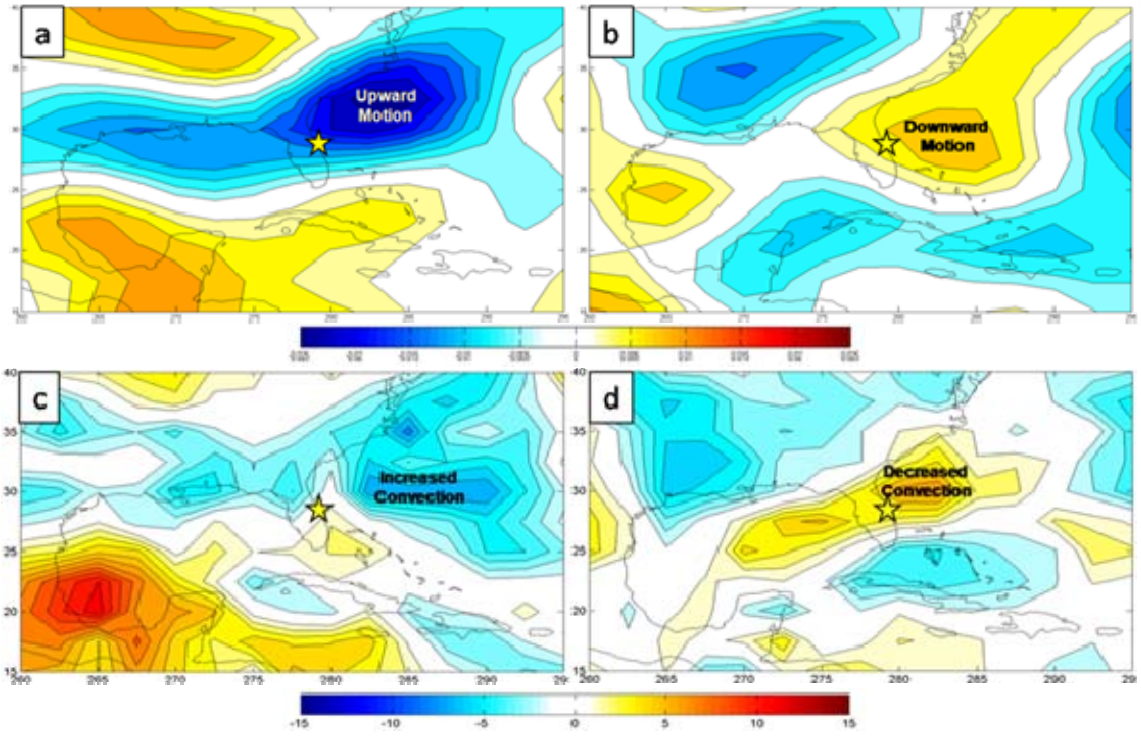

Figure 18. Composite anomalies for the main lightning season during periods in which there were above normal lightning violations (panels a, c) and below normal lightning violations (panels b, d). The top two panels show composite anomalies of 500 mb omega (Pa/s) (a: above normal; b: below normal). The bottom two panels show composite anomalies of OLR (W/m^2) (c: above normal; d: below normal). The yellow star indicates the approximate location of KSC/CCAFS.

In the above normal main lightning seasons, the focus of the negative OLR and 500 mb omega anomalies is NE of KSC/CCAFS over the North Atlantic (Figure 18a, c). Further investigation of these anomalies indicate that they are associated with anomalous low-level convergence in the same region (note speed and directional convergence indicated by Figures 16a, 17a), consistent with the OLR and omega anomalies in indicating above normal convection in the region NE of KSC/CCAFS. In the below normal composites, this same region has positive OLR and omega anomalies, and anomalous low level speed

divergence, consistent with anomalously weak convection to the NE of KSC/CCAFS. Figure 19 summarizes these anomalous environmental factors for the above and below normal main lightning seasons.

These results suggest the following hypothesis: above (below) normal lightning violations at KSC/CCAFS is part of a larger synoptic feature that is centered to the NE of KSC/CCAFS. This is plausible, given that environmental conditions such as anomalously deep tropical moisture transport, anomalous WSW-erly flow, and anomalous troughing (reduced subsidence) would favor convection in this region and potentially increase lightning violations at KSC/CCAFS—and similarly for the periods of decreased violations. Such a connection between conditions in the relatively small KSC/CCAFS region and the larger region to the NE could be useful in developing skillful long-range forecasts of violation probabilities at KSC/CCAFS. This is in part because the large-scale conditions that affect lightning violations at KSC/CCAFS are likely to be much easier to analyze and forecast than the smaller scale conditions in the KSC/CCAFS region.

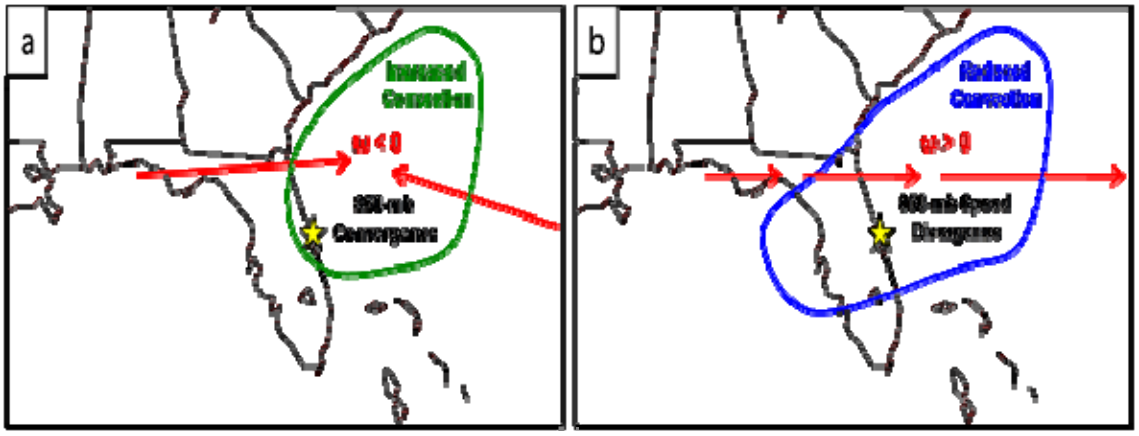

Figure 19. Schematic diagram of regional conditions associated with above normal (panel a) and below normal (panel b) lightning violations during the main lightning season at KSC/CCAFS.

To assess the global scale processes associated with lightning violations during the main lightning season, we analyzed the 200 mb GPH anomalies for the above and below normal violations composites (Figure 20). Height

anomalies at this level tend to provide useful information about teleconnections between remote regions of the climate system (e.g., Hildebrand 2001; Murphree 2008). In the above normal composite, a large anomalous upper level trough encompasses much of the U.S. east coast, consistent with the 850 mb negative height anomaly shown in Figure 16 and indicating equivalent barotropic structure and a dynamical linkage between the upper and lower level anomalies. Over the central tropical Pacific Ocean, positive height anomalies with twin anticyclones straddling the equator are evident, a pattern indicative of the above normal convection commonly linked to El Niño (EN) years. Rossby wave trains emanating from this region and from the east Asian region appear to contribute to the negative 200 and 850 mb GPH anomalies over the eastern U.S. that are associated with positive convection anomalies to the NE of Florida and above normal lightning violations at KSC/CCAFS (cf. Figures 16-20).

In the below normal composite, a weak positive 200 mb GPH anomaly occurs over the SE U.S., consistent with the corresponding weak positive GPH anomaly at 850 mb (Figure 16). Negative 200 mb GPH anomalies are located over the central tropical Pacific, a pattern typical of La Niña (LN) years. Rossby wave trains from this region and from east Asia appear to contribute to the positive 200 and 850 mb height anomalies over the SE U.S. that are associated with negative convection anomalies to the NE of Florida and below normal lightning violations at KSC/CCAFS (cf. Figures 16-20).

The oceanic Niño index (ONI), a measure of El Niño and La Niña (ENLN), also provides support for indications of teleconnections between the tropical Pacific and convection and lightning violations in the KSC/CCAFS region. Each of the above normal main lightning seasons is associated with positive ONI values, while the each of the below normal seasons is associated with either neutral or negative ONI values (CPC 2010).

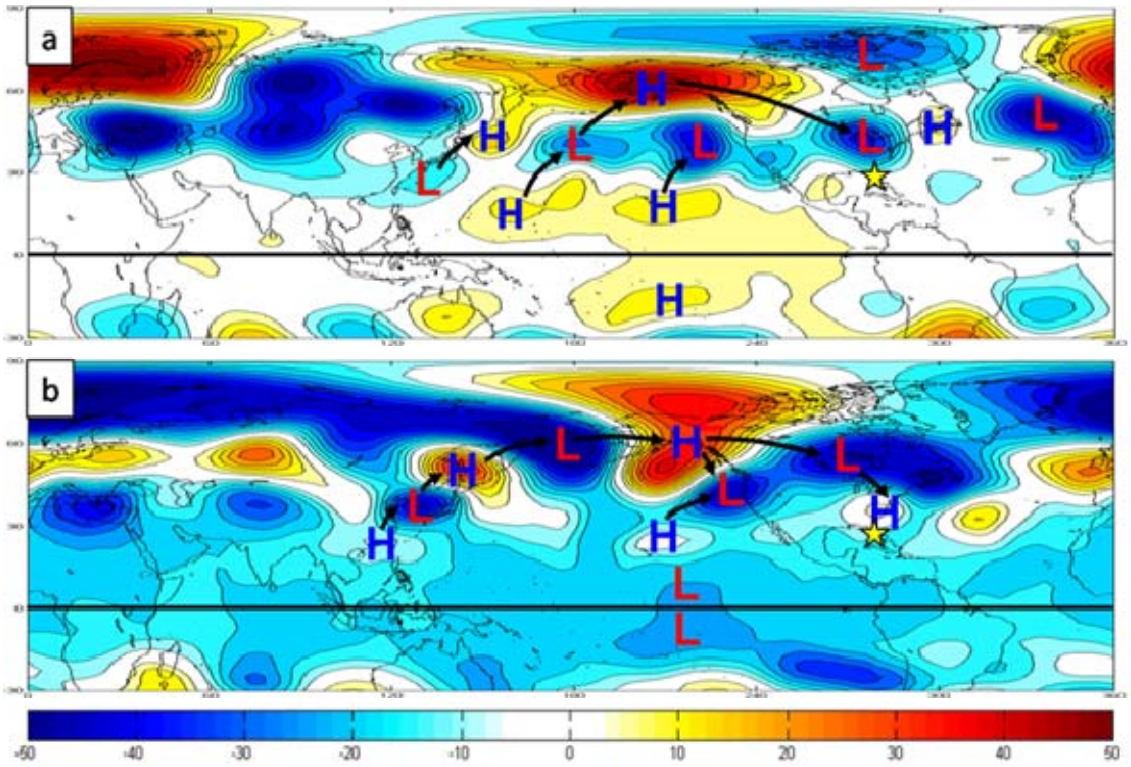

Figure 20. Composite 200 mb GPH anomalies (m) for the main lightning season during periods in which there were: (a) above normal lightning violations; and (b) below normal lightning violations. Anomalous Rossby wave trains that extend over the southeastern U.S. are marked with H and L, and black arrows. The H and L identify the center of the positive (negative) height anomalies that help define the wave trains. The black arrows link the centers that are part of individual wave trains and indicate the direction of anomalous energy propagation in the wave trains. The yellow star indicates the location of the Florida Peninsula.

2. Ramp-Up Season

The ramp-up season, defined by a rapid upward trend in the number of lightning violations, also displays more variability than any other season (Table 4; Appendix B, Figures 57-58). As was the case in the main lightning season, the Bermuda High is the dominant low-level synoptic feature (Figure 21). A ridge axis extends westward from the high across Florida and into the Gulf of Mexico, producing large-scale LTM westerly flow for KSC/CCAFS (Figure 21a). In the above normal cases, the actual composite mean again indicates a weaker ridge,

with the ridge axis farther to the south and more zonal than in the LTM (Figure 21b). This ridging favors more westerly to WSW-erly low level flow than normal, allowing more deep tropical moisture to be transported across the Florida Peninsula than normal (Figure 21b). Along with additional moisture, the weaker ridge leads to reduced subsidence, and makes conditions more favorable for convection and lightning violations, in the KSC/CCAFS region. In the below normal violation seasons, the ridge is significantly stronger than normal, with the axis oriented NW to SE across the Florida Peninsula (Figure 21c). Not only is there more subsidence over Florida, but the flow on the northern side of the ridge axis is from the west northwesterly (WNW-erly) and less favorable for deep moisture transport into the KSC/CCAFS region. The schematic of environmental conditions shown in Figure 15 for the main lightning season is also representative of the ramp-up season.

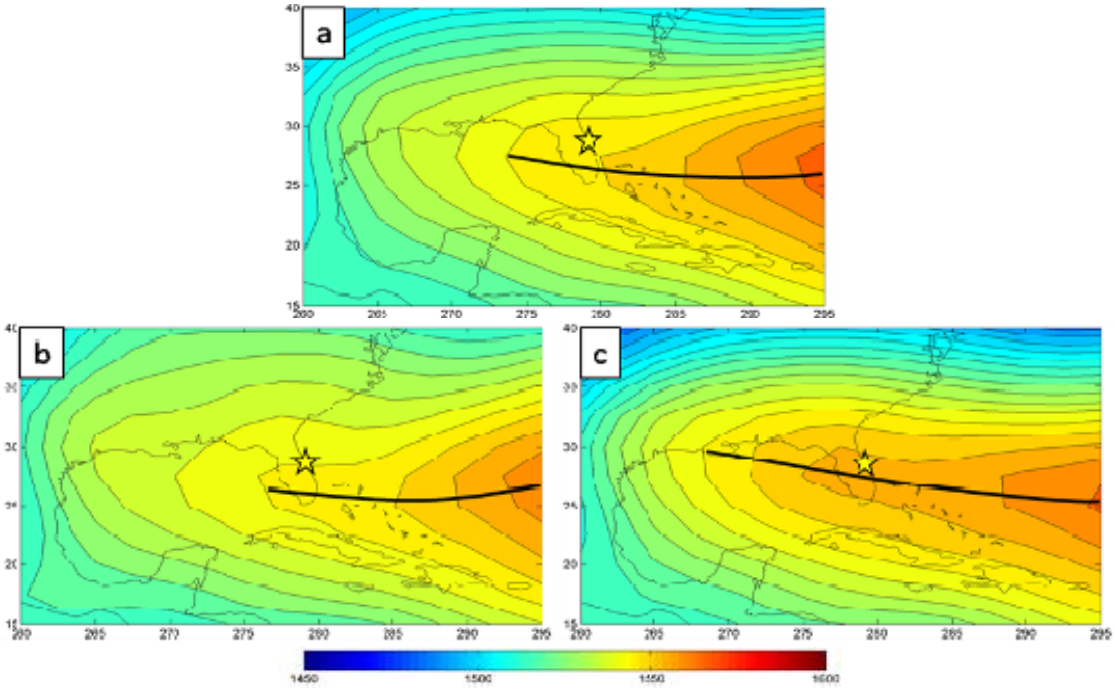

Figure 21. 850 mb GPH (m) for the lightning ramp-up season: (a) LTM; (b) composite mean for the three above normal lightning violation years (Table 6); and (c) composite mean for the three below normal lightning violation years. The bold black lines show the axis of the ridge at 850 mb. The yellow star indicates the approximate location of KSC/CCAFS.

Figure 22a shows a large negative 850 mb GPH anomaly positioned north of the Bahamas. The associated circulation on the western side of this anomaly produces anomalous NE-erly flow across most of the Florida Peninsula. Lambert et al. (2005) identified NE-erly flow as unfavorable for convection and lightning in the KSC/CCAFS region. However, the associated anomalous trough axis positioned across central Florida would favor increased convection in the KSC/CCAFS region. Sea breeze convection may be less frequent at KSC/CCAFS during the three above normal ramp-up seasons due to a farther inland propagation of the east coast sea breeze. However, the presence of the trough may compensate for the lack of sea breeze convection. Conversely, Figure 22b shows a large positive height anomaly centered west of KSC/CCAFS in the three below normal seasons. The associated anomalous flow is NE-erly, which would tend to decrease the potential for sea breeze convection over KSC/CCAFS. In addition, this anomalous flow would lead to anomalous advection of dry stable air into the region. The anomalous subsidence associated with the positive height anomaly would also tend to inhibit convection, making lightning violations infrequent.

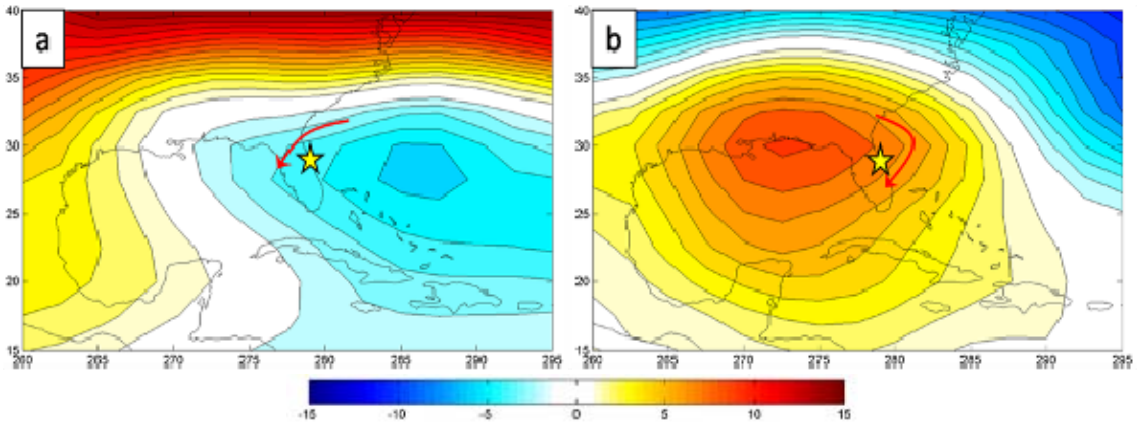

Figure 22. Composite 850 mb GPH anomalies (m) for the ramp-up season during periods in which there were: (a) above normal lightning violations and (b) below normal lightning violations. Red arrows represent anomalous 850 mb flow. The yellow star indicates the approximate location of KSC/CCAFS.

Figure 23 supports the implications of Figures 21-22. In particular, in the above (below) normal composite anomalies, the anomalous ridge axis is south (north) of KSC/CCAFS, leading to anomalously weak (strong) subsidence and strong (weak) convection over KSC/CCAFS. Recall from the discussion of Figure 17 that the anomalous ridge axes is at approximately the boundary between the anomalous easterlies and westerlies (marked by the black lines in Figure 23). The anomalies associated with the below normal number of lightning violations are especially striking. For both the above and below normal composite anomalies, Figure 23 provides clear evidence that interannual variations in the number of lightning violations at KSC/CCAFS are part of larger scale variations that extend over much of the SE U.S., Gulf of Mexico, Caribbean, and western subtropical North Atlantic. In particular, the convection anomalies that affect the KSC/CCAFS region tend to be part of larger convection anomalies that are centered to the east of KSC/CCAFS. This is similar to the findings for the main lightning season.

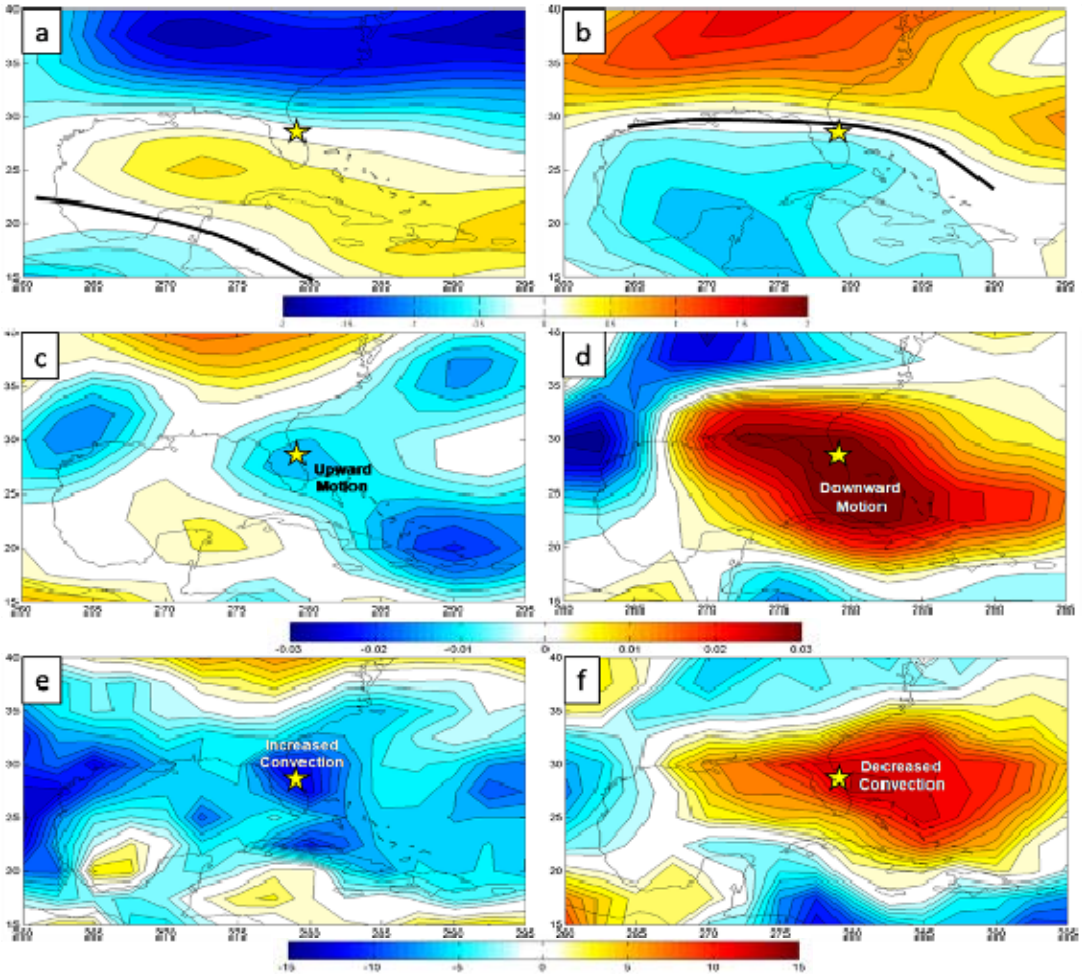

Figure 23. Composite anomalies for the ramp-up season during periods in which there were above normal lightning violations (panels a, c, e) below normal lightning violations (panels b, d, f). The top two panels show composite anomalies of 850 mb zonal wind (m/s) (a: above normal; b: below normal). The middle two panels show composite anomalies of 500 mb omega (Pa/s) (c: above normal; d: below normal). The bottom two panels show composite anomalies of OLR (W/m^2) (e: above normal; f: below normal). The bold black lines in panels a and b show the axis of the anomalous ridge at 850 mb. The yellow star indicates the approximate location of KSC/CCAFS.

Figure 24 shows the above and below normal composite 200 mb GPH anomalies for the ramp-up season. A comparison of 200 mb GPH anomalies in the SE U.S. region with the corresponding 850 mb GPH anomalies (cf. Figures 22, 24) indicates that: (a) the anomalies have equivalent barotropic structure (e.g., negative GPH anomalies to the east of Florida at both levels in the above

normal composites, and positive GPH anomalies over the SE U.S. at both levels in the below normal composites); and (b) the upper and lower level anomalies are dynamically linked to each other (e.g., the anomalies at each level are driven by the same dynamical processes). Figure 24 also shows evidence of anomalous Rossby wave trains and teleconnections from the western tropical North Pacific and east Asian regions to the SE U.S. region. Unlike in the main lightning season, there is relatively little evidence for teleconnections between ENLN related anomalies in the tropical Pacific and anomalies in the SE U.S. This may be due in part to the tendency for EN and LN events to be weak during the northern hemisphere spring when the ramp-up season occurs.

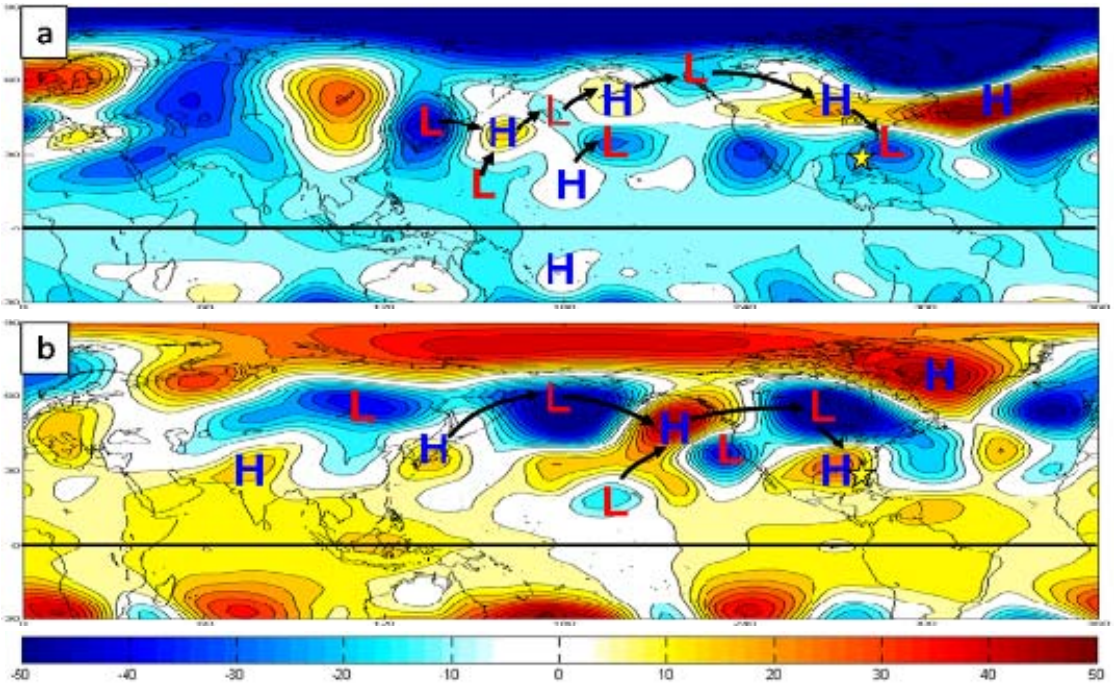

Figure 24. Composite 200 mb GPH anomalies (m) for the ramp-up season during periods in which there were: (a) above normal lightning violations; and (b) below normal lightning violations. Anomalous Rossby wave trains that extend over the SE U.S. are marked with H and L, and black arrows. The H and L identify the center of the positive (negative) height anomalies that help define the wave trains. The black arrows link the centers that are part of individual wave trains and indicate the direction of anomalous energy propagation in the wave trains. The yellow star indicates the location of the Florida Peninsula.

3. Ramp-Down I Season

The ramp-down I season, defined by a rapid downward trend in the number of lightning violations, also exhibits the second highest variability among all the seasons (Table 4; Appendix B, Figures 57–58). This season is slightly different from the other two peak periods of violations discussed thus far. The Bermuda High is the main low-level synoptic feature in the LTM for all three seasons (cf. Figures 13, 21a, 25a). But in the ramp-down I season, the ridge axis is centered much farther to the north and extends westward into South Carolina and the Gulf Coast states (Figure 25a). This results in a large-scale LTM flow for KSC/CCAFS that is SE-erly versus the WSW-erly flow that occurs in the previous two seasons. In the above (below) normal composite for the ramp-down I season, there are higher (lower) heights than normal across the Florida Peninsula (Figures 25b-c and 26a-b). The ridge axis in the above (below) normal seasons still remains south (north) of its LTM position as was the case in the main lightning and ramp-up seasons. In both the above and below normal ramp-down I seasons, mean SE-erly flow occurs across most of the peninsula. This flow regime, most common during the fall transition season, is less conducive for sea breeze convection, since the east coast sea breeze will be pushed inland by the mean flow (Lericos et al. 2002). Therefore, other mechanisms must account for the anomalous number of violations. One possible scenario, given the northern position of the ridge in both the above and below seasons, involves the mean SE-erly flow on the southern flank of the ridge that guides tropical waves, tropical cyclones, and other travelling convective systems toward the SE U.S. The stronger ridge in the above normal seasons would be more effective in guiding these systems toward Florida than the weaker ridge in the below normal seasons, which would tend to allow more recurvature to the north (Figure 25).

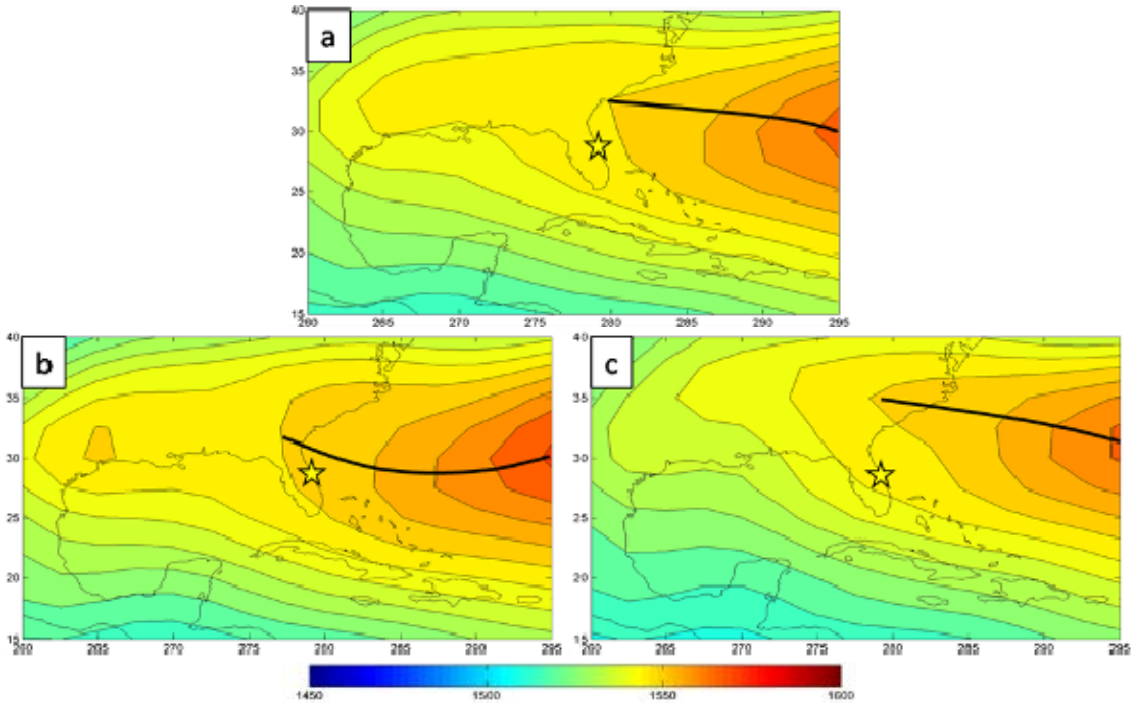

Figure 25. 850 mb GPH (m) for the lightning ramp-down I season: (a) LTM; (b) composite mean for the three above normal lightning violation years (Table 6); and (c) composite mean for the three below normal lightning violation years. The bold black lines show the axis of the ridge at 850 mb. The yellow star indicates the approximate location of KSC/CCAFS.

Figure 26 shows the corresponding 850 mb GPH anomalies, which produce weak anomalous SW-erly (SE-erly) flow for most of the Florida Peninsula in the above (below) normal periods that: (a) opposes (reinforces) the mean SE flow; and (b) potentially causes the east coast sea breeze convection to be more (less) frequent and/or intense (Figure 26). Another possible cause of the increased number of lightning violations is the influence of mid-latitude weather systems. Figure 26a indicates an anomalous weakness in the ridging extending from the Tennessee Valley southeastward (SE-ward) to Florida. This would increase the potential for cold fronts or mesoscale convective systems to propagate SE-ward into Florida along the northern boundary of the anomalous ridge. In the below normal periods, anomalous easterly flow on the north side of the negative height anomaly would only further strengthen the mean SE-erly

flow, reducing the likelihood of sea breeze convection along the east coast of Florida. With a significant negative anomaly positioned over the western Gulf of Mexico, the focus for increased convection would remain well east of the Florida peninsula along the central Gulf Coast in the below normal periods (Figure 26b).

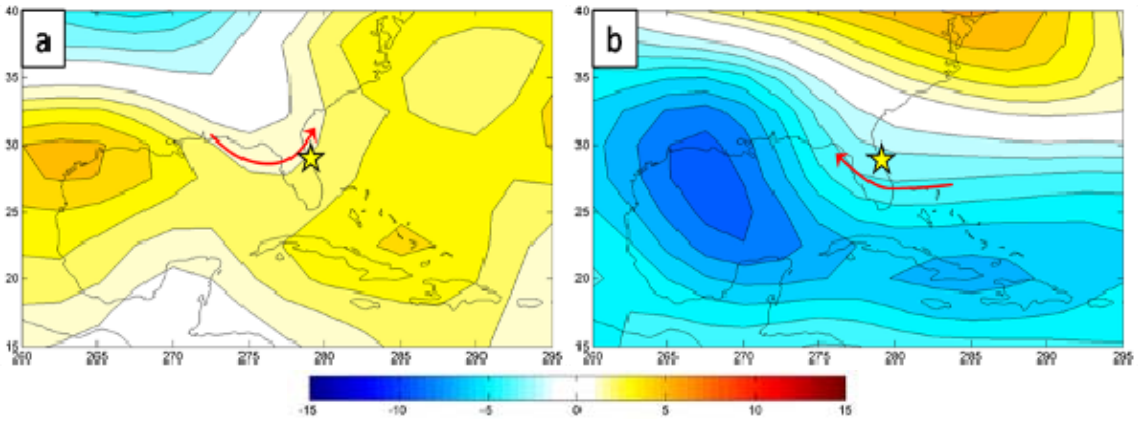

Figure 26. Composite 850 mb GPH anomalies (m) for the ramp-down I season during years in which there were: (a) above normal lightning violations; and (b) below normal lightning violations. Red arrows represent anomalous 850 mb flow. The yellow star indicates the approximate location of KSC/CCAFS.

Figure 27 shows the zonal wind, vertical motion, and OLR anomalies associated with anomalous violations in the ramp-down I season. Figure 27a indicates that in the three above normal seasons, the location of the anomalous ridge axis (in the 850 mb zonal wind field) south of the Florida Peninsula increases the likelihood of westerly flow across the peninsula. This tends to decrease the mean SE-erly flow and increase the likelihood of sea breeze related lightning violations along the east coast of the peninsula. The corresponding upward vertical motion and decreased OLR anomalies (Figure 27c, e) indicate that increased violations at KSC/CCAFS during the ramp-down I season are associated with increased convection over and to the west of Florida. The opposite is true in the below normal ramp-down I seasons, with anomalous easterly flow across the majority of the interest region strengthening the already unfavorable SE-erly flow and decreasing the likelihood of sea breeze convection along the east coast of the peninsula (Figure 27b, d, f). Positive 500 mb omega

and OLR anomalies indicate that reduced convection across much of the peninsula and to the east-northeast of Florida is likely during below normal ramp-down I seasons. So, as with the main lightning and ramp-up seasons, anomalous lightning violations during the ramp-down I season appear to be part of anomalous convective activity over a much larger region than just the KSC/CCAFS or east coast of the peninsula regions.

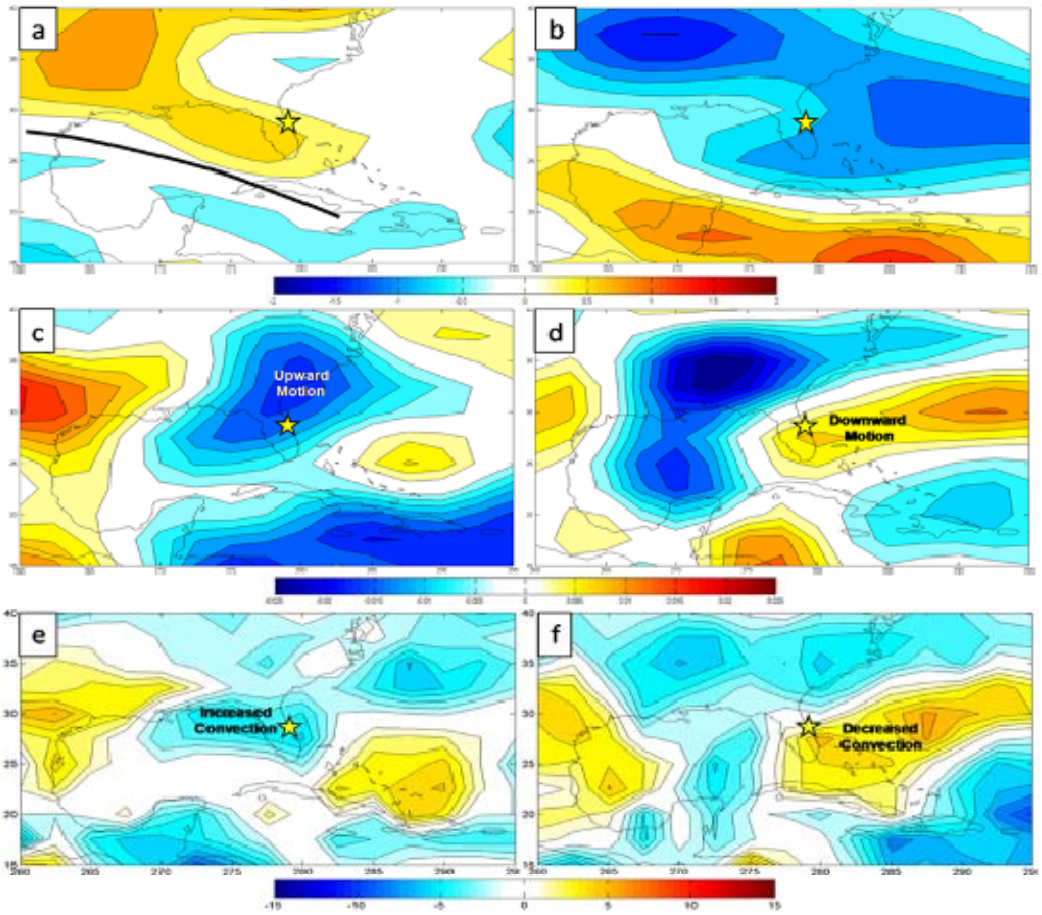

Figure 27. Composite anomalies for the ramp-down I season during three years in which there were above normal lightning violations (panels a, c, e) and the three years with below normal lightning violations (panels b, d, f). The top two panels show composite anomalies of 850 mb zonal wind (m/s) (a: above normal; b: below normal). The middle two panels show composite anomalies of 500 mb omega (Pa/s) (c: above normal; d: below normal). The bottom two panels show composite anomalies of OLR (W/m^2) (e: above normal; f: below normal). The bold black line in panel a shows the axis of the anomalous ridge in the 850 mb zonal wind field. The yellow star indicates the approximate location of KSC/CCAFS.

The corresponding upper level anomalies provide evidence of anomalous Rossby wave trains and teleconnections linking the SE U.S. to climate variations in the tropical Pacific and Indian Ocean regions. The origins of the wave trains may be: (a) ENLN conditions, as suggested by the paired anticyclones (cyclones) in the central tropical Pacific in Figure 28a (28b); and/or (b) Indian Ocean Zonal Mode (IOZM) conditions in the tropical Indian Ocean region, as suggested by the paired anticyclones (cyclones) in the south Asia – south Indian Ocean region (Figure 28a and 28b respectively).

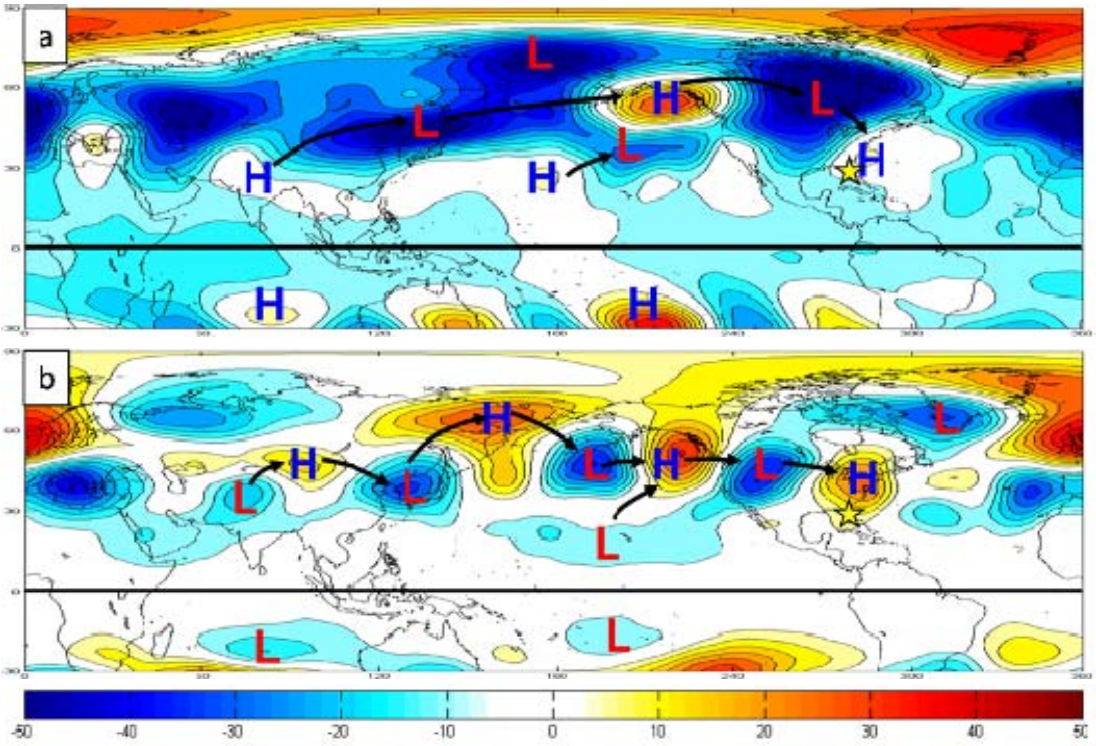

Figure 28. Composite 200 mb GPH anomalies (m) for the ramp-down I season during periods in which there were: (a) above normal lightning violations; and (b) below normal lightning violations. Anomalous Rossby wave trains that extend over the SE U.S. are marked with H and L, and black arrows. The H and L marks identify the centers of the positive (negative) height anomalies that help define the wave trains. The black arrows link the centers that are part of individual wave trains and indicate the direction of anomalous energy propagation in the wave trains. The yellow stars indicate the location of the Florida Peninsula.

4. Ramp-Down II Season

The 19-day ramp-down II transition period is shorter in duration and different from the other seasons in many other respects (see Tables 2–4 and Figures 11-12). In the transition from the ramp-down I season to the ramp-down II season, the Bermuda High weakens and its center shifts eastward, leaving the SE U.S. more susceptible to mid-latitude weather systems (compare Figures 25a and 29a). As shown in Figure 29b, the 850 mb GPH composite mean for the three years (see Table 6) with above normal ramp-down II seasons indicates a stronger than normal influence from the Bermuda High with the ridge axis extending westward, over or just south of KSC/CCAFS. With the axis very near KSC/CCAFS, calm or weak westerly winds are likely. This stronger ridge would inhibit mid-latitude influences, allowing the sea breeze to continue later into the fall than normal, thus increasing the likelihood of lightning violations over KSC/CCAFS. In the three below normal cases (Figure 29c), the ridge axis is well north of its LTM position for the ramp-down II season, and a large, closed high pressure system is positioned over the entire Gulf Coast. There is also a low level trough east of the U.S. over the western North Atlantic. This atmospheric setup is more favorable than the LTM for the advection of cold, dry air from the northwest into the SE U.S., and the passage of extratropical systems through the SE U.S. (cf. Hodanish et al. 1997).

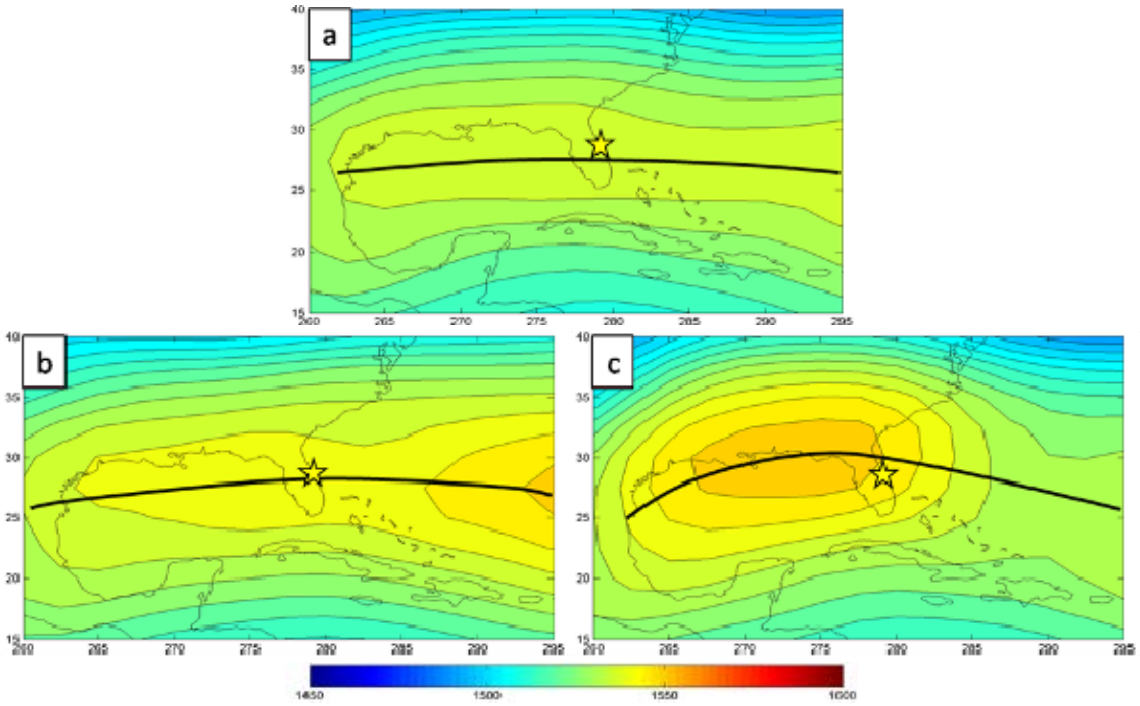

Figure 29. 850 mb GPH (m) for the lightning ramp-down II season: (a) LTM; (b) composite mean for the three above normal lightning violation years (Table 6); and (c) composite mean for the three below normal lightning violation periods (Table 6). The bold black lines show the axis of the ridge at 850 mb. The yellow star indicates the approximate location of KSC/CCAFS.

Figure 30a shows positive 850 mb GPH anomalies encompassing the entire region in the three above normal ramp-down II seasons. The circulation around the positive anomaly center near the Yucatan Channel produces a weak NW flow, acting to strengthen the already weak westerly LTM flow. This will tend to promote increased sea breeze related convection along the east coast of Florida (cf. Lericos et al. 2002). In the below normal composite (Figure 30b), a large positive height anomaly is centered just north of Florida, producing a strong NE flow anomaly and the transport of cool, dry across the entire Florida peninsula. This cool, dry, NE-erly flow would tend to produce anomalously weak convection in the KSC/CCAFS area.

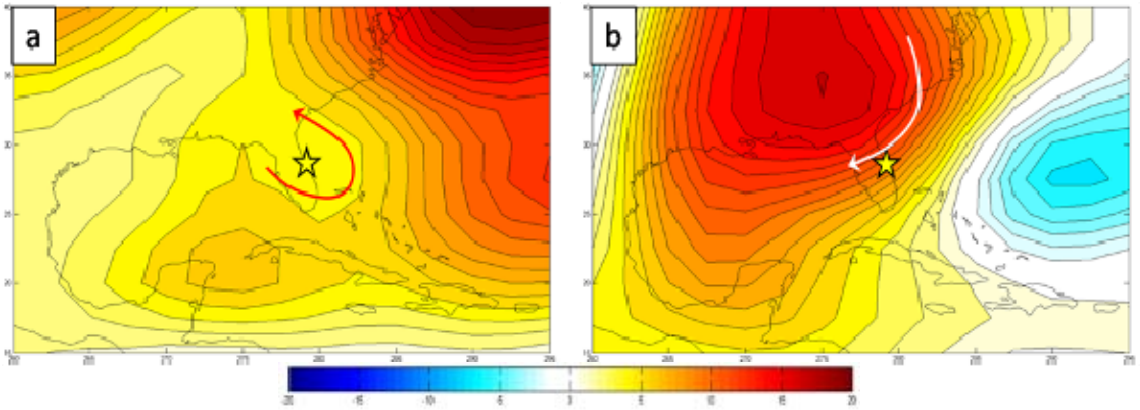

Figure 30. Composite 850 mb GPH anomalies (m) for the ramp-down II season during the three years in which there were: (a) above normal lightning violations; and (b) below normal lightning violations (see Table 6). Arrows represent anomalous 850 mb flow. The yellow star indicates the approximate location of KSC/CCAFS.

Figure 31a shows that the anomalous ridge axis in the 850 mb zonal wind field for the composite of the three above normal seasons is located south of the Florida Peninsula, similar to its position in the main lightning season. The position of this anomalous axis is associated with weak westerly zonal wind anomaly across the Gulf of Mexico and the southern half of the Florida Peninsula, opposing the east coast sea breeze and tending to keep it positioned along the eastern side of Florida. In the three below normal seasons, the anomalous ridge axis is far to the north across the Carolinas in response to the significant 850 mb height anomaly centered nearby (Figure 30b). Across the central Florida peninsula, a strong easterly wind anomaly tends to strengthen the easterly flow already occurring, reducing the likelihood of sea breeze convection. Abundant anomalous upward vertical motion over the eastern half of Florida and adjacent North Atlantic, along with anomalously low OLR values, support the increased convection over and to the ENE of KSC/CCAFS during above normal seasons (Figure 31c, e). Conversely, significant anomalous downward vertical motion and increased OLR values indicate the anomalous suppression convection and lightning favorable conditions that would be expected in the presence of strong NE-erly flow anomalies (see also the discussion of Figure 30).

As with the lightning season anomalies discussed earlier in this chapter, the ramp-down II anomalies indicate that interannual variations of lightning in the KSC/CCAFS region are closely linked to larger scale variations in low level flow and convection over the SE U.S. Gulf of Mexico, Caribbean, and western subtropical North Atlantic—especially to variations in convection centered over the North Atlantic to the east and NE of KSC/CCAFS.

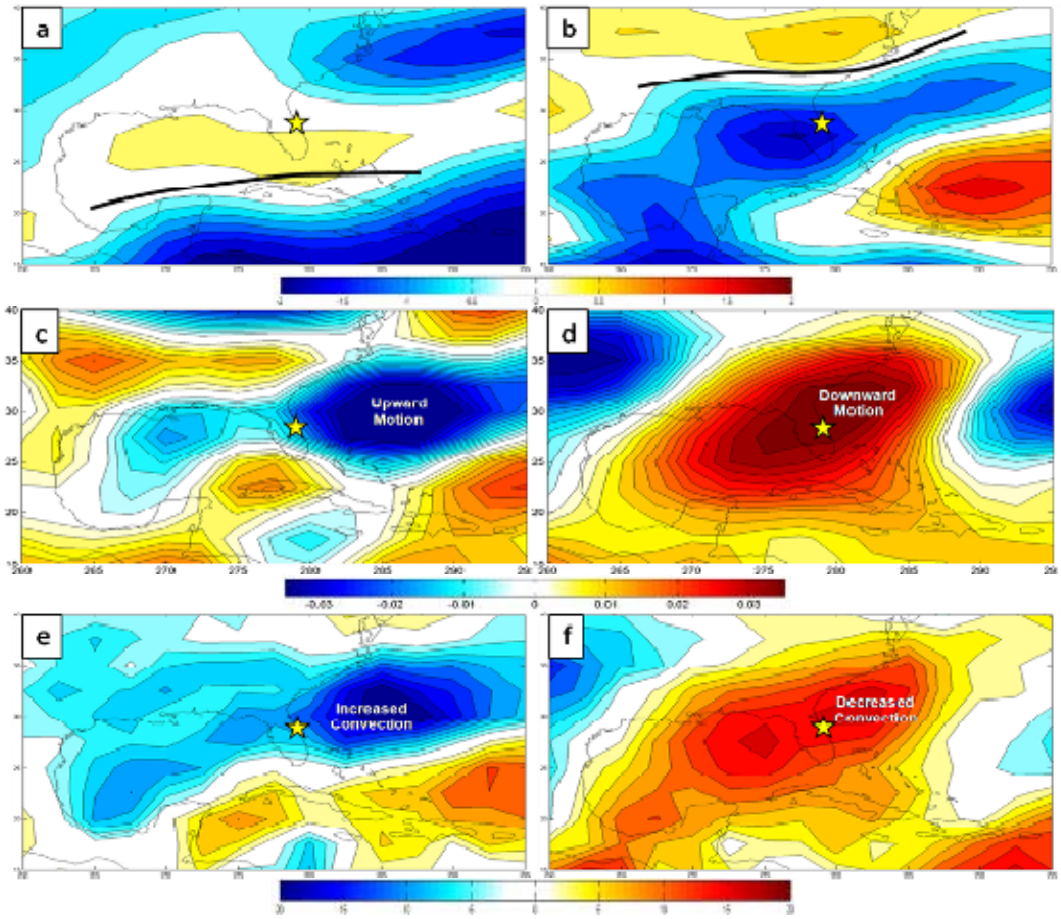

Figure 31. Composite anomalies for the ramp-down II season during three seasons in which there were above normal lightning violations (panels a, c, e) and the three seasons with below normal lightning violations (panels b, d, f). The top two panels show composite anomalies of 850 mb zonal wind (m/s) (a: above normal; b: below normal). The middle two panels show composite anomalies of 500 mb omega (Pa/s) (c: above normal; d: below normal). The bottom two panels show composite anomalies of OLR (W/m^2) (e: above normal; f: below normal). The bold black lines in panels a and b show the axis of the anomalous ridge in the 850 mb zonal wind field. The yellow star indicates the approximate location of KSC/CCAFS.

In the upper levels, anomalous Rossby wave trains are evident in both the above and below normal violation season anomaly composites (Figure 32). The anomalous wave trains emanate mainly from south and east Asia. In the below normal composite, there is evidence for the negative phase of the IOZM in the form of twin anticyclones located at approximately 30° N over south Asia and 30° S latitude over the southern Indian Ocean (Figure 32b). The height anomalies for the above and below normal composites are roughly opposite over much of the North Pacific and North America. In particular, the wave trains tend to produce opposite 200 mb GPH anomalies over Canada, the U.S., and the western North Atlantic. The equivalent barotropic structure of the 200 and 850 mb GPH anomalies indicates that these anomalies are dynamically linked to each other. By implication, the 850 GPH and associated low level circulation anomalies leading to the convection anomalies shown in Figure 31 are linked at least in part to the global scale upper level anomalies and teleconnections indicated by Figure 32.

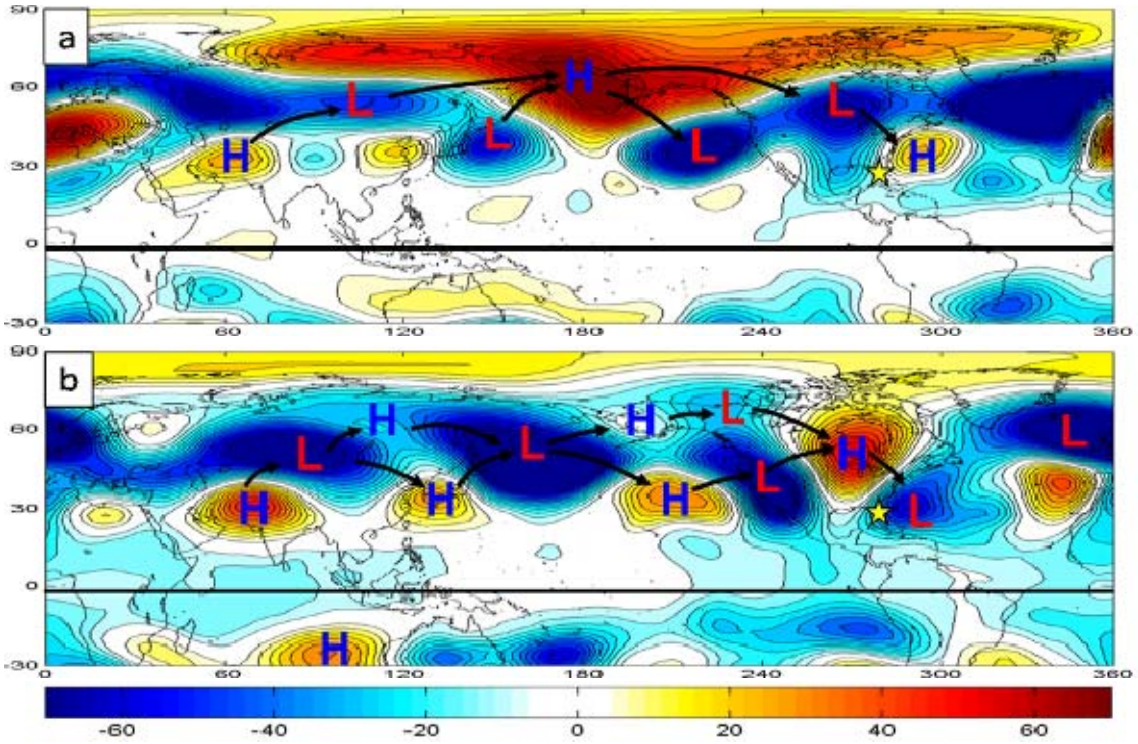

Figure 32. Composite 200 mb GPH anomalies (m) for the ramp-down II season during the three years in which there were: (a) above normal lightning violations; and (b) below normal lightning violations. Anomalous Rossby wave trains that extend over the SE U.S. are marked with H and L, and black arrows. The H and L identify the centers of the positive (negative) height anomalies that help define the wave trains. The black arrows link the centers that are part of individual wave trains and indicate the direction of anomalous energy propagation in the wave trains. The yellow stars indicate the location of the Florida Peninsula.

5. Winter Season

The winter season produces the fewest number of lightning violations and the least amount of variability (see Tables 2-4). During this season, the LTM shows the Bermuda High has weakened and shifted to the east, leaving only weak ridging in place over Florida and the Gulf of Mexico, with westerly flow over the KSC/CCAFS region (Figure 33a). In the composite of the three above normal years (Figure 33b), the ridge is weaker, contracted to the east, and with its axis located further to the south than in the LTM. In the composite of the three below normal years (Figure 33c), the ridge is slightly weaker than in the LTM but

with a similar location to the LTM. The below normal composite also shows greater than normal troughing over the western North Atlantic.

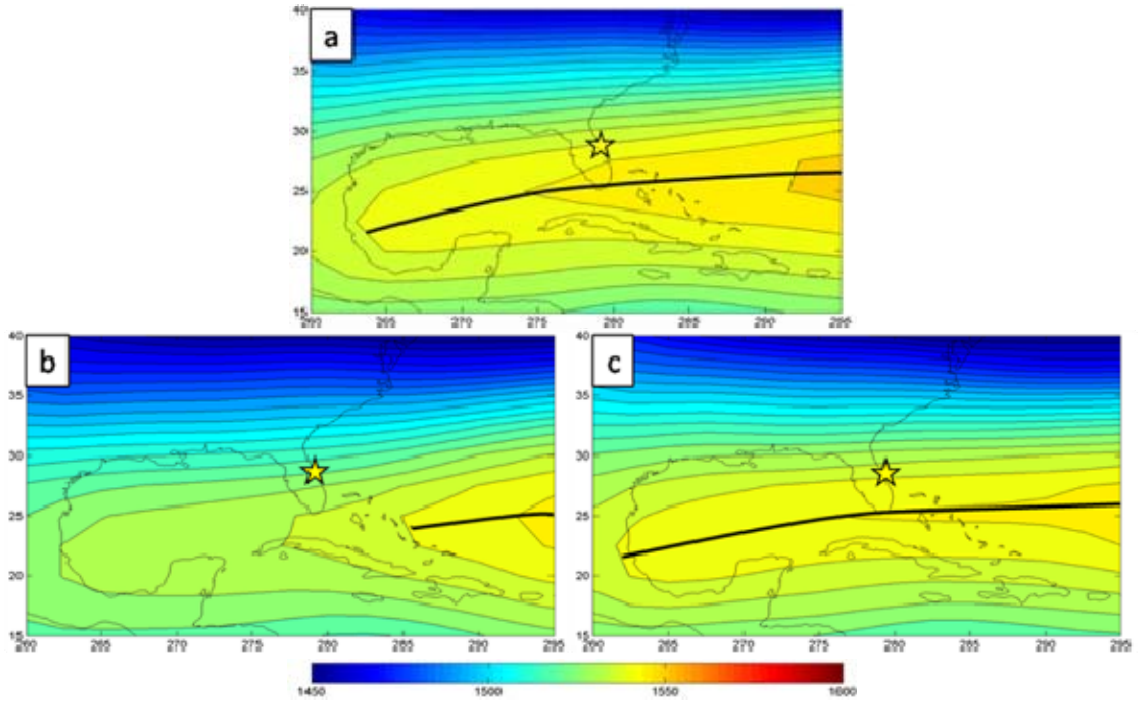

Figure 33. 850 mb GPH (m) for the lightning winter season: (a) LTM; (b) composite mean for the three years with above normal number of lightning violation (see Table 6); and (c) composite mean for the three below normal number of lightning violation years. The bold black lines indicate the position of the 850 mb ridge axis. The yellow star indicates the approximate location of KSC/CCAFS.

The anomalies for the winter season highlight the differences in the above and below normal seasons. Figure 34 shows a large negative 850 mb height anomaly affecting much of the focus region, suggesting more frequent than normal occurrence of mid-latitude weather systems in the above normal seasons. With anomalous low-level flow from the west off the Gulf of Mexico, abundant moisture would be available for these systems. A large negative 850 mb height anomaly is also present in the below normal cases, however centered more to the east. Flow around the backside of this feature produces anomalous northerly and NW-erly flow over the SE U.S., ushering in cooler, drier air which creates stable conditions for the region.

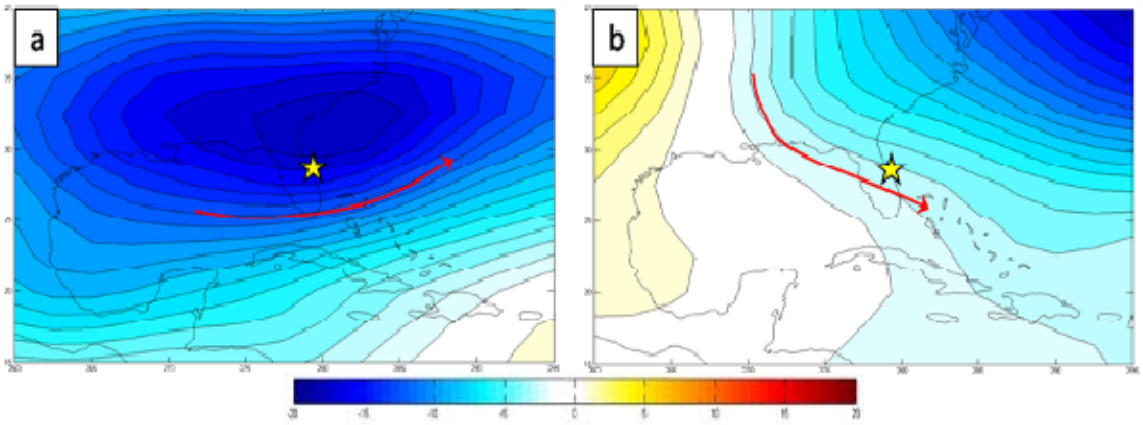

Figure 34. Composite 850 mb GPH anomalies (m) for the winter season during the three years in which there were: (a) above normal lightning violations; and (b) below normal lightning violations. Red arrows represent anomalous 850 mb flow. The yellow star indicates the approximate location of KSC/CCAFS.

Figure 35a indicates strong 850 mb zonal wind anomalies are present across the Gulf of Mexico, Florida, and the western North Atlantic in the composite of the three above normal winter seasons. This suggests more frequent and potentially stronger low-pressure systems, with anomalously strong warm moist air advection across Florida. The main area of lift is east of the Florida peninsula, ahead of the anomalous low (Figure 34a), and is associated with above normal upward vertical motion and above normal convection (Figure 35c, e). The composite of the three below normal seasons is also associated with above normal, but relatively weak, westerly zonal flow over Florida (Figure 35b). However, Figure 34b indicates that the anomalous meridional flow is the dominant flow anomaly, due to the negative height anomaly being centered to the NE of Florida. The associated anomalous southward flow of unusually cool, dry air over the SE U.S. (Figure 34b) is consistent with the downward vertical motion anomalies over and near the SE U.S. and the below normal convection to the west and east of Florida.

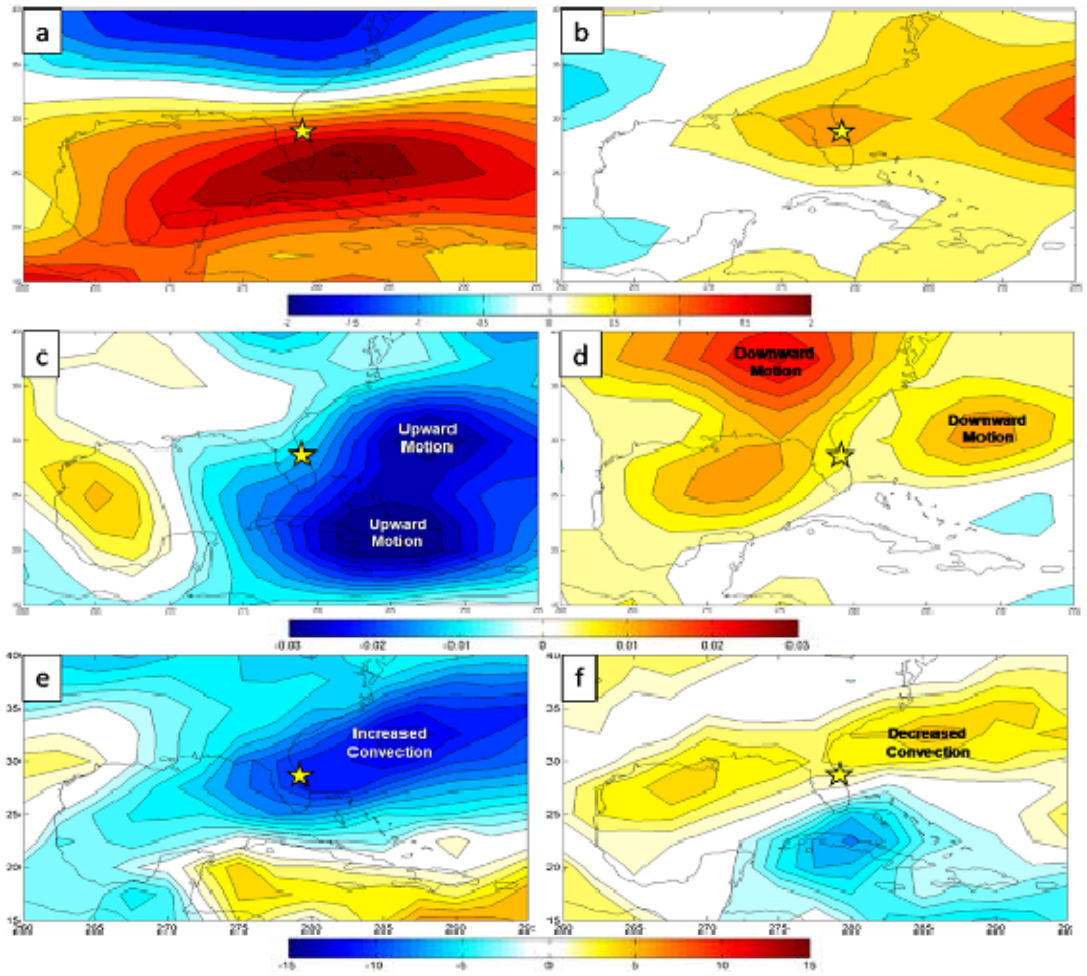

Figure 35. Composite anomalies for the winter season during three years in which there were above normal lightning violations (panels a, c, e) and below normal lightning violations (panels b, d, f). The top two panels show composite anomalies of 850 mb zonal wind (m/s) (a: above normal; b: below normal). The middle two panels show composite anomalies of 500 mb omega (Pa/s) (c: above normal; d: below normal). The bottom two panels show composite anomalies of OLR (W/m^2) (e: above normal; f: below normal). Yellow stars indicate the approximate location of KSC/CCAFS.

Figure 36 shows the 200 mb GPH anomalies for the above and below normal winter lightning season composites. The twin anticyclones (cyclones) straddling the equator in the tropical Pacific, and anomalous Rossby wave trains emanating from Asia and extending over North America and the North Atlantic, indicate strong teleconnections to ENLN. The ONI supports this connection as

each of the above (below) normal seasons are associated with positive (negative) ONI values (CPC 2010). The paired anticyclones over the far western Indian Ocean in above normal composite indicates that above normal lightning violations in the winter season may be linked to the positive phase of the IOZM. The net effect of the wave trains and teleconnections is the development of interannual variations in upper and lower level conditions over the SE U.S. that produce interannual variations in winter season lightning violations.

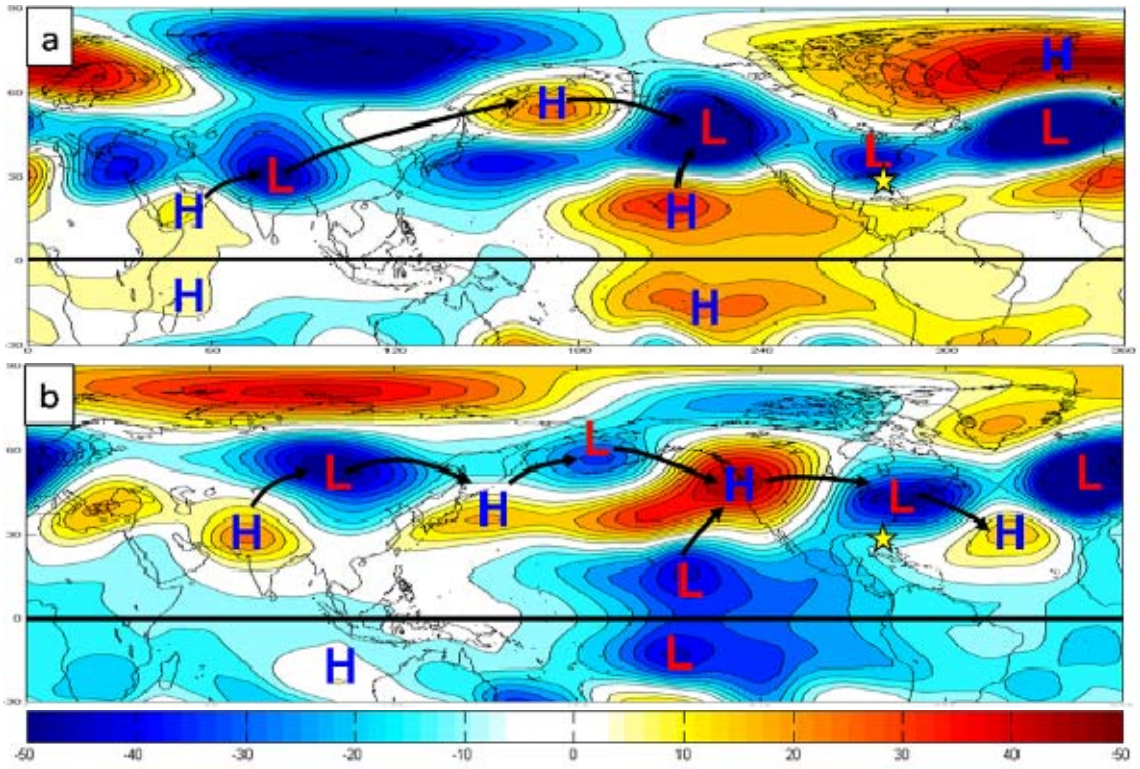

Figure 36. Composite 200 mb GPH anomalies (m) for the winter season during the years in which there were: (a) above normal number of lightning violations; and (b) below normal number of lightning violations. Anomalous Rossby wave trains that extend over the SE U.S. are marked with H and L, and black arrows. The H and L identify the center of the positive (negative) height anomalies that help define the wave trains. The black arrows link the centers that are part of individual wave trains and indicate the direction of anomalous energy propagation in the wave trains. The yellow star indicates the location of the Florida Peninsula.

6. Spring Season

The spring season features even less ridging than the winter (compare Figures 33a and 37a), with LTM westerly flow remaining over the Florida Peninsula. In the composite of the three years with above (below) normal number of lightning violations (see Table 6), weaker (stronger) than normal ridging occurs, allowing more (less) frequent passages of mid-latitude systems over Florida (Figure 37b, c).

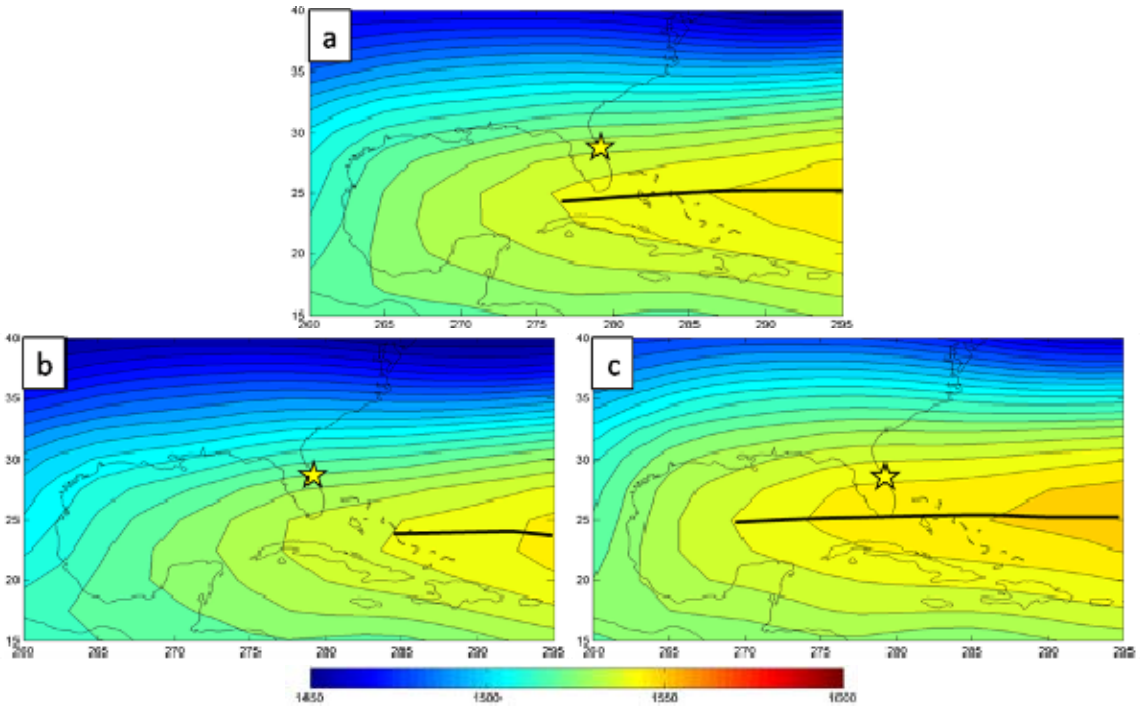

Figure 37. 850 mb GPH (m) for the lightning spring season: (a) LTM; (b) composite mean for the three years of above normal number of lightning violations; and (c) composite mean for the three years with below normal number of lightning violations. The bold black lines show the 850 mb ridge axis. The yellow star indicates the approximate location of KSC/CCAFS.

Starkly opposite patterns exist in the 850 mb GPH anomalies for the above and below normal spring seasons (Figure 38). Similar to the above normal winter season composite, the above normal spring season composite shows a large negative height anomaly over most of the SE U.S., Gulf of Mexico, and western Caribbean (Figure 38a). Anomalous low level SW-erly flow occurs

over the Gulf of Mexico, Florida, and the subtropical western North Atlantic. The below normal composite is nearly opposite (Figure 38b). A large positive height anomaly centered just north of Florida produces strong anomalous easterly flow across the entire peninsula (Figure 38b).

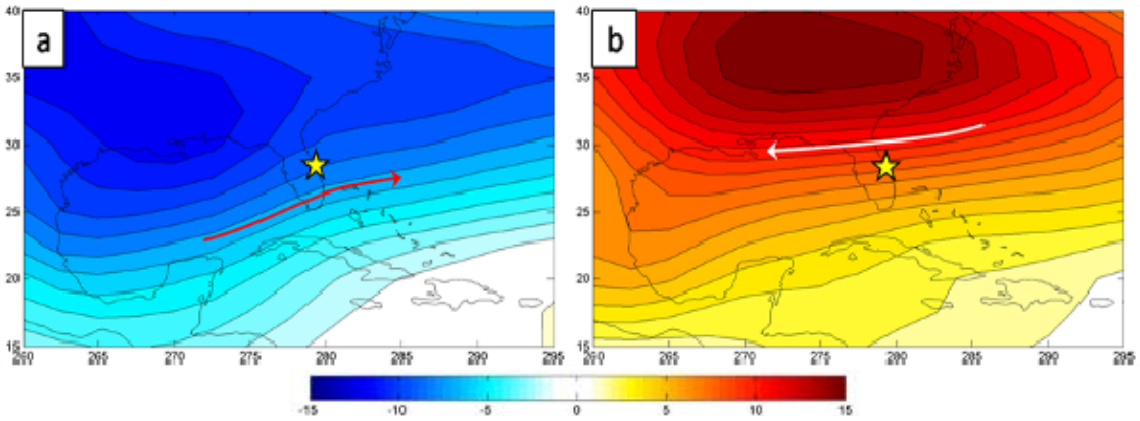

Figure 38. Composite 850 mb GPH anomalies (m) for the spring season during the three years in which there were: (a) above normal number of lightning violations; and (b) below normal number of lightning violations. Arrows represent anomalous 850 mb flow. The yellow star indicates the approximate location of KSC/CCAFS.

Figure 39 indicates strong zonal wind anomalies are present in both the above and below normal spring seasons. In the above normal composites, warm, moist air advected across the peninsula by an anomalous westerly zonal wind aids in the development of convection, and increases the probability of lightning violations at KSC/CCAFS (Figure 39a, c, e). In the below normal composites, a strong easterly zonal wind anomaly is located over Florida (Figure 39 b, d, f). Since the spring season runs until mid-May, sea breeze convection is possible. However, in the below normal composite, the strong easterly anomaly significantly decreases the chances of the sea breeze convection being located near KSC/CCAFS. In the above normal composites, the positive vertical motion anomalies on the southern flank of the anomalous low favor (compare Figure 39 c, e and Figure 38a) the development of thunderstorms, as indicated by the negative OLR anomalies. The opposite is true in the below normal composites, with anomalous downward vertical motion and positive OLR anomalies on the

southern flank of the anomalous high (compare Figure 39d, f and Figure 38b). The results shown in Figure 39 indicate that in the spring season, lightning violation anomalies at KSC/CCAFS are strongly tied to anomalies in regional scale mechanisms that extend across the SE U.S., Gulf of Mexico, Caribbean, and western North Atlantic—as in the other lightning violation seasons discussed in prior sections.

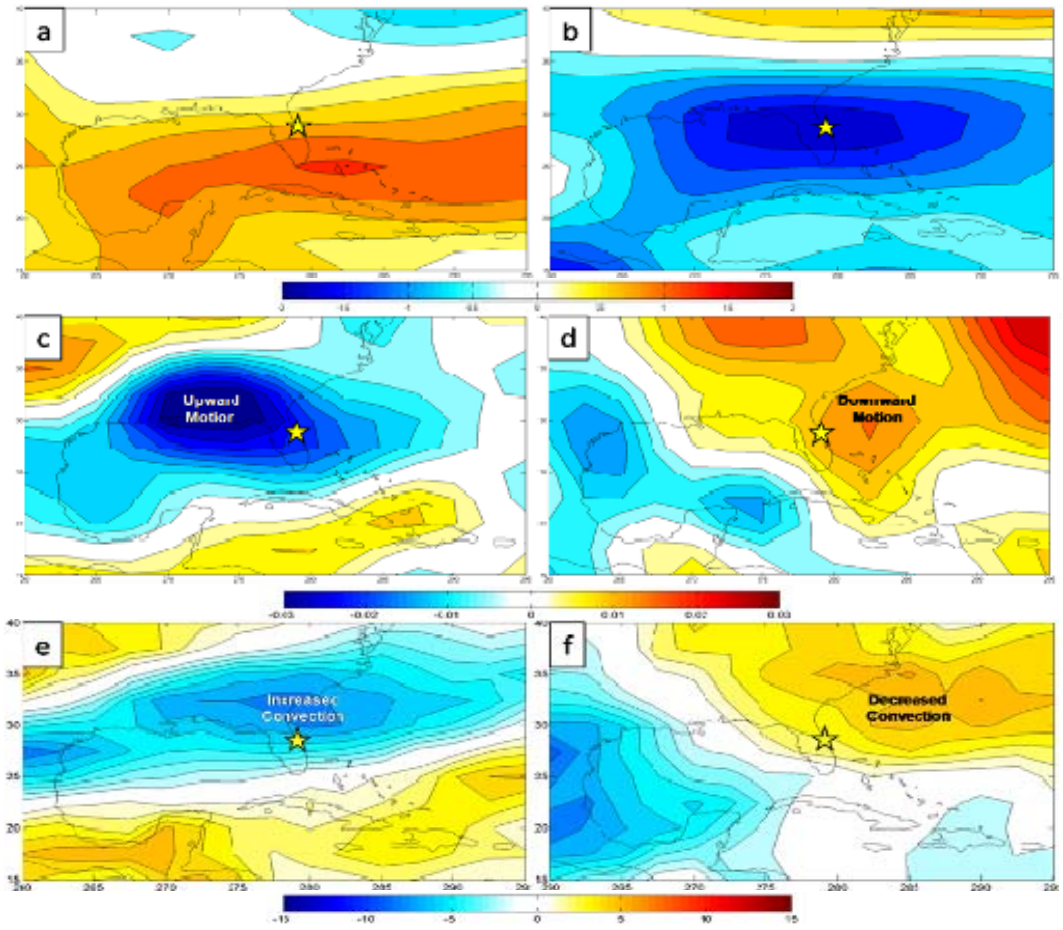

Figure 39. Composite anomalies for the spring season during the three years (see Table 6) with above normal number of lightning violations (panels a, c, e) and below normal number of lightning violations (panels b, d, f). The top two panels show composite anomalies of 850 mb zonal wind (m/s) (a: above normal; b: below normal). The middle two panels show composite anomalies of 500 mb omega (Pa/s) (c: above normal; d: below normal). The bottom two panels show composite anomalies of OLR (W/m^2) (e: above normal; f: below normal). Yellow stars indicate the approximate location of KSC/CCAFS.

Figure 40 shows the 200 mb GPH anomalies for the above and below normal spring season composites. The twin anticyclonic anomalies straddling the equator in the tropical Pacific indicate a strong teleconnection to EN during the above normal spring seasons (Figure 40a). Additionally, the upper level positive height anomalies stretching from the central Pacific into the Caribbean indicate a stronger than normal subtropical jet and extratropical storm track, resulting in stronger and/or more frequent low-pressure systems over Florida. The wave trains and signs of teleconnection to the SE U.S. are less clear in the below normal composite.

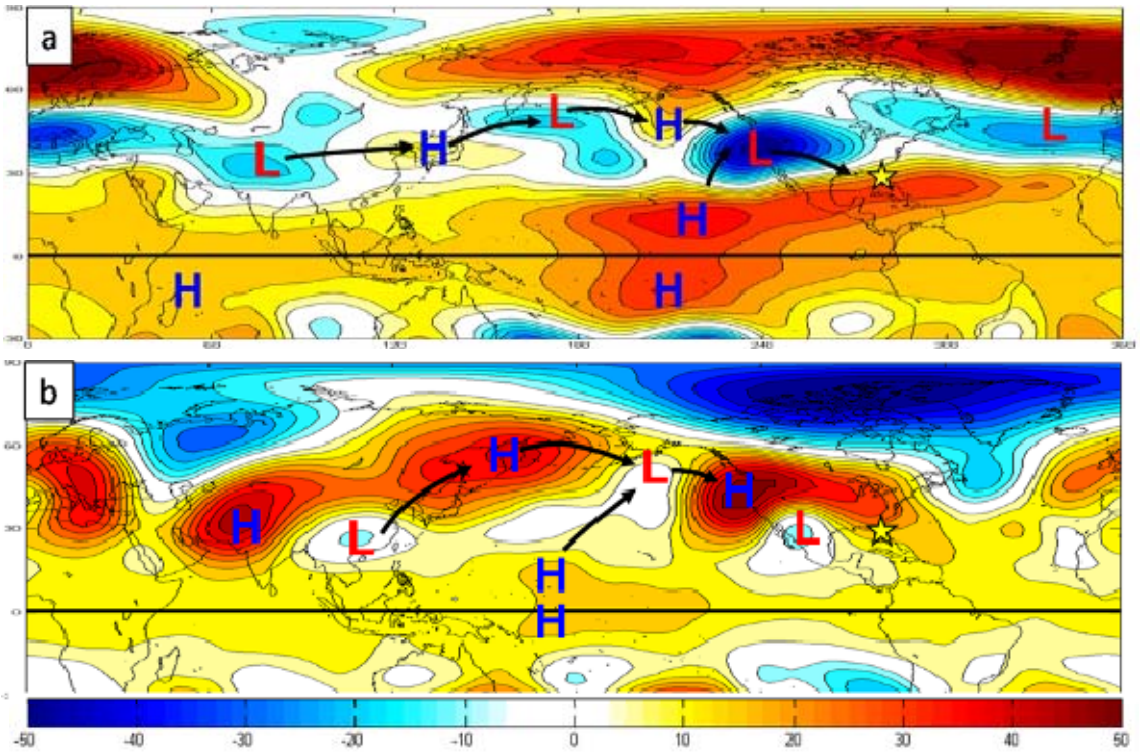

Figure 40. Composite 200 mb GPH anomalies (m) for the spring season during three years with (a) above normal number of lightning violations; and (b) below normal number of lightning violations. Anomalous Rossby wave trains that extend over the southeastern U.S. are marked with H and L and black arrows. The H and L identify the center of the positive (negative) height anomalies that help define the wave trains. The black arrows link the centers that are part of individual wave trains and indicate the direction of anomalous energy propagation in the wave trains. The yellow stars indicate the location of the Florida Peninsula.

C. ANOMALOUS START AND END DATES OF THE MAIN LIGHTNING SEASON

Considerable interannual variability not only exists in the number of violations for the main lightning season, but also in the start and end dates for this season. Table 7 lists the three earliest start and end dates, and the three latest start and end dates for the main lightning season. Note that the early and late starts and ends occur in different months (i.e., May for the early starts, June for the late starts, August for the early ends, October for the late ends). This indicates that the LTM conditions for the early and late starts are significantly different, and also for the early and late ends. This complicates the analyses of the associated anomalies, since different LTMs must be used for the early and for the late starts, and also for the early and late ends. For each of the four cases (early start, early end, late start, late end), we conducted analyses of the conditions during: (a) the ten days prior to the dates listed in Table 7; and (b) the ten days after those dates. Using the three early start dates as an example, the ten days before each of the early start dates of 5/07/99, 5/21/01, and 5/16/03 were composited, and the ten days after the same dates were composited. These composites representing the atmospheric conditions before and after the early start dates were then compared. Similarly, composites representing the atmospheric conditions during the 10 days before and after the late start dates were developed and compared. The remainder of this section discusses the atmospheric conditions responsible for producing these anomalously early and late starts of the main lightning season.

Table 7. Four cases are defined in this table: Early Start, Late Start, Early End, and Late End of the main lightning season. Using the 1989–2008 data record, the dates of the three earliest start dates of the main lightning season are listed. Similarly, the three dates of the latest start, earliest end, and latest end are also listed.

Early Start	**5/07/1999** **5/23/2001** **5/16/2003**
Late Start	**6/24/2000** **6/25/2006** **6/30/2007**
Early End	**8/03/1993** **8/10/1995** **8/05/2006**
Late End	**10/14/1990** **10/25/2002** **10/12/2008**

1. Early Start of the Main Lightning Season

Investigation of the early starts to the main lightning season revealed subtle but key differences between the ten-day period before and after the early start dates. The composite 850 mb GPH anomaly for the ten days prior to the early start dates of the lightning season (Figure 41a) indicates the Florida Peninsula is under the influence of anomalous WNW-erly flow on the southern flank of a negative height anomaly over the eastern U.S. and western North Atlantic. The period after the start of the lightning season also features a negative height anomaly centered over the mid-south region of the U.S., plus a weak positive height anomaly over Cuba and the Bahamas, with anomalous WSW-erly flow over Florida and directional convergence in the anomalous zonal flow to the east of Florida. Based on low-level wind flow alone, both of these flows would support an increase in sea breeze convection over the east coast of Florida. However, in the composite ten days prior to the early start dates of the season, a low level anticyclonic anomaly and weak anomalous ridging was

centered over the eastern Gulf of Mexico and Florida (Figure 41a), which would tend to suppress convection over that region. Conversely, in the composite ten days following the early start dates, a low level cyclonic anomaly and weak anomalous troughing occurred over the Gulf of Mexico and Florida, with its center over the mid-south region of the U.S. (Figure 41b), which would tend to support convection in the region.

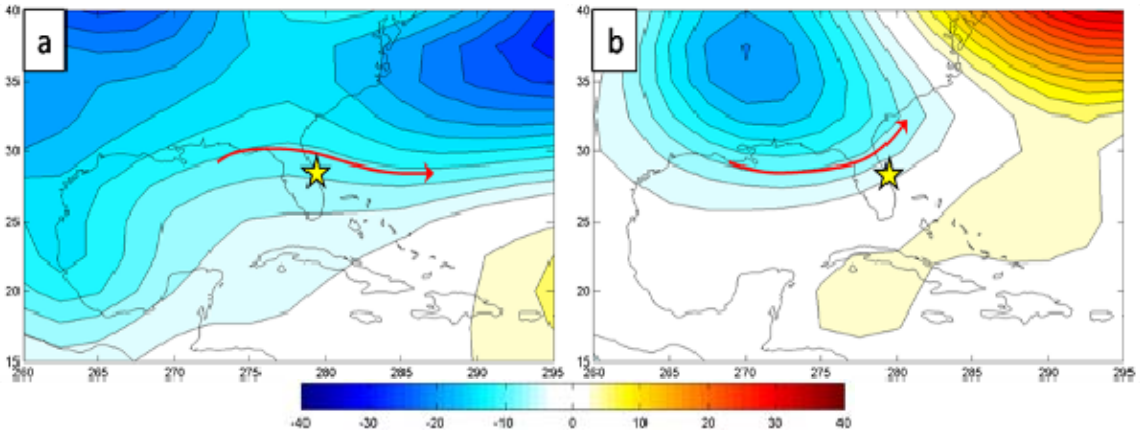

Figure 41. Composite 850 mb GPH anomalies (m) for the main lightning season during (a) the ten days immediately prior to the early start dates and (b) the ten days following the early start dates. Red arrows represent anomalous 850 mb flow. The yellow star indicates the approximate location of KSC/CCAFS.

The 500 mb omega field for the ten days prior to the early starts indicates a large area of anomalous downward vertical motion and anomalously weak convection in the region of weak ridging at 850 mb (compare Figure 41a and Figure 42a, c). For the 10-day period following the early starts of the main lightning season, the region of troughing at 850 mb is an area of anomalously upward vertical motion and anomalously strong convection (compare Figure 41b and Figure 42b, d).

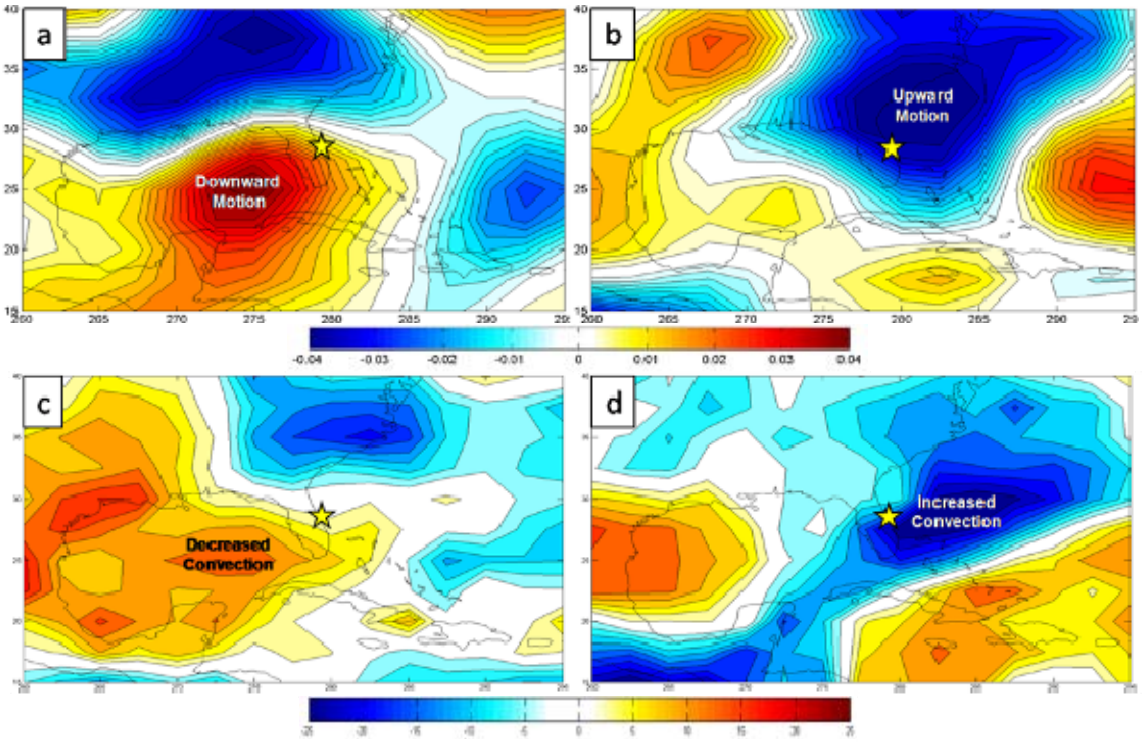

Figure 42. Composite anomalies for the main lightning season during the ten days immediately prior to the early start dates (panels a, c) and the ten days following the early start dates (panels b, d). The top two panels show composite anomalies of 500 mb omega (Pa/s) (a: ten days prior; b: ten days following). The bottom two panels show composite anomalies of OLR (W/m^2) (c: ten days prior; d: ten days following). Yellow stars indicate the approximate location of KSC/CCAFS.

2. Late Start of the Main Lightning Season

The 850 mb GPH anomaly for the 10 days prior to the late starts of the main lightning season features a large positive height anomaly centered north of Florida and anomalously easterly flow over Florida (Figure 43a). In the 10 days after the late start, a weak negative height center is centered over the KSC/CCAFS region, creating a weak cyclonic flow anomaly around KSC/CCAFS.

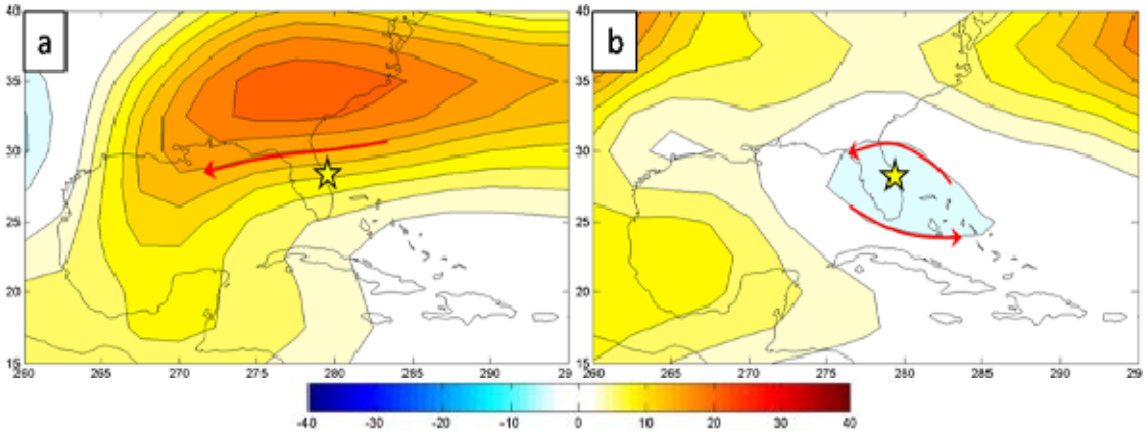

Figure 43. Composite 850 mb GPH anomalies (m) for the main lightning season during (a) the ten days immediately prior to late start dates and (b) the ten days following the late start dates. Red arrows represent anomalous 850 mb flow. The yellow star indicates the approximate location of KSC/CCAFS.

By late June and early July, sea breeze convection is well underway. Therefore, the anomalously weak easterly flow of the 10-day period following the late start dates is significantly more favorable for sea breeze convection to occur over KSC/CCAFS than the stronger easterly flow of the 10-days prior to the normal start of the main lightning season. In the composite of the 10-day period prior to the late start date, the positive height anomaly area in the SE U.S. (Figure 43a) is a region of anomalously strong downward vertical motion and anomalously weak convection (Figure 44a, c). Likewise, the weak negative height anomaly in the period following the late start date corresponds to anomalously upward vertical motion and anomalously strong convection over and/or to the east of the eastern half the Florida Peninsula.

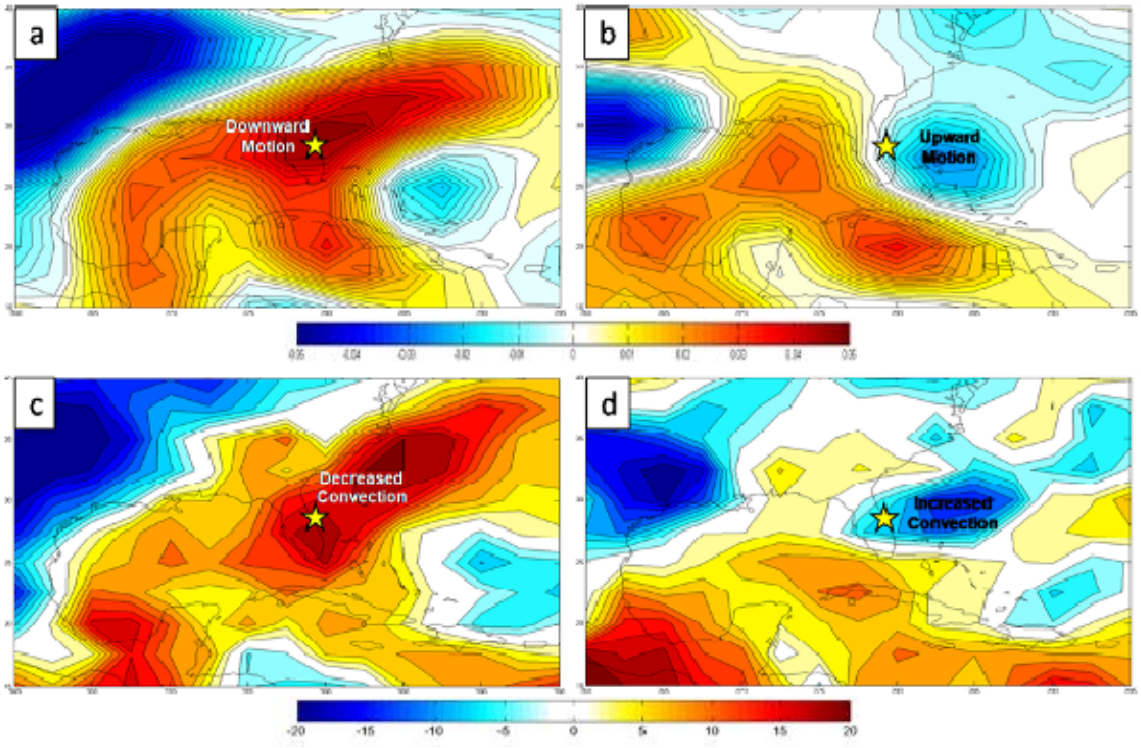

Figure 44. Composite anomalies for the main lightning seasons during the ten days immediately prior to late start dates (panels a, c) and the first ten days following the late start dates (panels b, d). The top two panels show composite anomalies of 500 mb omega (Pa/s) (a: ten days prior; b: ten days following). The bottom two panels show composite anomalies of OLR (W/m^2) (c: ten days prior; d: ten days following). Yellow stars indicate the approximate location of KSC/CCAFS.

3. Early Start vs. Late Start of the Main Lightning Season

The differences in the 10-day periods before and after the early and late start dates are somewhat subtle (see Figures 41–44). But our analyses of the differences between the early and late start dates themselves show some striking patterns. We determined the best way to analyze the two anomalous events separated by almost a month (see Table 7) was to compare the 10-day period after the beginning of the early start dates of the main lightning season with the 10-day period prior to the beginning of the late start dates of the main lightning season. This comparison allowed us to investigate a 10-day composite period with an anomalously large number of lightning violations and a 10-day composite

period with an anomalously small number of lightning violations, and thereby analyze the processes that contributed to these anomalies in lightning violations.

The 850 mb GPH anomalies for the early start dates (Figure 45a, c) show a weak ridge centered south of Florida, a trough over the central U.S., and a large negative height anomaly over much of the southern U.S., including the northern half of the Florida Peninsula. The corresponding low level flow and flow anomaly are WSW-erly, and a positive specific humidity anomaly, over the Florida Peninsula (Figure 45c and Appendix B, Figure 65). This flow and its corresponding moisture advection are favorable for enhanced sea breeze convection over the Florida east coast. Additionally, with an anomalous low affecting the region, reduced subsidence and increased instability would aid in widespread synoptic convection. The late start dates to the main lightning season feature a strong and extensive positive height anomaly over the SE U.S. (Figure 45b). This height anomaly represents a significant northern shift in the Bermuda High ridge axis, which creates a strong actual and anomalous east southeasterly (ESE-erly) to easterly flow over Florida (Figure 45b). This flow not only ushers in drier air (Appendix B, Figure 65), but also creates unfavorable conditions for sea breeze convection at KSC/CCAFS by pushing the east coast sea breeze farther inland than normal.

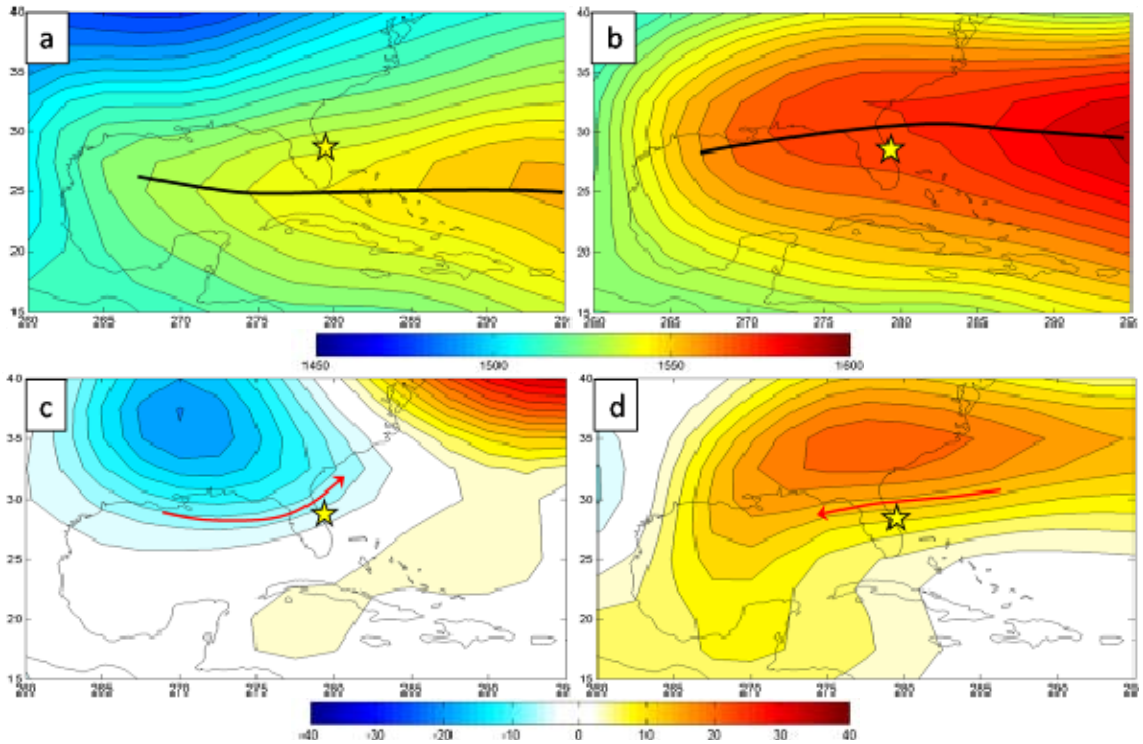

Figure 45. Composites of 850 mb GPH (m). The panels on the left (a, c) represent conditions during the first ten days following an early start of the main lightning violation season. The panels on the right (b, d) represent conditions during the ten days immediately prior to late start dates of the main lightning violation season (late starts). Panel (a) is the composite 850 mb GPH for the first ten days after the early start dates of the main lightning violation season; panel (b) is the composite 850 mb GPH for the ten days prior to the late start dates of the main lightning violation season; panel (c) is the composite 850 mb GPH anomaly for the first ten days after the early start dates of the main lightning violation season; and panel (d) is the composite 850 mb GPH anomaly for the ten days prior to the late starts of the main lightning violation season. The bold black lines show the axis of the ridge at 850 mb with red arrows representing anomalous 850 mb flow. Yellow stars indicate the approximate location of KSC/CCAFS.

Figures 46a, b highlights the zonal wind anomalies around the ridge and the height anomalies during early and late start dates of the main lightning seasons (Figure 45). The anomalous westerly flow in the early start of the main lightning seasons would set up conditions favorable for early season sea breeze convection. The days before the late start of the main lightning season feature anomalous easterly flow, opposing the LTM flow and shifting convection inland

and west of KSC/CCAFS. The circulation on the southern flank of the anomalous low over the Gulf Coast (Figure 45c) involves low level speed convergence over and to the east of Florida and generates abundant anomalous upward vertical motion and enhanced convection over the Florida Peninsula and the adjacent North Atlantic (Figure 46c), consistent with conditions of the early start dates to the main lightning season. For the late start dates, dry, stable easterly flow on the eastern side of the positive height anomaly (Figure 45d) leads to low level speed divergence, and a large region of anomalous downward vertical motion and anomalously low convection centered over and to the NE of the Florida Peninsula, consistent with late starts to the main lightning season.

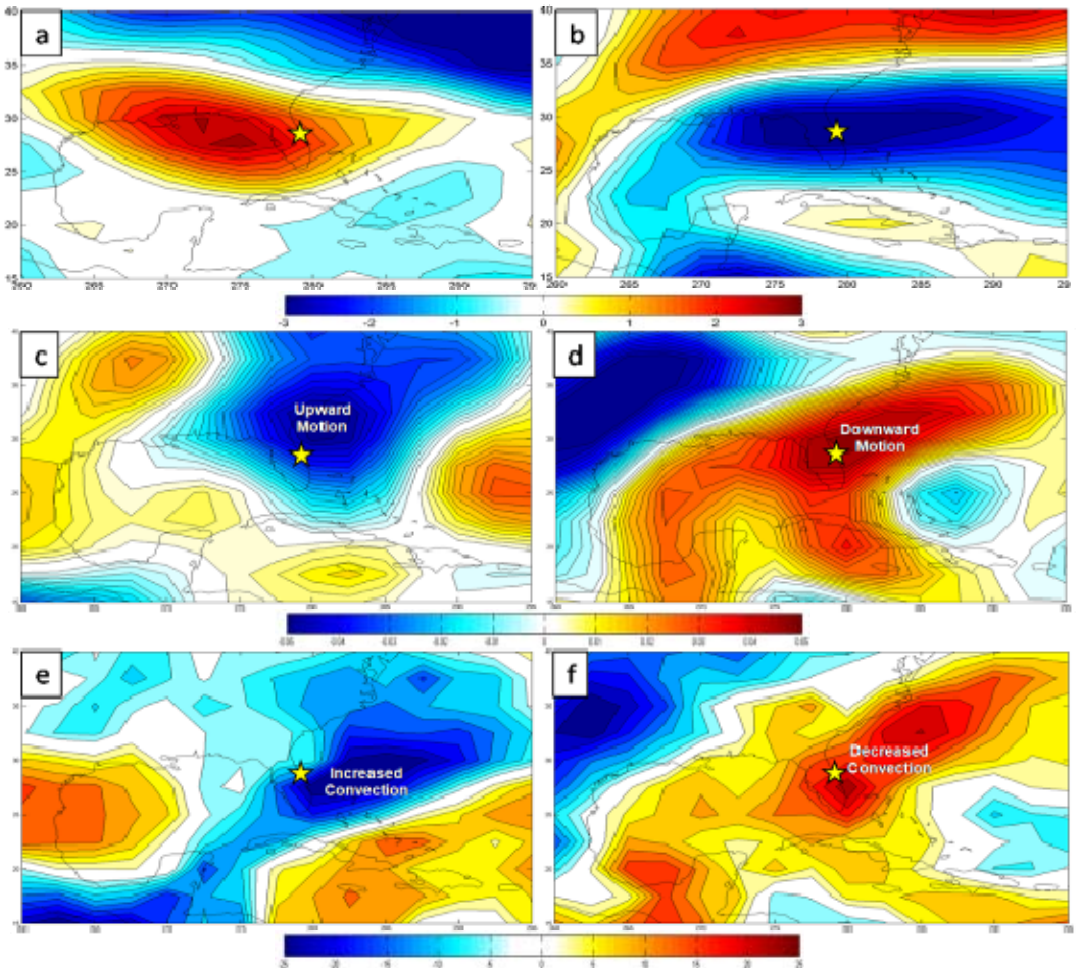

Figure 46. Composite anomalies of the 10-day period following the early start dates (panels a, c, e) and the 10-day period prior to the late start dates (panels b, d, f) of the main lightning season are compared. In particular: (a) composite 850 mb zonal wind (m/s) anomaly for the ten days following the early start dates; (b) composite 850 mb zonal wind (m/s) anomaly for the ten days prior to late start dates; (c) composite 500 mb omega (Pa/s) anomaly for the ten days following the early start dates; (d) composite 500 mb omega (Pa/s) anomaly for the ten days prior to late start dates; (e) composite OLR (W/m^2) anomaly for the ten days following the early start dates; and (f) composite OLR (W/m^2) anomaly for the ten days prior to late start dates of the main lightning violation season. Yellow stars indicate the approximate location of KSC/CCAFS.

The composite 200 mb GPH anomalies for the 10 days following the early start dates and 10 days prior to the late start dates show equivalent barotropic structure over the SE U.S. (compare Figures 45c, d and Figure 47). The

anomalous wave trains indicate teleconnections from east Asia and the tropical western North Pacific into the SE U.S. The predominantly negative anomalies along the equator (Figure 47a) are suggestive of a relationship between early starts and the occurrence of LN in the tropical Pacific.

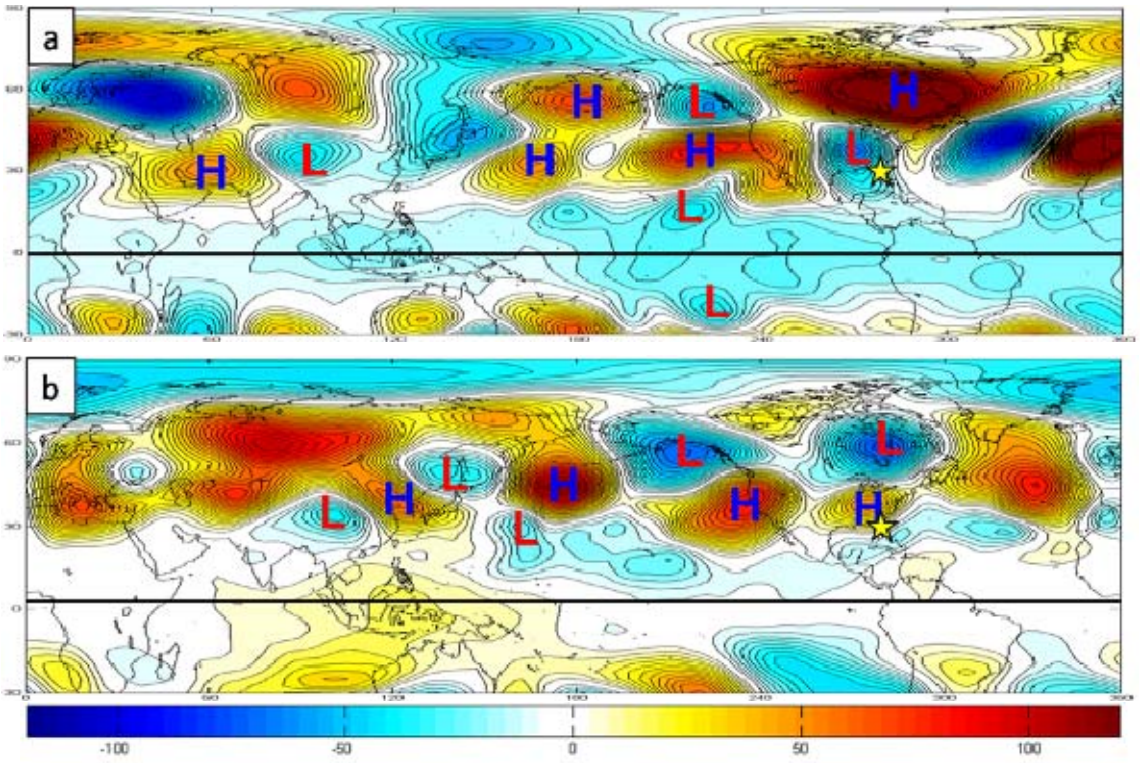

Figure 47. Composite 200 mb GPH anomalies (m) for the main lightning season during (a) the first ten days following the composite early start and (b) the first ten days immediately prior to the composite late start. Anomalous Rossby wave trains that extend over the SE U.S. are marked with H and L and black arrows. The H and L identify the center of the positive (negative) height anomalies that help define the wave trains. The black arrows link the centers that are part of individual wave trains and indicate the direction of anomalous energy propagation in the wave trains. Yellow stars indicate the approximate location of the Florida Peninsula.

The schematic diagrams in Figure 48 provide a basic conceptual summary of the anomaly patterns associated with the ten days after early starts, and the ten days prior to late starts, of the main lightning season. These schematics are directly based on the composites shown in Figures 45-47. The large spatial

scale of the anomalies, and the dramatic difference between the early start and late start patterns, indicate a relatively high potential for skillful long range forecasts (lead times of two weeks or longer) of the circulation and other anomalies that lead to early starts and late starts of the main lightning season.

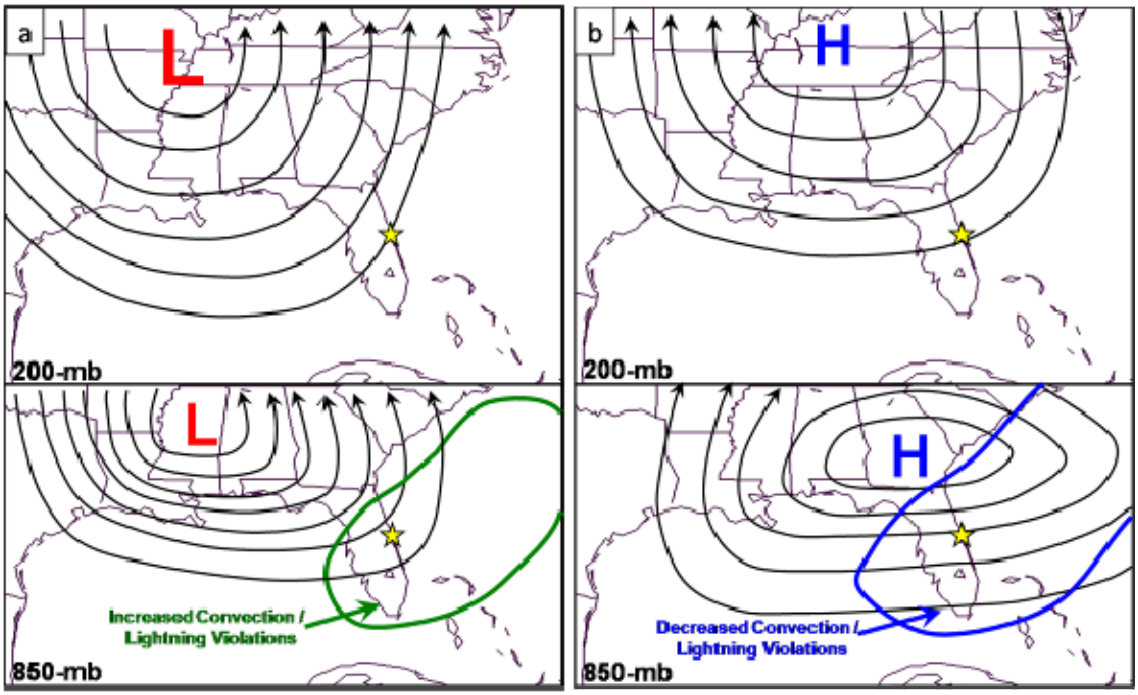

Figure 48. Schematic diagrams of the 200 mb and 850 mb geopotential height anomalies (m) associated with (a) the ten days after early start dates and (b) the ten days prior to late start dates of the main lightning season.

4. Early End of the Main Lightning Season

The earliest end dates of the main lightning season also produce subtle but key differences between the ten-day period before and after the end date. Ten days prior to the end of the lightning season, the composite 850 mb GPH anomaly indicates the Florida Peninsula is experiencing near normal conditions (Figure 49). A slight northward shift in the axis of the Bermuda High in the composite mean is represented by a positive height anomaly over the Carolinas. However, this seemingly minor shift produces anomalous easterly flow over the peninsula, which results in a reversal of the low level LTM wind direction and a

mean easterly flow. The 10-day period after the end dates of the main lightning season also features near normal conditions, with a weak positive height anomaly over the Florida panhandle. This anomaly is also a reflection of a northward shift in the Bermuda High, however its location yields an anomalous NE-erly flow for KSC/CCAFS.

The slight position difference of the two aforementioned positive height anomalies is probably critical in creating conditions favorable or unfavorable for lightning violations. While both of the anomalous wind directions are less than desirable, the NE-erly flow is probably more likely to suppress lightning at KSC/CCAFS. This is primarily because the anomalous NE-erly flow introduces drier more stable air into the region, limiting the necessary ingredients for convection (cf. Appendix B, Figure 66a). Additionally, the flow around the positive height centers, in conjunction with anomalous negative height centers well offshore of Cape Hatteras creates significant regions of low-level directional divergence. With the anomalous high farther west in the period following the early end of the main lightning season, this low level divergence is located in much closer proximity to the Florida Peninsula (compare Figure 50a and Figure 50b), inhibiting lightning violations. Both the 10-day periods prior and following the early end dates have positive anomalous vertical motion and OLR values. However, the magnitudes of these anomalies in the ten days prior to the early end dates of the main lightning season are considerably less, indicating more favorable conditions for lightning violations.

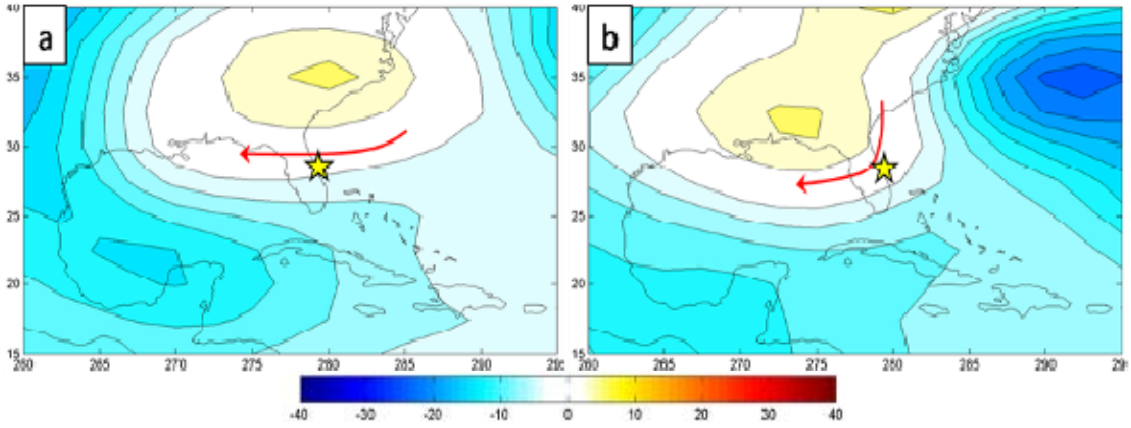

Figure 49. Composite 850 mb GPH anomalies (m) for the main lightning season during (a) the ten days immediately prior to the early end dates and (b) the first ten days following the early end dates. Red arrows represent the anomalous 850 mb flow. The yellow stars indicate the approximate location of KSC/CCAFS.

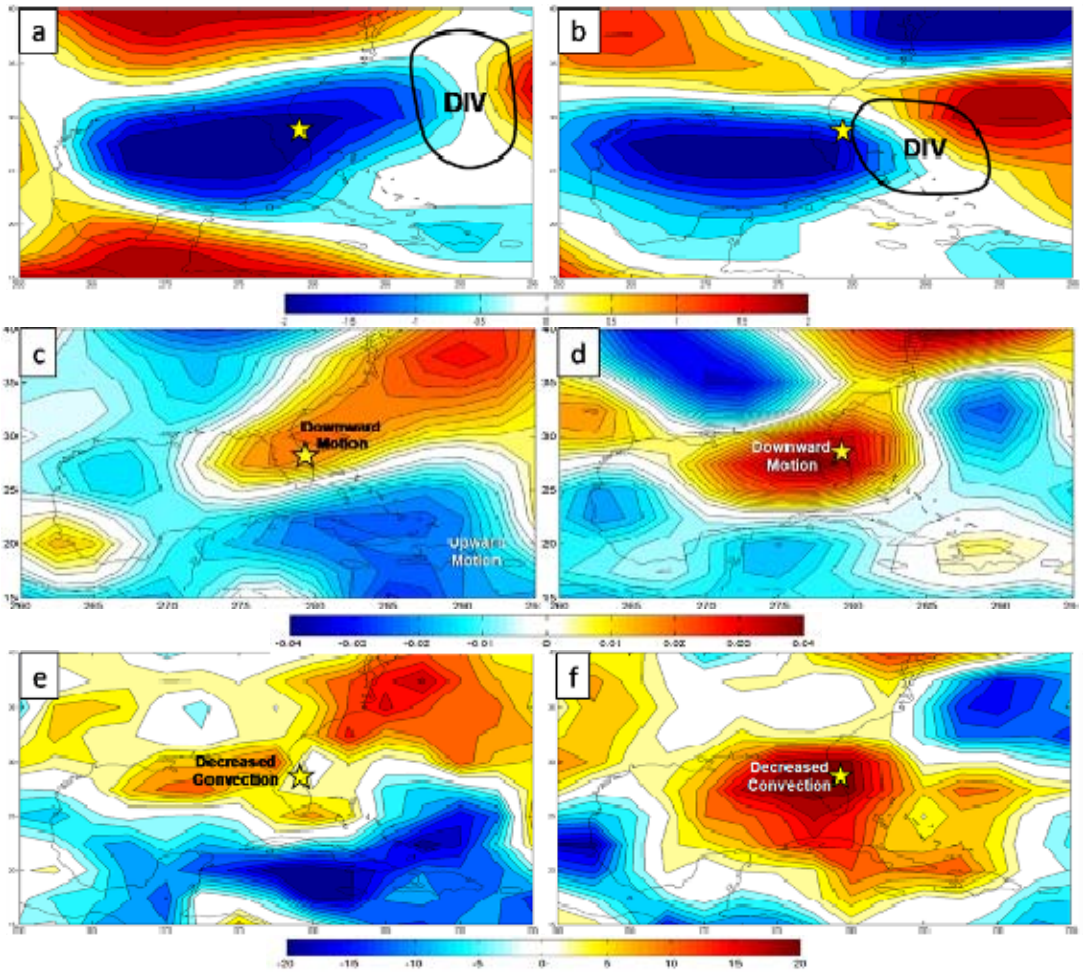

Figure 50. Composite anomalies for the main lightning seasons during the ten days immediately prior to the early end dates (panels a, c, e) and the ten days following the early end dates (panels b, d, f). The top two panels show composite anomalies of 850 mb zonal wind (m/s) (a: ten days prior; b: ten days following). The middle two panels show composite anomalies of 500 mb omega (Pa/s) (c: ten days prior; d: ten days following). The bottom two panels show composite anomalies of OLR (W/m^2) (e: ten days prior; f: ten days following). Yellow stars indicate the approximate location of KSC/CCAFS.

5. Late End of the Main Lightning Season

The periods before and after the late end dates of the main lightning season have some similarities to winter patterns. Figure 51a shows that in the ten days prior to the composite late end, the Bermuda high is located farther to the east than normal, and there are lower than normal heights across Florida and

the Gulf Coast. Figure 51b shows that in the days following the late ends to the main lightning season, a significant increase in heights occurs across the region creating a closed high-pressure system centered very near KSC/CCAFS, indicating anomalous strong subsidence and making lightning violations less likely. The zonal wind anomaly associated with the ten days before the end of the lightning season indicates anomalous low-level convergence occurs over the Florida Peninsula, associated with anomalous upward vertical motion and enhanced convection over and to the east of Florida (Figure 52a, c, e). The anomalies during the ten days following the composite late end dates show anticyclone low-level flow over KSC/CCAFS, and anomalously downward vertical motion and suppressed convection over and to the east and SE of the Florida Peninsula (Figure 52 b, d, f).

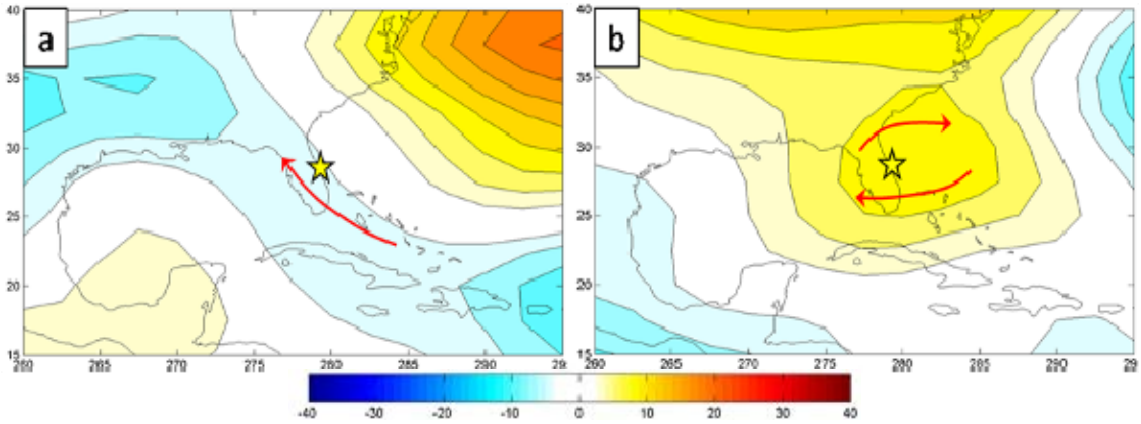

Figure 51. Composite 850 mb GPH anomalies (m) for the main lightning season during (a) the ten days immediately prior to the composite late end dates and (b) the ten days following the composite late end dates. Red arrows represent anomalous 850 mb flow. The yellow stars indicate the approximate location of KSC/CCAFS.

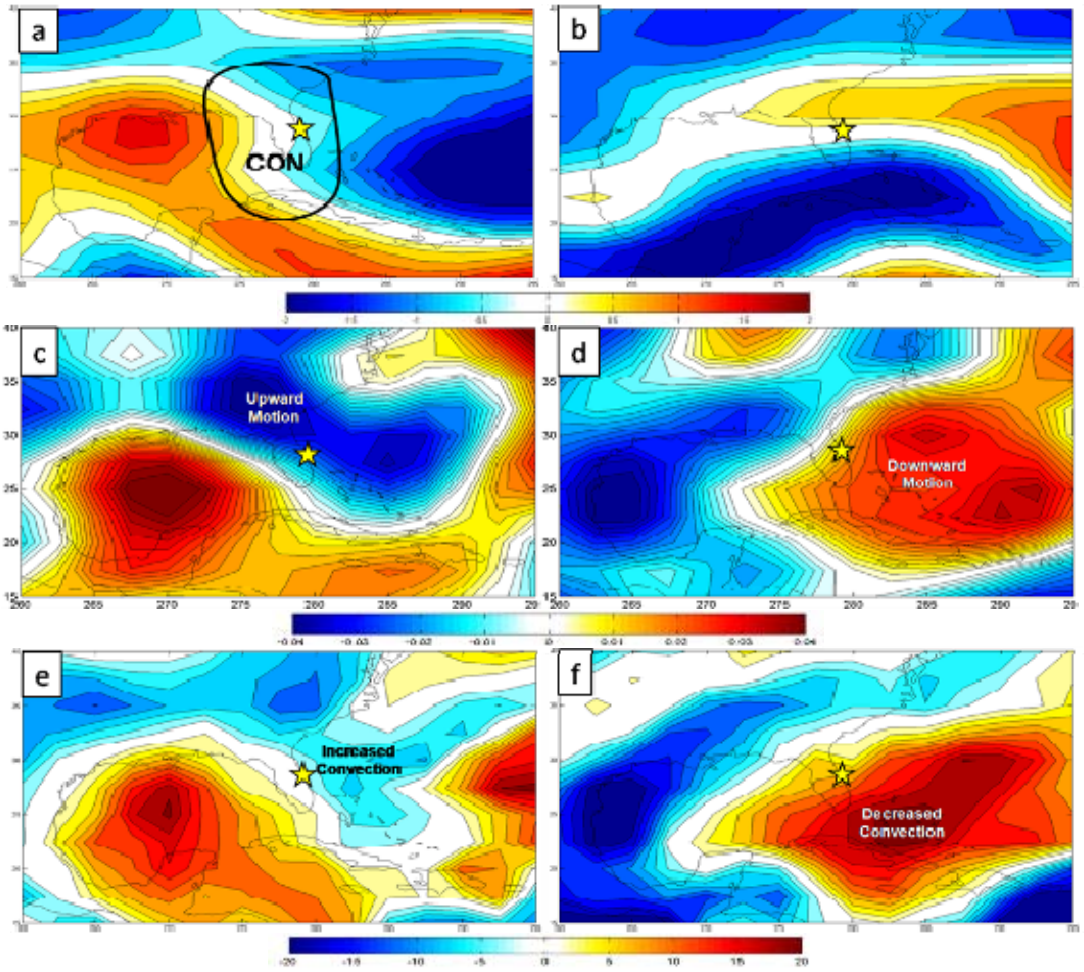

Figure 52. Composite anomalies for the main lightning season during the ten days immediately prior to the late end dates (panels a, c, e) and the ten days following the late end dates (panels b, d, f). The top two panels show composite anomalies of 850 mb zonal wind (m/s) (a: ten days prior; b: ten days following). The middle two panels show composite anomalies of 500 mb omega (Pa/s) (c: ten days prior; d: ten days following). The bottom two panels show composite anomalies of OLR (W/m^2) (e: ten days prior; f: ten days following). Yellow stars indicate the approximate location of KSC/CCAFS.

6. Early End vs. Late End of the Main Lightning Season

The differences in the 10-day periods before and after the early and late end dates are somewhat complex. But more striking differences are found by comparing the 10-day period after the early end dates with the 10-day period prior the late end dates of the lightning seasons. This comparison allowed us to

investigate a composite 10-day period with anomalously small numbers of lightning violations (the early end composite) with a composite 10-day period with anomalously high numbers of violations (the late end composite).

Figure 53 shows that the early (late) end composite is associated with: (a) anomalously positive (negative) 850 mb heights over the Gulf Coast; and (b) NE-erly (SE-erly) low level flow anomalies, and dry (moist) advection anomalies over the Florida Peninsula (cf. Appendix B, Figure 66). These anomalies are unfavorable (favorable) for dry stable (moist unstable) air advection into the peninsula and late season sea-breeze convection along the east coast of the peninsula.

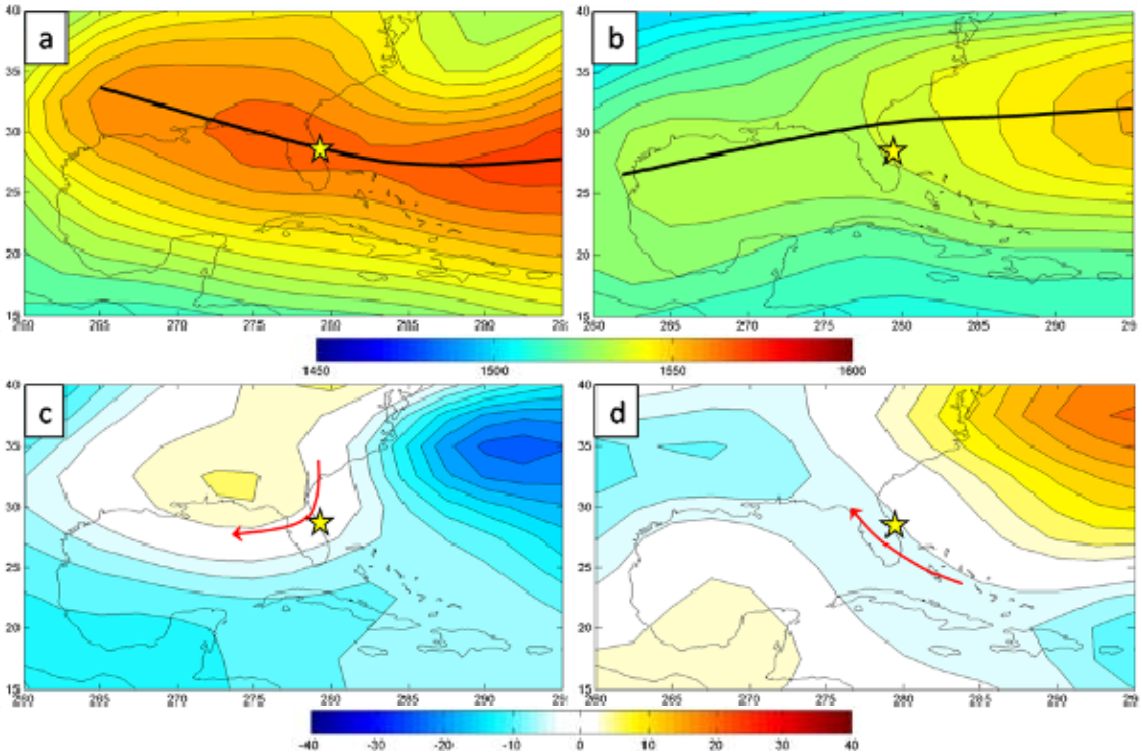

Figure 53. Composites of 850 mb GPH. The panels on the left (a, c) represent conditions during the first ten days following an early end of the main lightning violation season. The panels on the right (b, d) represent conditions during the ten days immediately prior to late ends of the main lightning violation season. Panel (a) is a composite 850 mb GPH (m) for the ten days following early end dates of the main lightning violation season; panel (b) is a composite 850 mb GPH (m) for the ten days prior to late end dates of the main lightning violation season; panel (c) is a composite 850 mb GPH anomaly (m) for the ten days following early end dates of the main lightning violation season; and panel (d) is a composite 850 mb GPH anomaly (m) for the ten days prior to late end dates of the main lightning violation season. The bold black lines show the axis of the ridge at 850 mb with red arrows representing anomalous 850 mb flow. Yellow stars indicate the approximate location of KSC/CCAFS.

The dry, stable NE-erly flow on the eastern side of the positive height anomaly In Figure 53a is associated with a large region of anomalous low-level divergence, downward vertical motion, and decreased convection (Figures 54a, c, e). Figures 54b, d, f shows that in the 10 days prior to the late end dates, the continued development of convection over the Florida Peninsula is aided by low-

level convergence over the peninsula, and anomalous upward vertical motion over southern Georgia and the northern half of the Florida Peninsula (Figure 54b, d, f). All these above factors combine to produce anomalously strong convection over and to the north and east of KSC/CCAFS, increasing the likelihood of an extended main lightning season and increased lightning violations.

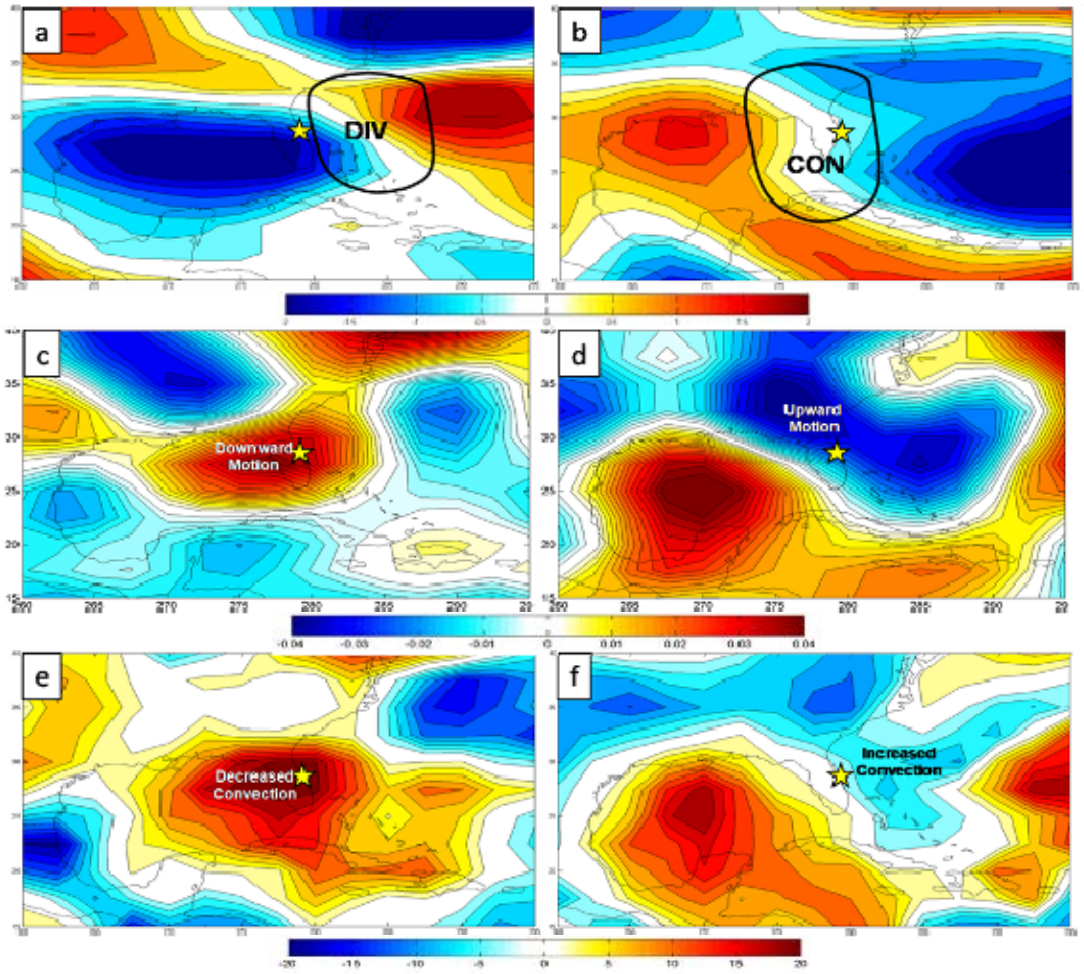

Figure 54. Composite anomalies panels on the left (a, c, e) represent conditions during the ten days immediately after early end dates of the main lightning violation season. The panels on the right (b, d, f) represent conditions during the ten days immediately prior to late ends of the main lightning violation season. In particular: (a) composite 850 mb zonal wind (m/s) anomaly for the ten days following early end dates; (b) composite 850 mb zonal wind (m/s) anomaly for the ten days prior to late end dates; (c) composite 500 mb omega (Pa/s) anomaly for the ten days following early end dates; (d) composite 500 mb omega (Pa/s) anomaly for the ten days prior to late end dates; (e) composite OLR (W/m^2) anomaly for the ten days following early end dates; and (f) composite OLR (W/m^2) anomaly for the ten days prior to late end dates of the main lightning violation season. Yellow stars indicate the approximate location of KSC/CCAFS.

The 200 mb GPH anomalies show some evidence of anomalous wave trains and extending from Asia into North America and the North Atlantic (Figure 55). A comparison of Figures 53 and 55 reveals equivalent barotropic structure over North America and the western North Atlantic, and indicates that the low-level anomalies shown in Figures 53 and 54 are dynamically linked to upper level anomalies. In particular, the upper level anomalies tend to support the low-level anomalies—for example, by supporting anomalously downward (upward) motion over and near Florida in the composite early (late) end to the main lightning season.

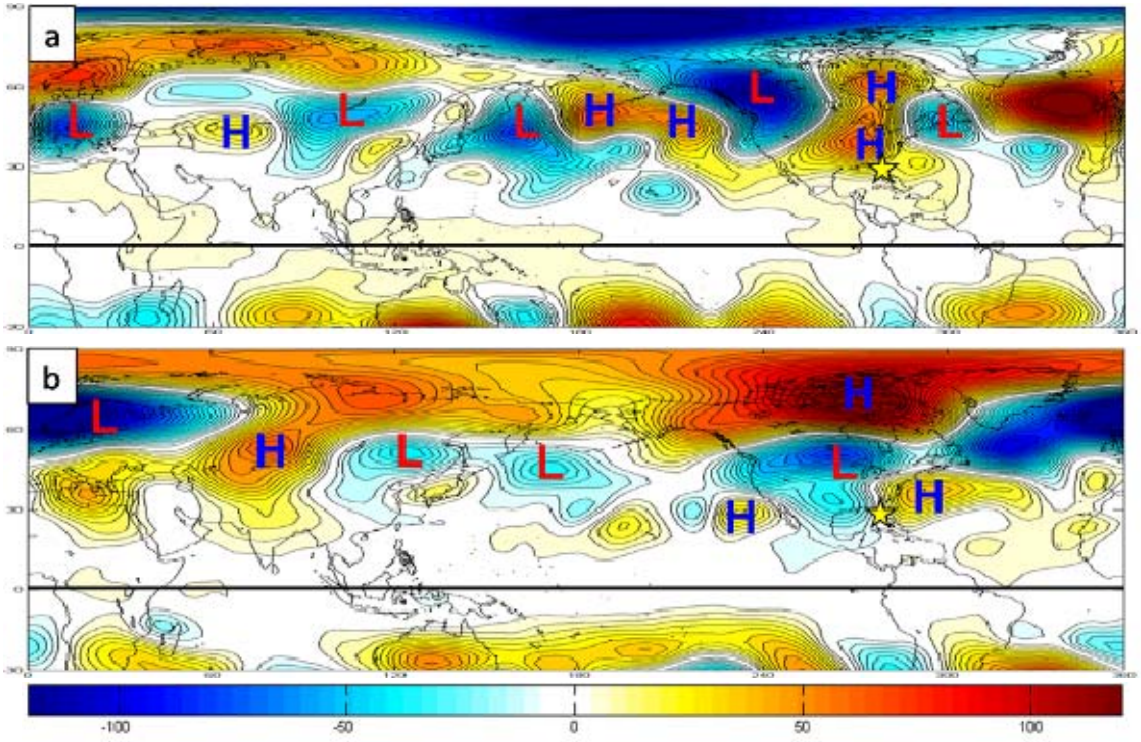

Figure 55. Composite 200 mb GPH anomalies (m) for the main lightning season during (a) the ten days following early end dates and (b) the first ten days immediately prior to late end dates. Anomalous Rossby wave trains that extend over the SE U.S. are marked with H and L and black arrows. The H and L identify the center of the positive (negative) height anomalies that help define the wave trains. The black arrows link the centers that are part of individual wave trains and indicate the direction of anomalous energy propagation in the wave trains. Yellow stars indicate the approximate location of the Florida Peninsula.

The schematic diagrams in Figure 56 provide a basic conceptual summary of the anomaly patterns associated with the ten days after early ends, and the ten days prior to late end, of the main lightning season. These schematics are directly based on the composites shown in Figures 53–55. The pronounced and relatively large-scale anomalies in Figure 56 suggest there is potential for long range forecasting of the regional anomalies that contribute to early and late ends of the main lightning season at KSC/CCAFS.

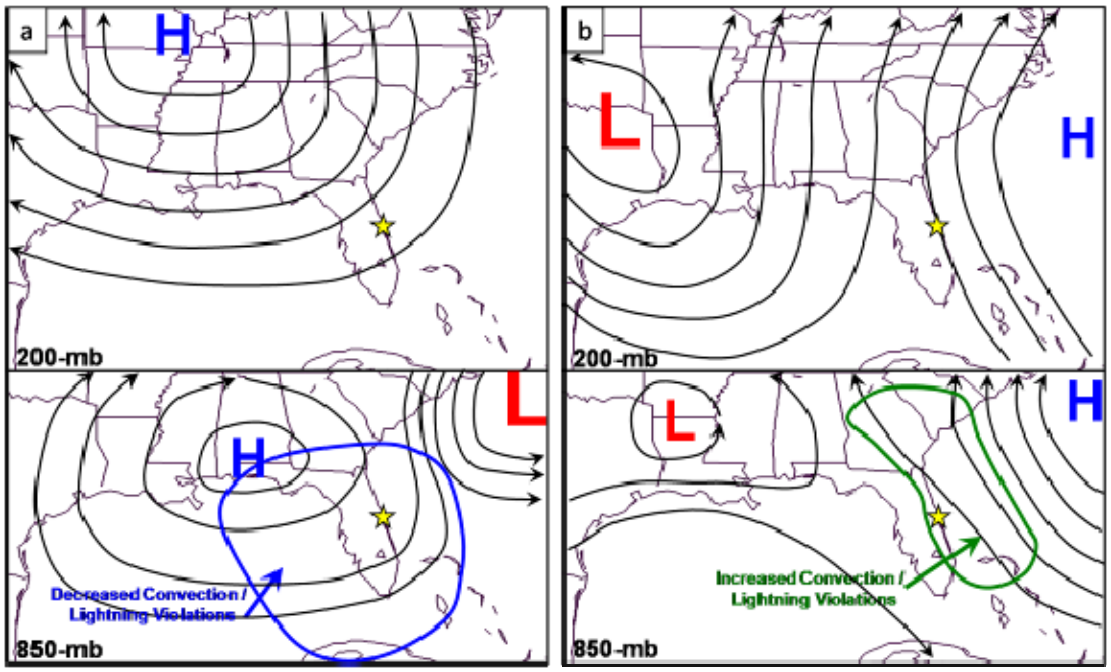

Figure 56. Schematic diagrams of the 200 mb and 850 mb geopotential height anomalies (m) associated with (a) the ten days after early end dates and (b) the ten days prior to late end dates of the main lightning season.

THIS PAGE INTENTIONALLY LEFT BLANK

IV. SUMMARY, CONCLUSIONS, AND RECOMMENDATIONS

A. KEY RESULTS AND CONCLUSIONS

This thesis explored the viability of recreating past LLCC violations to develop climatologies of the probability of natural lightning violations at KSC/CCAFS. We also investigated the physical processes that lead to interannual variability in lightning violations. The primary focus was to improve lightning forecasts and long range planning of space vehicle launches by limiting lightning related launch delays and cancellations at KSC/CCAFS.

We used CG lightning strike data from the NLDN to identify events in which the KSC/CCAFS natural lightning launch commit criterion was violated. These events allowed us to develop sub-daily, daily, and multi-day probabilities of lightning violations. We developed an objective statistical method for determining the seasonal tendencies of lightning and applied the method to identify six main lightning seasons spanning the full year. We used these seasons as a basis for characterizing patterns associated with climate scale variations in lightning at KSC/CCAFS. We applied conditional compositing methods to atmospheric reanalysis data to analyze climate variations that lead to interannual variations in violations in each season, as well as in the start and end dates of the main lightning season.

Our results indicated that regional and global scale processes are involved in altering the probability of lightning violations at KSC/CCAFS. These processes include shifts in the latitude and zonal extent of the Bermuda High, alterations of regional scale divergence and convection, and teleconnections to several well-known global scale climate variations. Several of these processes tend to be important in all or most lightning violation seasons, in addition to the start and end of the lightning season. These large-scale processes are generally easier to forecast, especially at long lead times. Therefore, relationships identified between these larger scale processes and lightning violations at KSC/CCAFS

improve the foundation for the development of skillful long range forecasts of the lightning violations. We expect our results will be useful improving the analysis and long range forecasting of natural lightning violations and in the planning of launches at KSC/CCAFS.

B. APPLICABILITY TO DOD OPERATIONS

The majority of scheduling and preparations for space launch operations begins several weeks to months prior to the actual launch dates. However, the space launch weather community primarily focuses on short-range pre-launch forecasting support (lead times of 72 hours or less). Very few, if any, operational products exist to aid launch weather officers in determining the likelihood for LLCC violations when planning space launches. However, it is in this planning phase when the space launch weather community can have arguably the greatest impact on the launch operations. Strategically selecting launch dates using the most complete and accurate climatological data available significantly decreases the likelihood of a launch delay or cancellation, saving DoD millions of dollars in preparation costs.

C. AREAS FOR FURTHER RESEARCH

Based on the results of this research, it is evident that creating comprehensive climatologies for the LLCC can rapidly provide benefits to the space launch weather community. This section highlights areas of future research to develop and improve LLCC climatologies and lightning related long range support for space launches.

1. This study focused on the natural lightning launch commit criterion. However, in order to improve operational relevancy, climatologies for the remaining criteria need to be created. The results from this study will prove instrumental in this process, since lightning violations are a vital part of most of the other criteria.

2. This study used CG lightning data from the NLDN, and excluded from detailed consideration data on lightning aloft. We made this decision because of the time required to process the large dataset from the LDAR / LDAR-II systems. In order to create climatologies that are as representative of the natural lightning criterion as possible, the LDAR and LDAR-II dataset needs to be analyzed. The comprehensive coverage of these systems would allow researchers to focus on the occurrence of lightning within 10 nm of KSC/CCAFS, rather than within 15 nm, as we did in this study.

3. Our study decided not to incorporate the electric field mill data from KSC/CCAFS into our evaluation of past LLCC violations. This again was primarily due to the time needed to process the large dataset. We recommend that data from this system get archived in a more accessible and usable format, to facilitate the use of this important data by researchers. Accounting for the electric field mill data in developing natural lightning climatologies is probably best done after evaluating the electric field mill LLCC (see Chapter I, Section B, and Appendix C). Merging the lightning and electric field mill datasets would then highlight if any adjustments are needed to the natural lightning climatologies.

4. The objective selection of the optimal threshold distance is complicated by a number of factors, especially the horizontal distance travelled by CG lightning (see Chapter II, Section C.2). We suggest that future research considering merging the results of McNamara (2002) and Nelson (2002) to develop an improved method for dealing with this horizontal distance issue.

5. The development and verification of LLCC climatologies is hindered by limited historical records of violations at KSC/CCAFS. We recommend that space launch weather personnel develop a daily electronic record of LLCC violations, especially those associated with planned and actual space launches. This would be a very valuable dataset for future research and development efforts.

6. This study analyzed regional and global scale processes that lead to interannual variations in lightning violations. We recommend that future research extend these analyses, and include analyses of intraseasonal variations of lightning violations. As part of these analyses, we recommend that future research further test the hypothesis developed in this study that above (below) normal numbers of lightning violations at KSC/CCAFS tend to be part of larger synoptic systems centered to the east of KSC/CCAFS. We also suggest that the results of these climate analyses be applied to: (a) create more advanced climatologies than those based just on long-term mean values; and (b) improve operational forecasting of LLCC violations at all lead times.

7. We recommend the use of newer, higher resolution reanalysis datasets such as the North American Regional Reanalysis (NARR) and Climate Forecast System Reanalysis (CFSR), to: (a) develop more advanced climatologies of several of the LLCC, and (b) further clarify the regional and global scale factors that help determine violations of the LLCC.

8. We suggest that the development of a long-range version of the LLCC be considered. The existing LLCC are focused on assessing near real time, mesoscale lightning related conditions or short range forecasts of those conditions. This is a reasonable focus but one that leads to complications in developing climatologies for the LLCC (e.g., complications related to the very high spatial and temporal resolution needed for such climatologies, and the corresponding very detailed and long term datasets needed to develop those climatologies). LLCC based on long range planning considerations, and on climate analyses and long range forecasts, would be a very useful complement to the existing LLCC. These longer range LLCC would be especially useful in developing long-range space launch plans.

APPENDIX A. CLIMATOLOGY TABLES

Table 8. Total number of lightning violations at KSC/CCAFS for each day of the year when summed over the 20-year study period, 1989-2008.

		Month											
		January	February	March	April	May	June	July	August	September	October	November	December
Days of Month	1	2.00	0.00	4.00	5.00	2.00	6.00	13.00	13.00	12.00	4.00	3.00	2.00
	2	2.00	1.00	4.00	4.00	2.00	11.00	11.00	14.00	15.00	4.00	4.00	3.00
	3	3.00	4.00	3.00	3.00	5.00	9.00	11.00	16.00	8.00	6.00	6.00	0.00
	4	0.00	2.00	4.00	0.00	5.00	7.00	11.00	15.00	11.00	6.00	6.00	0.00
	5	0.00	1.00	0.00	5.00	3.00	12.00	11.00	15.00	13.00	6.00	6.00	1.00
	6	0.00	1.00	2.00	2.00	5.00	12.00	13.00	10.00	12.00	5.00	5.00	1.00
	7	2.00	0.00	4.00	1.00	3.00	9.00	9.00	12.00	13.00	5.00	5.00	1.00
	8	2.00	2.00	2.00	2.00	1.00	11.00	15.00	12.00	11.00	8.00	8.00	1.00
	9	1.00	0.00	4.00	4.00	3.00	9.00	12.00	12.00	12.00	6.00	6.00	0.00
	10	1.00	4.00	1.00	4.00	2.00	12.00	12.00	16.00	9.00	7.00	7.00	3.00
	11	1.00	1.00	2.00	1.00	3.00	14.00	12.00	13.00	8.00	6.00	6.00	2.00
	12	1.00	3.00	0.00	3.00	5.00	13.00	15.00	12.00	6.00	5.00	5.00	1.00
	13	2.00	2.00	3.00	3.00	4.00	11.00	14.00	14.00	5.00	3.00	3.00	1.00
	14	3.00	1.00	2.00	2.00	7.00	11.00	15.00	14.00	3.00	5.00	5.00	0.00
	15	1.00	0.00	2.00	6.00	3.00	10.00	13.00	14.00	5.00	3.00	3.00	1.00
	16	1.00	2.00	4.00	6.00	4.00	9.00	9.00	8.00	5.00	4.00	4.00	0.00
	17	0.00	1.00	5.00	1.00	4.00	11.00	11.00	12.00	9.00	1.00	1.00	0.00
	18	1.00	0.00	3.00	1.00	2.00	13.00	14.00	12.00	12.00	4.00	4.00	0.00
	19	1.00	0.00	5.00	2.00	7.00	12.00	13.00	13.00	8.00	3.00	3.00	1.00
	20	3.00	2.00	2.00	2.00	4.00	11.00	17.00	14.00	7.00	4.00	4.00	1.00
	21	1.00	2.00	6.00	4.00	4.00	16.00	12.00	14.00	8.00	3.00	3.00	0.00
	22	1.00	5.00	1.00	4.00	5.00	15.00	14.00	12.00	8.00	3.00	3.00	0.00
	23	3.00	4.00	3.00	5.00	4.00	15.00	12.00	14.00	4.00	3.00	3.00	2.00
	24	2.00	2.00	1.00	1.00	2.00	13.00	14.00	8.00	10.00	6.00	6.00	2.00
	25	1.00	0.00	2.00	5.00	2.00	14.00	9.00	11.00	10.00	4.00	4.00	3.00
	26	0.00	2.00	4.00	5.00	6.00	13.00	14.00	12.00	14.00	2.00	2.00	2.00
	27	2.00	2.00	3.00	5.00	6.00	13.00	13.00	10.00	10.00	1.00	1.00	2.00
	28	1.00	5.00	5.00	2.00	12.00	14.00	8.00	9.00	11.00	2.00	2.00	1.00
	29	2.00		4.00	3.00	9.00	14.00	8.00	10.00	7.00	2.00	2.00	0.00
	30	1.00		3.00	7.00	5.00	14.00	11.00	11.00	5.00	2.00	2.00	0.00
	31	1.00		8.00		7.00		14.00	15.00		2.00		

Table 9. Lightning violation probability by month and day for KSC/CCAFS for the study period of 1989–2008.

Days of Month	Month											
	January	February	March	April	May	June	July	August	September	October	November	December
1	0.10	0.00	0.20	0.25	0.10	0.30	0.65	0.65	0.60	0.20	0.15	0.00
2	0.10	0.05	0.20	0.20	0.10	0.55	0.55	0.70	0.75	0.20	0.10	0.00
3	0.15	0.20	0.15	0.15	0.25	0.45	0.55	0.80	0.40	0.30	0.05	0.00
4	0.00	0.10	0.20	0.00	0.25	0.35	0.55	0.75	0.55	0.30	0.00	0.00
5	0.00	0.05	0.00	0.25	0.15	0.60	0.55	0.75	0.65	0.30	0.15	0.05
6	0.00	0.05	0.10	0.10	0.25	0.60	0.65	0.50	0.60	0.25	0.10	0.05
7	0.10	0.00	0.20	0.05	0.15	0.45	0.45	0.60	0.65	0.25	0.00	0.05
8	0.10	0.10	0.10	0.10	0.05	0.55	0.75	0.60	0.55	0.40	0.10	0.05
9	0.05	0.00	0.20	0.20	0.15	0.45	0.60	0.60	0.60	0.30	0.05	0.00
10	0.05	0.20	0.05	0.20	0.10	0.60	0.60	0.80	0.45	0.35	0.10	0.15
11	0.05	0.05	0.10	0.05	0.15	0.70	0.60	0.65	0.40	0.30	0.05	0.10
12	0.05	0.15	0.00	0.15	0.25	0.65	0.75	0.60	0.30	0.25	0.05	0.05
13	0.10	0.10	0.15	0.15	0.20	0.55	0.70	0.70	0.25	0.15	0.15	0.05
14	0.15	0.05	0.10	0.10	0.35	0.55	0.75	0.70	0.15	0.25	0.10	0.00
15	0.05	0.00	0.10	0.30	0.15	0.50	0.65	0.70	0.25	0.15	0.00	0.05
16	0.05	0.10	0.20	0.30	0.20	0.45	0.45	0.40	0.25	0.20	0.15	0.00
17	0.00	0.05	0.25	0.05	0.20	0.55	0.55	0.60	0.45	0.05	0.05	0.00
18	0.05	0.00	0.15	0.05	0.10	0.65	0.70	0.60	0.60	0.20	0.00	0.00
19	0.05	0.00	0.25	0.10	0.35	0.60	0.65	0.65	0.40	0.15	0.00	0.05
20	0.15	0.10	0.10	0.10	0.20	0.55	0.85	0.70	0.35	0.20	0.00	0.05
21	0.05	0.10	0.30	0.20	0.20	0.80	0.60	0.70	0.40	0.15	0.10	0.00
22	0.05	0.25	0.05	0.20	0.25	0.75	0.70	0.60	0.40	0.15	0.05	0.00
23	0.15	0.20	0.15	0.25	0.20	0.75	0.60	0.70	0.20	0.15	0.20	0.10
24	0.10	0.10	0.05	0.05	0.10	0.65	0.70	0.40	0.50	0.30	0.10	0.10
25	0.05	0.00	0.10	0.25	0.10	0.70	0.45	0.55	0.50	0.20	0.10	0.15
26	0.00	0.10	0.20	0.25	0.30	0.65	0.70	0.60	0.70	0.10	0.05	0.10
27	0.10	0.10	0.15	0.25	0.30	0.65	0.65	0.50	0.50	0.05	0.00	0.10
28	0.05	0.25	0.25	0.10	0.60	0.70	0.40	0.45	0.55	0.10	0.10	0.05
29	0.10		0.20	0.15	0.45	0.70	0.40	0.50	0.35	0.10	0.10	0.00
30	0.05		0.15	0.35	0.25	0.70	0.55	0.55	0.25	0.10	0.10	0.00
31	0.05		0.40		0.35		0.70	0.75		0.10		0.00

Table 10. 15-day mean of lightning violation probability by month and day for KSC/CCAFS for the study period of 1989–2008

Day of Month	Month											
	January	February	March	April	May	June	July	August	September	October	November	December
1	0.06	0.06	0.14	0.17	0.18	0.41	0.63	0.61	0.58	0.37	0.09	0.05
2	0.06	0.06	0.14	0.18	0.19	0.44	0.63	0.62	0.58	0.36	0.08	0.04
3	0.05	0.07	0.13	0.18	0.18	0.46	0.62	0.63	0.57	0.35	0.08	0.05
4	0.05	0.07	0.13	0.17	0.17	0.48	0.62	0.63	0.56	0.32	0.08	0.05
5	0.05	0.08	0.13	0.16	0.17	0.49	0.62	0.64	0.55	0.30	0.08	0.05
6	0.06	0.08	0.13	0.16	0.18	0.49	0.62	0.66	0.54	0.28	0.08	0.05
7	0.07	0.08	0.13	0.16	0.19	0.51	0.63	0.67	0.51	0.27	0.08	0.04
8	0.07	0.07	0.12	0.15	0.18	0.52	0.62	0.67	0.48	0.26	0.08	0.04
9	0.07	0.08	0.12	0.15	0.18	0.53	0.61	0.66	0.45	0.26	0.08	0.04
10	0.06	0.08	0.13	0.14	0.19	0.53	0.61	0.65	0.43	0.25	0.07	0.04
11	0.05	0.07	0.13	0.14	0.18	0.55	0.62	0.64	0.45	0.25	0.07	0.04
12	0.06	0.06	0.13	0.14	0.19	0.56	0.63	0.63	0.44	0.24	0.07	0.04
13	0.07	0.06	0.14	0.13	0.19	0.56	0.65	0.63	0.42	0.23	0.06	0.04
14	0.07	0.07	0.15	0.14	0.19	0.57	0.64	0.64	0.40	0.22	0.06	0.04
15	0.07	0.08	0.14	0.15	0.19	0.59	0.66	0.64	0.39	0.22	0.06	0.04
16	0.07	0.09	0.14	0.16	0.20	0.61	0.65	0.65	0.36	0.20	0.07	0.04
17	0.07	0.10	0.13	0.15	0.20	0.62	0.66	0.63	0.36	0.20	0.07	0.05
18	0.07	0.08	0.14	0.15	0.20	0.63	0.65	0.62	0.36	0.19	0.07	0.05
19	0.07	0.09	0.14	0.17	0.21	0.62	0.65	0.61	0.38	0.18	0.07	0.05
20	0.07	0.08	0.15	0.17	0.21	0.62	0.65	0.61	0.39	0.16	0.07	0.05
21	0.07	0.09	0.16	0.17	0.24	0.63	0.63	0.59	0.41	0.16	0.07	0.05
22	0.07	0.10	0.17	0.17	0.25	0.64	0.60	0.58	0.43	0.15	0.07	0.05
23	0.07	0.12	0.17	0.18	0.25	0.66	0.60	0.57	0.43	0.15	0.07	0.05
24	0.07	0.12	0.18	0.16	0.26	0.67	0.61	0.59	0.42	0.14	0.06	0.05
25	0.07	0.13	0.18	0.17	0.27	0.67	0.62	0.59	0.41	0.15	0.06	0.05
26	0.07	0.13	0.19	0.18	0.30	0.66	0.62	0.60	0.39	0.14	0.06	0.06
27	0.08	0.14	0.18	0.19	0.31	0.66	0.63	0.58	0.38	0.13	0.06	0.07
28	0.07	0.14	0.17	0.19	0.32	0.66	0.62	0.57	0.38	0.12	0.06	0.06
29	0.07		0.17	0.20	0.34	0.65	0.63	0.57	0.37	0.12	0.06	0.06
30	0.07		0.17	0.19	0.37	0.63	0.62	0.57	0.36	0.12	0.06	0.06
31	0.06		0.17		0.38		0.62	0.57		0.11		0.06

Table 11. 15-day mean of the number of lightning violation hours per day for KSC/CCAFS for the study period of 1989–2008.

Days of Month	Month											
	January	February	March	April	May	June	July	August	September	October	November	December
1	0.18	0.16	0.35	0.54	0.52	1.36	2.25	2.32	2.24	1.33	0.25	0.10
2	0.15	0.14	0.38	0.56	0.54	1.42	2.20	2.40	2.24	1.30	0.17	0.07
3	0.14	0.16	0.35	0.53	0.50	1.52	2.17	2.37	2.20	1.22	0.18	0.10
4	0.13	0.15	0.34	0.51	0.49	1.63	2.15	2.41	2.18	1.07	0.18	0.11
5	0.13	0.18	0.34	0.51	0.50	1.67	2.15	2.45	2.20	0.98	0.18	0.12
6	0.14	0.20	0.36	0.50	0.50	1.70	2.24	2.58	2.17	0.84	0.20	0.11
7	0.18	0.20	0.37	0.46	0.58	1.75	2.27	2.63	2.07	0.74	0.19	0.10
8	0.19	0.20	0.37	0.43	0.58	1.72	2.29	2.63	1.91	0.73	0.17	0.09
9	0.17	0.21	0.36	0.43	0.59	1.79	2.25	2.56	1.87	0.75	0.19	0.09
10	0.13	0.21	0.37	0.42	0.60	1.78	2.20	2.55	1.86	0.69	0.18	0.09
11	0.11	0.16	0.35	0.40	0.53	1.83	2.18	2.51	1.93	0.65	0.18	0.09
12	0.12	0.14	0.39	0.42	0.50	1.88	2.25	2.51	1.94	0.65	0.18	0.10
13	0.13	0.17	0.42	0.39	0.51	1.91	2.30	2.48	1.81	0.62	0.15	0.10
14	0.14	0.17	0.46	0.40	0.53	1.95	2.27	2.49	1.73	0.58	0.15	0.09
15	0.14	0.19	0.42	0.46	0.56	2.11	2.31	2.53	1.63	0.59	0.16	0.09
16	0.14	0.21	0.45	0.51	0.56	2.13	2.30	2.55	1.49	0.53	0.17	0.09
17	0.15	0.23	0.41	0.49	0.55	2.20	2.37	2.47	1.43	0.55	0.20	0.12
18	0.16	0.21	0.43	0.50	0.56	2.21	2.36	2.49	1.49	0.55	0.19	0.13
19	0.16	0.21	0.48	0.54	0.59	2.24	2.36	2.46	1.58	0.52	0.17	0.11
20	0.18	0.19	0.51	0.54	0.58	2.26	2.33	2.43	1.57	0.50	0.17	0.12
21	0.17	0.21	0.51	0.54	0.68	2.30	2.21	2.31	1.67	0.49	0.14	0.12
22	0.13	0.25	0.53	0.54	0.65	2.32	2.14	2.21	1.74	0.47	0.15	0.12
23	0.13	0.28	0.54	0.52	0.68	2.38	2.10	2.17	1.74	0.46	0.16	0.12
24	0.13	0.31	0.61	0.49	0.78	2.39	2.20	2.28	1.65	0.45	0.13	0.12
25	0.13	0.31	0.59	0.48	0.82	2.41	2.23	2.28	1.56	0.46	0.12	0.14
26	0.14	0.31	0.61	0.56	0.96	2.41	2.25	2.30	1.45	0.44	0.12	0.18
27	0.18	0.33	0.58	0.61	1.02	2.36	2.29	2.24	1.37	0.43	0.12	0.19
28	0.18	0.35	0.55	0.62	1.08	2.40	2.26	2.14	1.39	0.39	0.13	0.19
29	0.18		0.54	0.62	1.10	2.37	2.35	2.19	1.34	0.39	0.12	0.19
30	0.18		0.57	0.57	1.18	2.26	2.30	2.20	1.28	0.37	0.12	0.19
31	0.15		0.52		1.24		2.31	2.17		0.33		0.19

Table 12. Probability of natural lightning criterion violation by hour for KSC/CCAFS for each season during the study period of 1989–2008.

	Hour of Day (UTC)																							
	1	2	3	4	5	6	7	8	9	10	11	12	13	14	15	16	17	18	19	20	21	22	23	24
Winter	0.01	0.01	0.01	0.01	0.01	0.01	0.01	0.01	0.01	0.01	0.01	0.01	0.00	0.01	0.01	0.01	0.01	0.01	0.01	0.01	0.01	0.02	0.01	0.01
Spring	0.02	0.02	0.01	0.01	0.01	0.01	0.01	0.01	0.01	0.01	0.00	0.01	0.00	0.00	0.00	0.01	0.01	0.01	0.02	0.02	0.02	0.02	0.02	0.02
Ramp-Up	0.09	0.09	0.07	0.04	0.05	0.03	0.03	0.02	0.02	0.02	0.03	0.02	0.02	0.01	0.02	0.06	0.10	0.14	0.19	0.22	0.21	0.21	0.15	0.13
Main Lightning	0.15	0.10	0.07	0.05	0.04	0.03	0.04	0.03	0.04	0.03	0.03	0.03	0.03	0.03	0.05	0.11	0.17	0.26	0.34	0.39	0.38	0.34	0.25	0.19
Ramp-Down	0.11	0.10	0.09	0.08	0.07	0.06	0.06	0.05	0.05	0.05	0.05	0.05	0.05	0.06	0.06	0.08	0.13	0.17	0.21	0.23	0.22	0.19	0.15	0.12
Post Lightning	0.05	0.04	0.03	0.02	0.02	0.02	0.02	0.01	0.02	0.02	0.01	0.01	0.01	0.02	0.01	0.02	0.01	0.02	0.03	0.03	0.04	0.04	0.05	0.06

THIS PAGE INTENTIONALLY LEFT BLANK

APPENDIX B. ADDITIONAL FIGURES

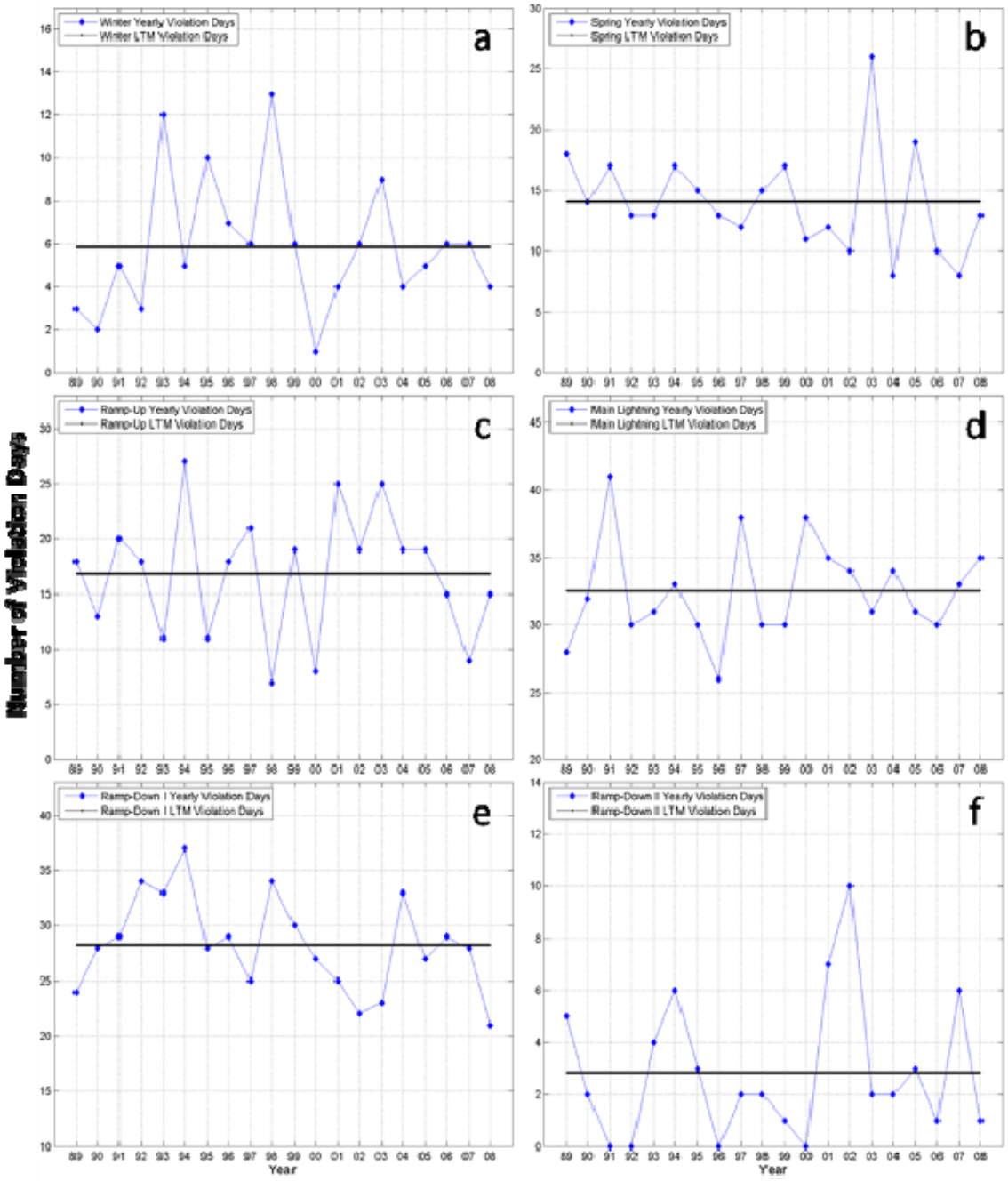

Figure 57. Total number of lightning violations days for (a) winter, (b) spring, (c) ramp-up, (d) main lightning, (e) ramp-down I, and (f) ramp-down II for KSC/CCAFS during the study period of 1989–2008. Scales are different for each of the six seasons.

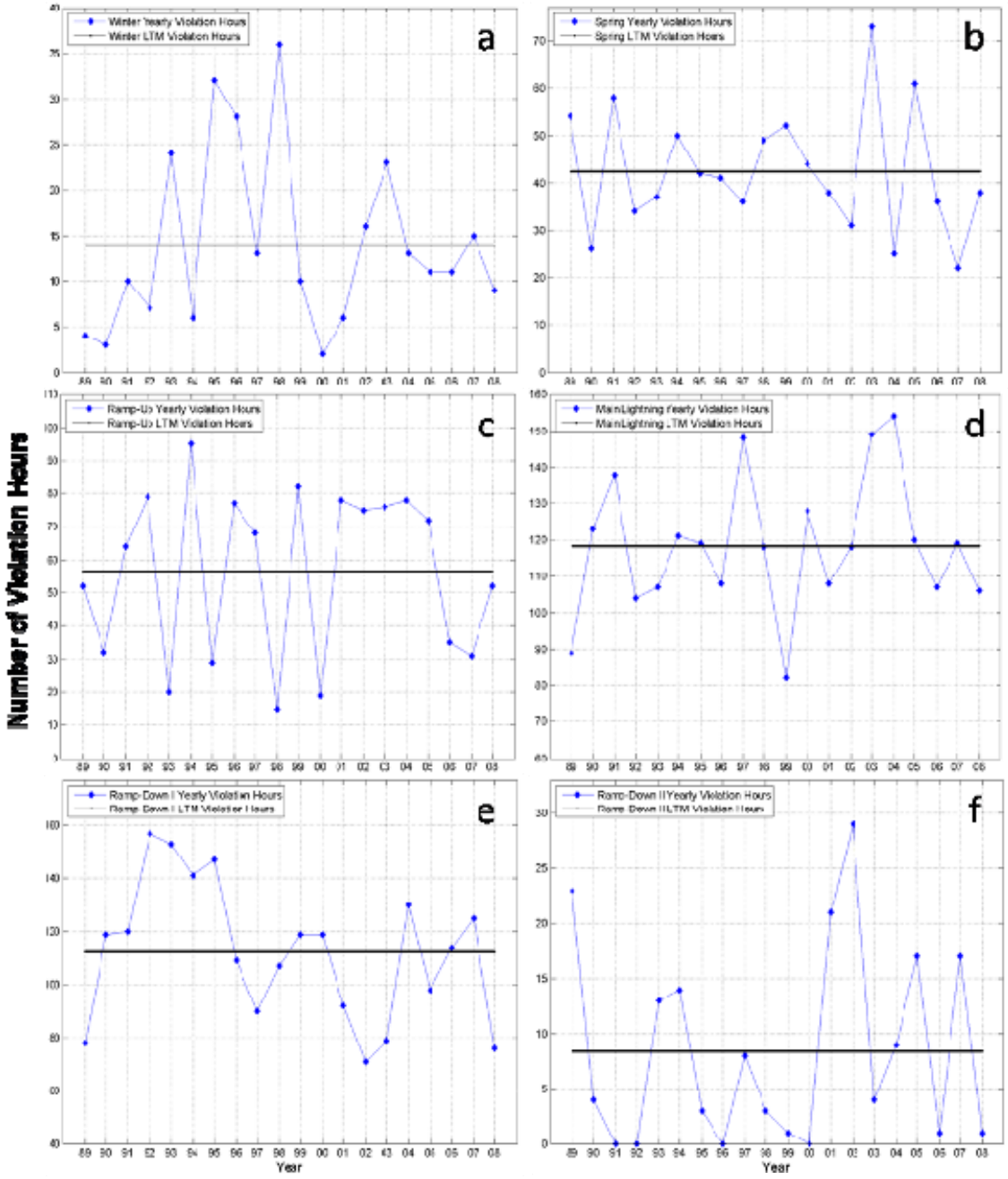

Figure 58. Total number of lightning violation hours for (a) winter, (b) spring, (c) ramp-up, (d) main lightning, (e) ramp-down I, and (f) ramp-down II for KSC/CCAFS during the study period of 1989–2008. Scales are different for each of the three seasons.

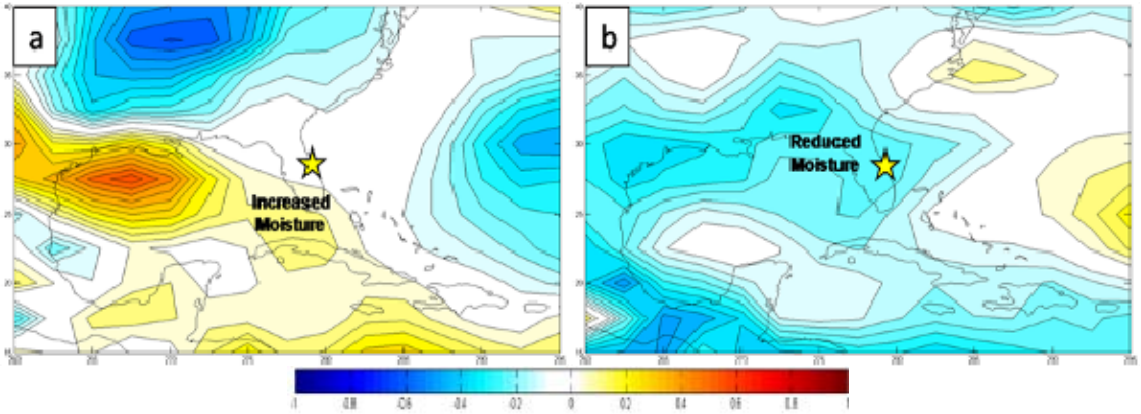

Figure 59. Composite 850 mb specific humidity (g/kg) anomalies during the main lightning season for periods in which there were: (a) above normal lightning violations and (b) below normal lightning violations. Yellow stars indicate the approximate location of KSC/CCAFS.

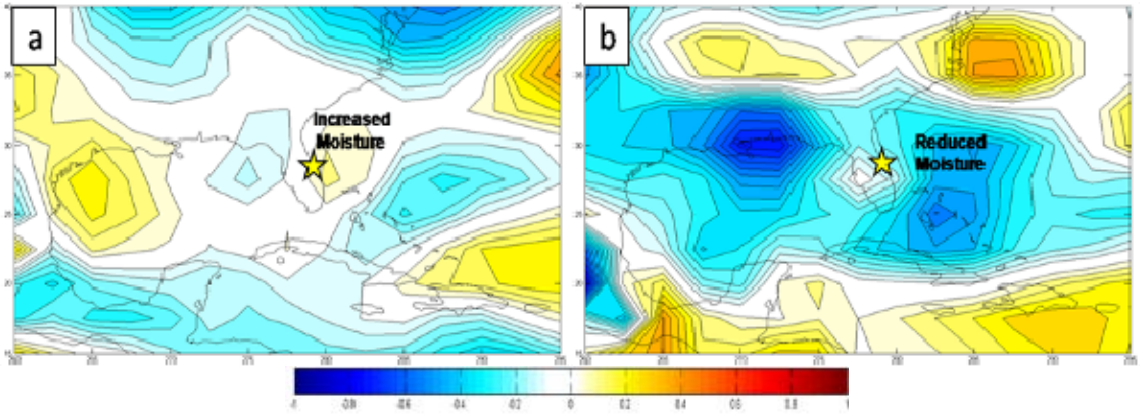

Figure 60. Composite 850 mb specific humidity (g/kg) anomalies during the ramp-up season for periods in which there were: (a) above normal lightning violations and (b) below normal lightning violations. Yellow stars indicate the approximate location of KSC/CCAFS.

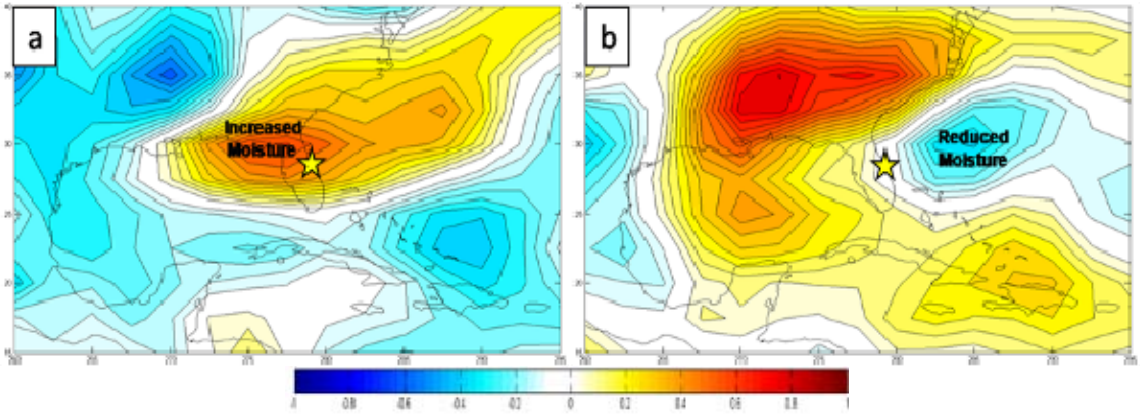

Figure 61. Composite 850 mb specific humidity (g/kg) anomalies during the ramp-down I season for periods in which there were: (a) above normal lightning violations and (b) below normal lightning violations. Yellow stars indicate the approximate location of KSC/CCAFS.

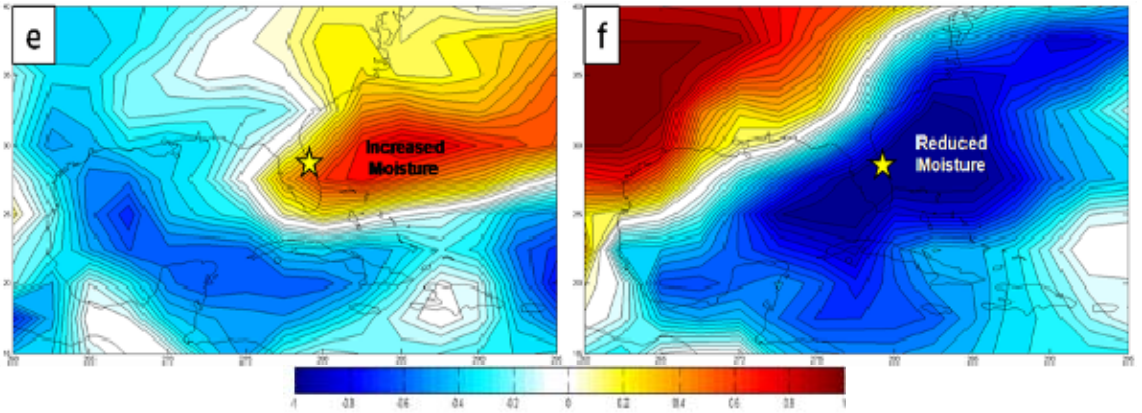

Figure 62. Composite 850 mb specific humidity (g/kg) anomalies during the ramp-down II season for periods in which there were: (a) above normal lightning violations and (b) below normal lightning violations. Yellow stars indicate the approximate location of KSC/CCAFS.

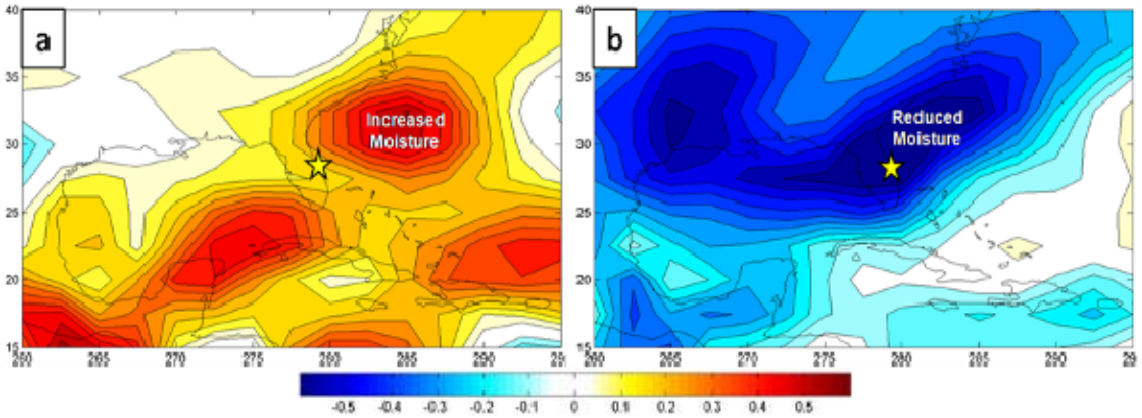

Figure 63. Composite 850 mb specific humidity (g/kg) anomalies during the winter season for periods in which there were: (a) above normal lightning violations and (b) below normal lightning violations. Yellow stars indicate the approximate location of KSC/CCAFS.

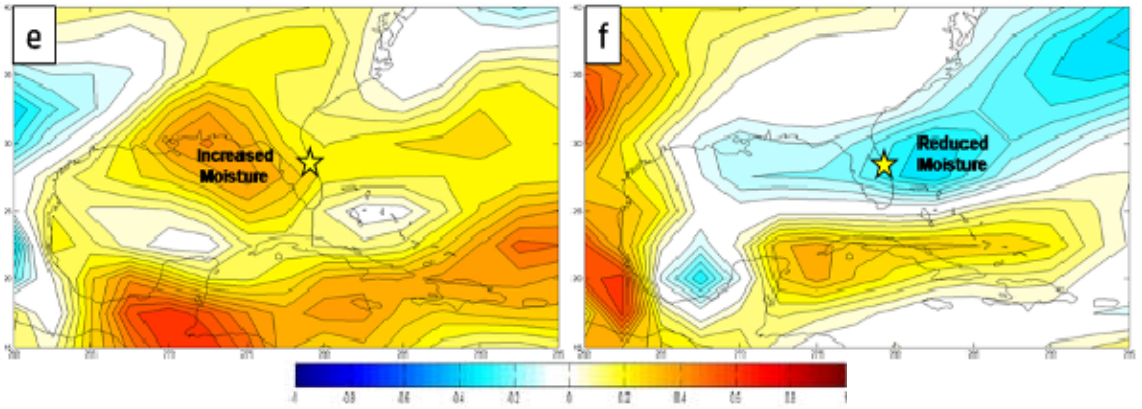

Figure 64. Composite 850 mb specific humidity (g/kg) anomalies during the spring season for periods in which there were: (a) above normal lightning violations and (b) below normal lightning violations. Yellow stars indicate the approximate location of KSC/CCAFS.

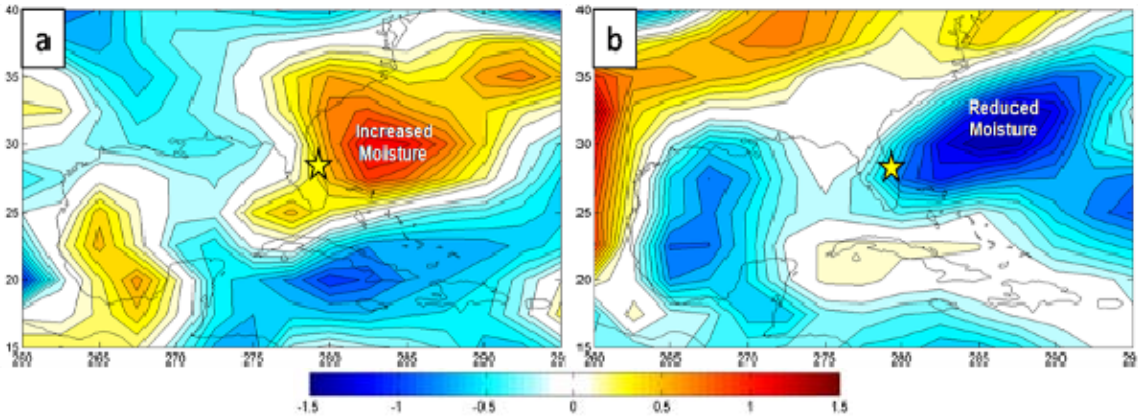

Figure 65. Composites of 850 mb specific humidity (g/kg) anomalies. The panel on the left (a) represents conditions during the first ten days in which there was an early start of the main lightning violation season (early starts). The panel on the right (b) represents conditions during the ten days immediately prior to late starts of the main lightning violation season (late starts). Yellow stars indicate the approximate location of KSC/CCAFS.

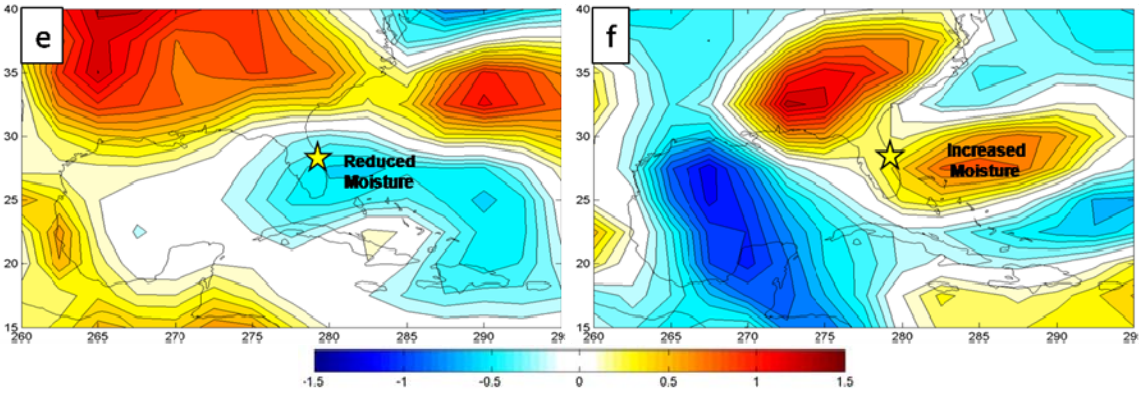

Figure 66. Composites of 850 mb specific humidity (g/kg) anomalies. The panel on the left (a) represents conditions during the first ten days in which there was an early end of the main lightning violation season (early ends). The panel on the right (b) represents conditions during the ten days immediately prior to late ends of the main lightning violation season (late ends). Yellow stars indicate the approximate location of KSC/CCAFS.

LIST OF REFERENCES

14th Weather Squadron (14 WS), cited 2010: Patrick AFB, FL Narrative. [Available online at http://www.meted.ucar.edu/afwa/climo/operations/media/patrick_narr.pdf] Accessed January 2010.

45th Weather Squadron (45 WS), 2007: Sea Breeze Forecasting. *Basic orientation and lightning training DVD*. Vol. 2.2, Sigmatech, Inc.

Air Force Space Command (AFSPC), 2004. Range safety user requirements– Ground and launch personnel, equipment, systems, and material operations safety requirements, APSPC Manual 91-710 Volume 6, 143 pp.

Applied Meteorology Unit (AMU), 2009: Applied Meteorology Unit quarterly report. AMU 3rd Quarter Rep. FY-09, 26 pp.

Cox, C. C., 1999: A comparison of horizontal cloud-to-ground lightning flash distance using weather surveillance radar and the distance between successive flashes method. M.S. thesis, Department of Engineering Physics, Air Force Institute of Technology, 130 pp.

Climate Prediction Center (CPC), cited 2010: Cold and warm episodes by season. [Available online at http://www.cpc.noaa.gov/products/analysis_monitoring/ensostuff/ensoyears.shtml.] Accessed February 2010.

Cummins, K.L., M.J. Murphy, E.A. Bardo, W.L. Hiscox, R.B. Pyle, and A.E. Uman, 1998: A combined TOA/MDF technology upgrade of the U.S. national lightning detection network. *J. Geophys. Res.,* 98, 9035-9044.

————, J. A. Cramer, C. J. Biagi, E. P. Krider, J Jerauld, M. A. Uman, and V. A. Rakov, 2006: The U.S. national lightning detection network: Post-upgrade status, Preprints, *Second Conf on Meteorological Applications of Lightning Data*, Atlanta, GA, Amer. Meteor. Soc., 9 pp.

Earth Systems Research Laboratory (ESRL), cited 2010. [Accessed online at http://www.esrl.noaa.gov/psd/cgi-bin/data/composites/printpage.pl.] Accessed January 2010.

Everitt, J. A., 1999: An improved thunderstorm forecast index for Cape Canaveral, Florida. M.S. thesis, Dept. of Engineering Physics, Air Force Institute of Technology, 98 pp.

Federal Aviation Administration (FAA): United States Department of Transportation, 2003: Commercial space transportation quarterly launch report. FAA 2nd Quarter Rep., 18 pp.

Free Map Tools, cited 2010: Radius around point map. [Available online at http://www.freemaptools.com/radius-around-point.htm.] Accessed January 2010.

Glickman, T. S., Ed., 2000: *Glossary of Meteorology.* 2d ed. Amer. Meteor. Soc., 855 pp.

Goetz, E. C., 2001: Descriptive and conditional climatology for specific launch commit criteria for Cape Canaveral, Florida. M.S. thesis, Dept. of Engineering Physics, Air Force Institute of Technology, 110 pp.

Grogan, M.J., 2004: Report on the 2002–2003 U.S. NLDN system wide upgrade. Viasala News. 5 pp.

Hanson, C. M., 2007: Long range operational military forecasts for Iraq. M.S. thesis, Dept. of Meteorology, Naval Postgraduate School, 77 pp.

Hildebrand, P. E., 2001: El Nino and La Nina events and North Atlantic tropical cyclones. M.S.thesis, Dept. of Meteorology, Naval Postgraduate School, 113 pp.

Hodanish, S., D. Sharp, C. Paxton, W. Collins, and R. E. Orville, 1997: A 10-yr monthly lightning climatology of Florida: 1986-95. *Wea. Forecasting*, **12**, 439–448.

Kalnay, E., and Coauthors, 1996: The NCEP/NCAR 40-year reanalysis project. *Bull. Amer. Meteor. Soc*, **77**, 437–471.

Krider, E. P., 1988: Spatial distribution of lightning strikes to ground during small thunderstorms in Florida. *Proc. 1988 Int. Aerospace and Ground Conf. on Lightning and Static Electricity*, Oklahoma City, OK, 318-323.

LaJoie, M. R., 2006: The impact of climate variations on military operations in the Horn of Africa. M.S. thesis, Dept. of Meteorology, Naval Postgraduate School, 153 pp.

Lambert, W. C., M. Wheeler, and W. P. Roeder, 2005: Objective lightning forecasting at Kennedy Space Center and Cape Canaveral Air Force Station using cloud-to-ground lightning surveillance system data. Preprints, *Conf. on Meteorological Applications of Lightning Data,* San Diego, CA, Amer. Meteor. Soc., 4.1.

Lericos, T. P., H. E. Fuelberg, A. I. Watson, and R. L. Holle, 2002: Warm season lightning distributions over the Florida Peninsula as related to synoptic patterns. *Wea. Forecasting*, **17**, 83–98.

Lopez, R. E., and R. L. Holle, 1999: The distance between successive lightning flashes. NOAA Tech. Memo. ERL NSSL-105, National Severe Storms Laboratory, Norman, OK, 29 pp.

McNamara,T. M., 2002: The horizontal extent of cloud-to-ground lightning over the Kennedy Space Center. M.S. thesis, Department of Engineering Physics, Air Force Institute of Technology, 100 pp.

Moss, S. M., 2007: Long range operational military forecasts for Afghanistan. M.S. thesis, Dept. of Meteorology, Naval Postgraduate School, 99 pp.

Mundhenk, B. D., 2009: A statistical-dynamical approach to intraseasonal prediction of tropical cyclogenesis in the western North Pacific. M.S. thesis, Dept of Meteorology, Naval Postgraduate School, 129 pp.

Murphree, T., 2008: *MR3610 Course Module 5: Introduction to Climate Science*. Dept. of Meteorology, Naval Postgraduate School, Monterey, California, 48 pp.

————, 2008b: *MR3610 Course Module 6: Smart Climatology*. Dept. of Meteorology, Naval Postgraduate School, Monterey, California, 52 pp.

Murphy, M. J., K. L. Cummins, N. W. S. Demetriades, W. P. Roeder, 2008: Performance of the new Four-Dimensional Lightning Surveillance System (4DLSS) at the Kennedy Space Center/Cape Canaveral Air Force Station complex. *Extended Abstracts, 13th Conf. on Aviation, Range and Aerospace Meteorology*, New Orleans, LA, *Amer. Meteor. Soc.*, 7.6.

National Aeronautics and Space Administration (NASA), cited 2009: Spaceport Weather Data Archive. [Available online at ftp://trmm.ksc.nasa.gov/lightning/archives/4DLSS/.]

Nelson, L. A., 2002: Synthesis of 3-dimensional lightning data and weather radar data to determine the distance that naturally occurring lightning travels from thunderstorms. M.S. thesis, Department of Engineering Physics, Air Force Institute of Technology, 85 pp.

Neumann, C. J., 1971: Thunderstorm forecasting at Kennedy Space Center. *J. Appl. Meteor.,* **10,** 921–936.

Parsons, T. L., 2000: Determining horizontal distance distribution of cloud-to-ground lightning. M.S. thesis, Department of Engineering Physics, Air Force Institute of Technology, 88 pp.

Poehler, H. A., 1978: LDAR observations of a developing thunderstorm correlated with field mill, ground strike location, and weather radar data including the first report of the design and capabilities of a new, time-of-arrival ground-strike location system (GSLS). NASA Contract Report CR-154626, 135pp.

Poniatowski, K. S., 1987: Manned/Unmanned launch vehicle weather history at lift-off 1960 to present. Unpublished, NASA Headquarters, 55 pp. [Cited in Roeder and McNamara 2006.]

Raynak, C.S., 2009: Statistical-dynamical forecasting of tropical cyclogenesis in the North Atlantic at intraseasonal lead times. M.S. thesis, Dept. of Meteorology, Naval Postgraduate School, 93 pp.

Renner, S. L., 1998: Analyzing horizontal distances between WSR-88D thunderstorm centroids and cloud-to-ground lightning strikes. M.S. thesis, Department of Engineering Physics, Air Force Institute of Technology, 123 pp.

Roeder, W. P., J. E. Sardonia, S. C. Jacobs, M. S. Hinson, A. A. Guiffrida, and J. T. Madura, 1999: Avoiding triggered lightning threat to space launch from the Eastern Range/Kennedy Space Center. Preprints, *Eighth Conf. on Aviation, Range, and Aerospace Meteorology,* Dallas, TX, Amer. Meteor. Soc., 120–124.

————, and T. M. McNamara, 2006: A survey of the lightning launch commit criteria. Preprints, *Second Conf on Meteorological Applications of Lightning Data*, Atlanta, GA, Amer. Meteor. Soc., 18 pp.

Simpson, J. E., 1994: *Sea Breeze and Local Wind.* Cambridge University Press, 234 pp.

Stepanek, A. J., 2006: North Pacific – North American circulation and precipitation anomalies associated with the Madden-Julian Oscillation. M.S. thesis, Dept. of Meteorology, Naval Postgraduate School, 143 pp.

Uman, M. A., and E. P. Krider, 1989: Natural and artificially initiated lightning. *Science*, **246**, 457–464.

van den Dool, H., 2007: *Empirical Methods in Short-Term Climate Prediction*. Oxford University Press, 215 pp.

Vorhees, D. C., 2006: The impacts of global scale climate variations on Southwest Asia. M.S. thesis, Dept. of Meteorology, Naval Postgraduate School, 175 pp.

Ward, J. G., K. L. Cummins, and E. P. Krider, 2008: Comparison of the KSC-ER cloud-to-ground lightning surveillance system (CGLSS) and the U.S. national lightning detection network (NLDN). Preprints, *Twentieth International Lightning Detection Conference*, Tucson, AZ, Amer. Meteor. Soc., 7 pp.

THIS PAGE INTENTIONALLY LEFT BLANK

INITIAL DISTRIBUTION LIST

1. Defense Technical Information Center
   Ft. Belvoir, Virginia

2. Dudley Knox Library
   Naval Postgraduate School
   Monterey, California

3. Prof. Tom Murphree
   Naval Postgraduate School
   Monterey, California

4. Ms. Mary Jordan
   Naval Postgraduate School
   Monterey, California

5. Mr. William Roeder
   45th Weather Squadron
   Patrick AFB, Florida

6. Air Force Weather Technical Library
   Asheville, North Carolina